ISTANBUL TECHNICAL UNIVERSITY ★ GRADUATE SCHOOL

NUMERICAL MODELING AND EXPERIMENTAL ANALYSIS ON COUPLED TORSIONAL-LONGITUDINAL AND LATERAL VIBRATIONS OF PROPULSION SHAFT SYSTEM

Ph.D. THESIS

Akile Neşe HALİLBEŞE

Department of Naval Architecture and Marine Engineering

Naval Architecture and Marine Engineering Programme

JUNE 2021

ISTANBUL TECHNICAL UNIVERSITY ★ GRADUATE SCHOOL

NUMERICAL MODELING AND EXPERIMENTAL ANALYSIS ON COUPLED TORSIONAL-LONGITUDINAL AND LATERAL VIBRATIONS OF PROPULSION SHAFT SYSTEM

Ph.D. THESIS

Akile Neşe HALİLBEŞE
(508152010)

Department of Naval Architecture and Marine Engineering

Naval Architecture and Marine Engineering Programme

Thesis Advisor: Prof. Dr. Osman Azmi ÖZSOYSAL

JUNE 2021

İSTANBUL TEKNİK ÜNİVERSİTESİ ★ LİSANSÜSTÜ EĞİTİM ENSTİTÜSÜ

GEMİ SEVK SİSTEMLERİNDE OLUŞAN TEKİL VE BİRLEŞİK EKSENEL, YANAL VE BURULMA TİTREŞİMLERİNİN İNCELENMESİ

DOKTORA TEZİ

Akile Neşe HALİLBEŞE
(508152010)

Gemi İnşaatı ve Gemi Makinaları Mühendisliği Anabilim Dalı

Gemi İnşaatı ve Gemi Makinaları Mühendisliği Programı

Tez Danışmanı: Prof. Dr. Osman Azmi ÖZSOYSAL

HAZİRAN 2021

Akile Neşe HALİLBEŞE, a Ph.D. student of İTU Graduate School student ID 508152010, successfully defended the thesis entitled "NUMERICAL MODELING AND EXPERIMENTAL ANALYSIS ON COUPLED TORSIONAL-LONGITUDINAL AND LATERAL VIBRATIONS OF PROPULSION SHAFT SYSTEM", which she prepared after fulfilling the requirements specified in the associated legislations, before the jury whose signatures are below.

Thesis Advisor : **Prof. Dr. Osman Azmi ÖZSOYSAL** .....
Istanbul Technical University

Jury Members : **Prof. Dr. Oğuz Salim SÖĞÜT** .....
Istanbul Technical University

Prof. Dr. Fuat ALARÇİN .....
Yıldız Technical University

Assoc. Prof. Bahadır UĞURLU .....
Istanbul Technical University

Assoc. Prof. İsmail BAYER .....
Yıldız Technical University

Date of Submission : 26 April 2021
Date of Defense : 09 June 2021

To all women in the world who have not got opportunity to get even basic education,

FOREWORD

I would like to express my deep appreciation and thanks for my supervisor Prof. Dr. Osman Azmi ÖZSOYSAL. I would also like to thank my committee members, Prof. Dr. Oğuz Salim SÖĞÜT and Prof. Dr. Fuat ALARÇİN for serving as my committee members. I would especially like to thank my parents for their support throghout the preparation of this thesis.

I would also like to thank the following people for their valuable contributions:

- Assoc. Prof. Bahadır UĞURLU, Ress. Ass. İsmail KAHRAMAN (staffs and lecturers at Istanbul Technical University),
- Prof. Xinping YAN, Dr. Cong ZHANG, Dr. Qianwen HUANG (staffs and lecturers at Wuhan University of Technology),

April 2021

Akile Neşe HALİLBEŞE
(MSc. BSc. Naval Architect and Marine Engineer)

TABLE OF CONTENTS

Page

FOREWORD ..... **ix**
TABLE OF CONTENTS ..... **xi**
SYMBOLS ..... **xiii**
LIST OF TABLES ..... **xv**
LIST OF FIGURES ..... **xvii**
SUMMARY ..... **xix**
ÖZET ..... **xxiii**
1. INTRODUCTION **1**
1.1 Purpose of Thesis 1
1.2 Methodology 2
1.3 Literature Review 2
2. COUPLED TORSIONAL AND LONGITUDINAL VIBRATIONS **7**
2.1 Numerical Model for the Coupled Torsional and Longitudinal Vibrations 8
2.2 Experimental Setup 11
2.3 Application and Discussion 15
2.4 Different Parameter Effects to Coupled Torsional-Longitudinal Vibration 22
2.4.1 Effect of diameter and length ratio of the shaft 22
2.4.2 Effect of damping coefficient and stiffness coefficient of the shaft 24
2.5 Permissible Torsional Vibration Stresses 27
2.6 Results 28
3. COUPLED TORSIONAL AND LATERAL VIBRATIONS **29**
3.1 Numerical Model for Coupled Torsional and Lateral Vibrations 30
3.2 Experimental Setup 32
3.3 Application and Discussion 34
3.4 Verification 35
3.5 Verification at Various Speed Range 37
3.6 Different Parameter Effects to the Coupled Torsional-Lateral Vibration 40
3.6.1 Coupling effect 41
3.6.2 Effect of diameter and length ratio of the shaft 41
3.6.3 Effect of stiffness and damping coefficient ratio of the shaft 42
3.6.4 Effect of eccentricity of cross section ratio 44
3.7 Permissible Torsional Vibration Stresses 45
3.8 Results 46
4. COUPLED LONGITUDINAL AND LATERAL VIBRATIONS OF SHAFT SYSTEM **49**
4.1 Numerical Model for Coupled Longitudinal and Lateral Vibrations 49
4.2 Experimental Setup 52
4.3 Application and Discussion 54
4.4 Numerical Simulation 54
4.5 Verification 56
4.6 Verification at Various Speed Range 58

4.7 Different Parameter Efffects to the Coupled Longitudinal-Lateral Vibration . 62
4.7.1 Coupling effect 62
4.7.2 Effect of the diameter and length ratio of the shaft 63
4.7.3 Effect of stiffness and damping coefficient ratio 65
4.7.4 The effect of the coupling coefficient 67
4.8 Results 67
5. CONCLUSION 69
REFERENCES 75
CURRICULUM VITAE 81

SYMBOLS

ρ	: Density
J	: Moment of inertia
L	: Length of each shaft segment
A	: Cross-sectional area
E	: Young's modulus
t	: Time
m	: Mass
I	: Second axial moment of inertia
d_t	: Torsional damping coefficient
d_x	: Longitudinal damping coefficient
k_t	: Torsional stiffness coefficient
k_x	: Longitudinal stiffness coefficient
k_{tx}	: Stiffness coefficient for coupled torsional-longitudinal vibration
k_{xt}	: Stiffness coefficient for coupled longitudinal- torsional vibration
δ	: Coupling coefficient
M	: The matrix of masses
D_T	: Torsional damping matrix
D_X	: Longitudinal damping matrix
K_T	: Torsional stiffness matrix
K_X	: Longitudinal stiffness matrix
K_{TX}	: Stiffness matrix for coupled torsional-longitudinal vibration
K_{XT}	: Stiffness matrix for coupled longitudinal- torsional vibration
G	: Shear modulus
I_P	: Second polar moment
E	: Young's modulus
DNV	: DNV is an IACS member
τ_c	: Vibration stress
σ_B	: Minimum tensine strength
λ	: Speed ratio
C_K	: The particular shaft design factor
C_D	: Size factor
TVC	: Torsional vibration calculation report

LIST OF TABLES

Page

Table 2.1: Geometrical properties of the shaft segments. **12**
Table 2.2: Loadings for each rotational speed. **15**
Table 2.3: Natural frequencies predicted by the coupled and uncoupled form (Hz). **19**
Table 2.4: Error margin for each rotational speed. **22**
Table 3.1: Loadings for each rotational speed……**34**
Table 3.2: Error margin for each rotational speed. **40**
Table 3.3: Natural frequencies predicted by the coupled and uncoupled form (Hz). **40**
Table 3.4: Natural frequencies predicted by the coupled and uncoupled form (Hz). **41**
Table 3.5: The relative errors of numerical results compared to experimental results.. ..... **47**
Table 4.1 : Loadings for each rotational speed. **53**
Table 4.2 : The geometrical properties of the shaft segments. **54**
Table 4.3 : Properties of the propulsion shaft. **54**
Table 4.4 : Error margin for each rotational speed. **61**
Table 4.5 : Naturel frequencies predicted by the coupled and uncoupled form (Hz). **61**

LIST OF FIGURES

Page

Figure 2.1 : Schematic of the beam with a mass payload (Hassan and Mehrdaad, 2006). **7**
Figure 2.2 : Schematic of lumped-mass model of the shaft (Huang, 2017). **9**
Figure 2.3 : Details of the shaft system. **9**
Figure 2.4 : Propulsion shaft system test plan. **12**
Figure 2.5 : Vibration measurement points layout. **13**
Figure 2.6 : Longitudinal and torsional vibration measurement points layout. **13**
Figure 2.7 : Vibration measurement points layout. **14**
Figure 2.8 : The signal acquisition and analysis system. **14**
Figure 2.9 : Experimental and numerical coupled longitudinal vibration results. **16**
Figure 2.10 : Experimental and numerical coupled longitudinal vibration results. **16**
Figure 2.11 : Experimental and numerical coupled torsional vibration results. **17**
Figure 2.12 : Experimental and numerical coupled torsional vibration results. **17**
Figure 2.13 : Longitudinal displacement for coupled and uncoupled form. **18**
Figure 2.14 : Torsional angle for coupled and uncoupled form. **18**
Figure 2.15 : Numerical method results for 100–190 rpm in the longitudinal direction. **19**
Figure 2.16 : Numerical method results for 100–190 rpm in the torsional direction. **20**
Figure 2.17 : Experiment results for 100–190 rpm in the longitudinal direction. **21**
Figure 2.18 : Experiment results for 100–190 rpm in torsional direction. **21**
Figure 2.19 : The effect of the shaft length. **23**
Figure 2.20 : The effect of the shaft diameter. **23**
Figure 2.21 : The effect of damping coefficient. **24**
Figure 2.22 : The effect of torsional stiffness coefficient. **25**
Figure 2.23 : The effect of longitudinal stiffness coefficient. **25**
Figure 2.24 : The effect of coupled vibration coefficient. **26**
Figure 3.1 : Unbalanced shaft model. **29**
Figure 3.2 : Measurement points layout for the shaft lateral and torsional vibrations. **33**
Figure 3.3 : Hydraulic loading system and torque measurement point. **34**
Figure 3.4 : Vertical displacements results (a) at 100 rpm (b) between 0-5 Hz. **35**
Figure 3.5 : Horizontal displacements results (a) at 100 rpm (b) between 0-5 Hz. **36**
Figure 3.6 : Torsional angles results (a) at 100 rpm (b) between 0-5 Hz **37**
Figure 3.7 : Numerical results between 100-190 rpm (a) vertical (b) horizontal (c) torsional. **38**
Figure 3.8 : Experimental results between 100-190 rpm (a) vertical (b) horizontal (c) torsional. **39**
Figure 3.9 : Displacements for different shaft length. **41**
Figure 3.10 : Displacements for different shaft diameter. **42**
Figure 3.11 : Displacements for different damping coefficients. **43**

Figure 3.12 : Displacements for different lateral stiffness coefficients. **43**
Figure 3.13 : Displacements for different torsional stiffness coefficients **44**
Figure 3.14 : Displacements at different eccentricity of cross sections. **45**
Figure 4.1 : Schematic of the beam with a mass payload. **49**
Figure 4.2 : Measurement points layout for the shaft longitudinal and lateral vibrations. **53**
Figure 4.3 : Finite element model with boundary conditions. **55**
Figure 4.4 : Longitudinal displacements results (a) at 100 rpm (b) between 0-5 Hz. **56**
Figure 4.5 : Vertical displacements results (a) at 100 rpm (b) between 0-5 Hz. **57**
Figure 4.6 : Horizontal displacements results (a) at 100 rpm (b) between 0-5 Hz. .. **58**
Figure 4.7 : Numerical results between 100-190 rpm (a) longitudinal (b) vertical (c) horizontal **59**
Figure 4.8 : Experimental results between 100–190 rpm (a) longitudinal (b) vertical (c) horizontal. **60**
Figure 4.9 : Longitudinal displacement for coupled and uncoupled form. **62**
Figure 4.10 : Lateral displacement for coupled and uncoupled form (a) vertical (b) horizontal. **63**
Figure 4.11 : Displacements for different shaft length. **64**
Figure 4.12 : Displacements for different shaft diameter. **64**
Figure 4.13 : Displacements for different damping coefficients. **65**
Figure 4.14 : Displacements for different longitudinal stiffness coefficients. **66**
Figure 4.15 : Displacements for different lateral stiffness coefficients. **66**
Figure 4.16 : Displacements for different coupled vibration coefficient. **67**

NUMERICAL MODELING AND EXPERIMENTAL ANALYSIS ON COUPLED TORSIONAL-LONGITUDINAL AND LATERAL VIBRATIONS OF PROPULSION SHAFT SYSTEM

SUMMARY

Ships are the most leading option for the development and progress of water transportation. The main engine, which is one of the main components of the propulsion system, is to produce more power than ever with oversizing the ship because of increased tonnage demands. As an inevitable result of this fact, the number of failures increases due to the increased drive power of ships because of the complex running conditions under harmonic and impact loads. The propulsion shaft system is the heart of the ship. When the operating conditions cannot be predicted correctly and the impact loads miscalculated, the reliability of the propulsion systems will be reduced.

The main purpose of this thesis is to develop a multi-purpose computer code to investigate the behavior of a conventional propulsion shaft system in where three different coupled vibration case occurs and to observe how the vibration responses vary. Simultane vibration responses are in different directions. Excitation frequency and ultimate amplitudes that may occur with the coupled vibration are generally ignorable and so done. Whenever the vibration forms are considered separately instead of coupled, the numerical results can be quite different from the actual measurements. Ignoring the coupled vibration approach or pure uncoupled vibration calculations is not realistic since the harmonic forces do not excite only the power transmission shaft in the propulsion chain but also the bearings and ship hull, and causes a significant raising at noise level. Similarly, it negatively affects the running performance of the shaft system and leads to loss of durability, breakage, tribological problems, and finally failures. For this reason, it always needs to examine the coupled vibration modes for the cruising reliability of each ship.

It is noticed that the unwanted vibration reactions generally occur in the longitudinal, torsional, and lateral modes and their coupled forms. Even if the numerical error margin will increase during the coupled vibration modeling (i.e. torsional, longitudinal, and lateral), the interaction of two axes is inevitably taken into account. Common studied forms about the coupled vibration are coupled torsional-longitudinal vibration, coupled torsional-lateral, and coupled longitudinal-lateral vibration. In this research, taking advantage of the small-scaled model of a propulsion shaft system at the Wuhan University of Technology, the experimental results are compared with the results of numerical simulation codes about the coupled vibration cases such as the torsional-longitudinal, the torsional-lateral, and the longitudinal-lateral. Numerical outcomes were validated by examining the time-based displacement values at different shaft speeds and comparing them with test results.

The theoretical approach is based on a mass-spring system for coupled torsional-longitudinal vibrations. The theoretical model for coupled torsional-longitudinal

vibration is sufficiently compatible that it can respond quickly to changes in values such as the stiffness coefficient, damping coefficient, and rotational speed. External forces and forced vibration responses, including torque and longitudinal forces with different amplitudes, were taken into account. Besides, since the propeller is not included in the experimental mechanism, the numerical model is created using the coupled vibration coefficient in the literature. A theoretical solution has been obtained to verify the proposed mass-spring model. Depending on the change of rotational speed and loading condition, the change of frequency response and maximum ultimate amplitude.were presented. Coupled vibration effect is also investigated by comparing maximum displacement values for coupled and uncoupled vibration. The effect of the parameters such as the shaft length, shaft diameter, stiffness coefficient, and damping coefficient, etc., for coupled torsional-longitudinal vibrations were also examined. The vibration stress that occurs in the system was further compared with the allowable stress required by DNV.

Coupled torsional-lateral vibrations of the propulsion shaft system are caused by the rotation of the propeller, the mass of shaft components, the external and internal forces affecting the bearings, axial displacement caused by the transmission of the force of the gears to each other. As a result of the structural properties of the shaft and the imbalances that occur during the rotation process, axial displacements occur between the center of the mass and the center of the cross-section of the shaft. The movement of the shaft always results in axial displacement horizontally when not intervened externally in real operating conditions. This eccentric effect of the shaft causes the vibration response to be more complex and intense. In addition to vibration control techniques that reduce the wrong alignment of the bearing and shaft, the dissertation has focused mainly on theoretical and practical methods that support the prediction of shaft vibrations. Therefore, minimizing the vibration density of the propeller shaft on the horizontal and vertical axis is of great interest. The majority of the studies about coupled lateral-torsional vibration in literature are belong to aerospace engineering. In those studies, the shaft system is modeled according to the torsional-lateral vibrations with a disk of mass m located at the midpoint of a massless shaft called with the Jefcott Rotor model. Taking advantage of these studies, the Jefcott Rotor model has been revised and applied to the propeller-shaft system in this doctoral research work. Thus, a numeric model was obtained considering sufficiently suitable and responsive to influencing factors such as the eccentricity of the cross-section, the damping coefficient, stiffness coefficient, and the shaft length-diameter ratio. This method is suitable for predicting dynamic performance and numerical solutions with the above impact factors. The experiment was repeated at different shaft speed values to validate the proposed numerical model, and time-dependent displacement values were compared for validation. Based on the proposed model, the effect of the change of impact factors such as the eccentricity of the cross-section, the damping coefficient, the coefficient of stiffness, and the length-diameter ratio of the shaft were discussed. Additionally, a new coupling coefficient value has been proposed, and the importance of accurately defining the coupling coefficient value was shown.

At the final step of this doctoral work, the coupled longitudinal-lateral vibrations were investigated due to axial forces that occur in the propeller and cause misalignment of the shaft. The numerical model for the coupled longitudinal-lateral vibrations involves the equation of motion by the Energy Method. In the model, the equations are complex, and it is tough to simplify and bring into matrix form and solve in Matlab. Consequently, the equation of motion is solved with the help of the Ansys APDL

program by modeling the system with the mass-spring method. The coupled vibration effect is given in the system with the angular velocity. To verify the proposed mass-spring model, the results were compared with data obtained from the experimental setup. Depending on the change of rotational speed and loading condition, the change of frequency responses and maximum displacements are presented. The frequency response values of the system were obtained with the harmonic solution. The effect of parameters such as the shaft length-diameter and stiffness coefficient, damping coefficient of the bearing in the numerical method for coupled longitudinal-lateral vibrations were also examined. Validated numerical results by the experimental ones show that the code and the thesis offer suitable solutions for the safety performance of any power transmission system about significant problems by the multiple coupled vibrations.

GEMİ SEVK SİSTEMLERİNDE OLUŞAN TEKİL VE BİRLEŞİK EKSENEL, YANAL VE BURULMA TİTREŞİMLERİNİN İNCELENMESİ

ÖZET

Gemi sevk sistemi, gemilerin önemli bir parçası olarak görev yapar ve gemi operasyonunun güvenliği ve güvenilirliğinde önemli bir rol oynar. Gemilerin hareketi için, ana makina tarafından üretilen tork şaft sistemi yardımı ile pervaneye iletilir ayrıca şaft sistemi ana makina ve pervaneyi birbirine bağlar. Gemiler seyirleri sırasında dalga, rüzgar ve daha birçok kuvvet tarafından farklı şekillerde uyarılırlar ve tüm bu uyarımlar kuvvetin yönünde titreşim tepkisine yol açar. Şaft sisteminde burulma, boyuna ve enine modlarda ve bunların birleşik formlarında istenmeyen titreşim tepkileri gözlenir.Sonuç olarak titreşim tepkileri tek bir eksen yerine aynı anda farklı yönlerde meydana gelir. Ancak literatür incelendiğinde bu titreşim formlarını birbirinden ayrı olarak ele alınması sonucunda birleşik titreşim etkisi ile meydana gelebilecek zorlanmış titreşim frekans ve genliklerinin göz ardı edildiği ve gerçek ölçümlerle elde edilen sonuçlardan oldukça farklı sonuçlara varıldığı görülmüştür. Göz ardı edilen birleşik titreşim formları şaft sisteminde sadece şaftları değil, aynı zamanda temeli, yatakları ve gemi gövdesini de uyarır ve gürültü seviyesini artırmasıyla birlikte yapısal zararlar verir. Böylelikle, sistemin zayıf performansının yanı sıra şaft ve yataklar başta olmak üzere tüm şaft sistemi dayanıklılığını yitirme, kırılma ve tribolojik sorunlara ve arızalara yol açar. Sonuç olarak, geminin seyri sırasında güvenilirliği için birleşik titreşim modlarının incelenmesi elzemdir. Yaygın incelenen birleşik titreşim formları, birleşik burulma-boyuna titreşim, birleşik burulma-eksenel titreşim ve birleşik boyuna-eksenel titreşimdir. Birleşik titreşimin boyuna-yatay-dikey olarak 3 eksen ve burulma titreşiminin bütün olarak modellenmemesinin sebebi; sayısal olarak modellemede artan hata paylarıdır. Bunun sonucunda birleşik titreşim iki eksenin birbiri ile etkileşimi dikkate alınarak sayısal modellenir. Bu tez çalışmasında Wuhan Teknoloji Üniversite'sindeki deney imkanından yararlanarak; sevk sisteminin daha küçük bir modeli olan deney düzeneği için birleşik burulma-boyuna, burulma-aksenel ve boyuna-eksenel titreşimleri sayısal olarak modellenerek; farklı hız değerlerinde zamana bağlı yerdeğiştirme değerleri incelenerek deney sonuçları ile doğrulanmıştır.

Bu çalışmada, bir geminin pervane şaft sisteminin daha basit bir modeli olan deney düzeneği birleşik burulma-boyuna titreşimleri için bir kütle-yay sistemi ile modellenmiştir. Birleşik burulma-boyuna titreşimi için rijitlik katsayısı,sönümleme katsayısı ve dönme hızı ile ilişkili ve katsayıların değişimine yeterince elverişli bir sayısal metod önerilmiştir. Farklı genliklere sahip tork ve boyuna kuvvetler de dahil olmak üzere dış kuvvetler ve zorlama frekansları dikkate alınmıştır. Ek olarak, deney düzeneğinde pervane yer almaması sonucu; literatürde yer alan birleşik titreşim katsayısından yararlanılarak sayısal model oluşturulmuştur. Önerilen kütle-yay modelini doğrulamak için teorik çözüm elde edilmiştir. Dönme hızının ve yükleme koşulunun değişimine bağlı olarak doğal frekans ve maksimum genliğin değişimi sunulmuştur. Birleşik titreşim etkisi maximum yerdeğiştirme değerleri kıyaslanarak

incelenmiştir. Ayrıca birleşik titreşim etkisinin doğal frekansa etkisi sunulmuştur. Birleşik burulma-boyuna titreşimleri için sayısal yöntemde yer alan şaftın boyu, çapı, rijitlik katsayısı, sönümleme katsayısı gibi parametrelerin titreşime olan etkisi ayrıca incelenmiştir. Bunların yanısıra birleşik titreşim etkisi de incelenmiştir. Son olarak deney düzeneğinde meydana gelen birleşik burulma-boyuna titreşim genlikleri DNV tarafından müsade edilen maksimum değerler ile kıyaslanılmıştır.

Gemi sevk sisteminin birleşik burulma-eksenel titreşimleri pervanenin dönüşü, dişli gibi şafta takılı ekstra kütlelerin dönmesi, yataklara etki eden kuvvetler, dişlilerin birbirlerine kuvvet iletimi sonucu oluşan eksen kaçıklığından kaynaklanır. Şaftın yapısal özellikleri ve dönme işlemi sırasında meydana gelen dengesizlikler sonucunda kütle merkezi ile şaftın enine kesitinin merkezi arasında bir eksen kaçıklığı görülür. Şaftın hareketi her zaman gerçek çalışma şartlarında dışarıdan müdahale edilmediğinde yatay olarak eksen kaçıklığı ile sonuçlanır. Şaftın bu eksantrik etkisi, titreşim yanıtının daha karmaşık ve yoğun olmasına neden olur. Yatak ve şaftın yalnış hizalamasını azaltan titreşim kontrol tekniklerine ek olarak, araştırmalar esas olarak şaft titreşimlerinin tahminini destekleyen teorik ve pratik yöntemlere odaklanılmışlardır. Bu nedenle, pervane şaftının yatay ve dikey eksende titreşim yoğunluğunun en aza indirilmesi araştırmada büyük ilgi görmektedir. Yapılan çalışmalar incelendiğinde; çalışmalararın çoğunluğunun uçak-uzay mühendisliği alanında gerçekleştiği görülmüştür ve şaft sistemi enine- boyuna titreşimleri için Jefcott Rotor ile isimlendirilen kütlesiz bir şaftın orta noktasında yer alan m kütlesinde bir disk ile modellenmektedir. Bu çalışmalardan faydalanarak Jefcott Rotor modeli revize edilerek pervane-şaft sistemine uygulanmıştır. Böylelikle enine kesitin eksantrikliği, sönümleme katsayısı, rijitlik katsayısına bağlı ve uzunluk-çap oranı gibi etki faktörlerine bağlı nümerik bir model elde edilmiştir. Bu yöntem yukarıdaki etki faktörleri ile dinamik performansı tahmin edebilmekle beraber sayısal hesaplamalara uygundur. Önerilen sayısal modeli doğrulamak için farklı hız değerlerinde deney tekrarlanmış ve zamana bağlı yerdeğiştirme değerleri kıyaslanarak doğrulanmıştır. Önerilen modele dayanarak, enine kesitin eksantrikliği, sönümleme katsayısı, rijitlik katsayısı gibi katsayıların ve şaftın uzunluk-çap oranı gibi etki faktörlerinin değişiminin titreşime olan etkisi tartışılmıştır. Birleşik titreşim etkisi yaratan eksen kaçıklığı incelendiğinde ise, sayısal metod da kullanılan literatürden edinilen eksen kaçıklığı değerinin yeterli olmadığı ve her şaft sisteminde değişiklik göstereceği sonucuna varılmıştır. Bunun sonucunda yeni bir eksen kaçıklığı değeri önerilmiştir. Sonuç olarak, eksantrik katsayı değerinin doğru tanımlanmasının önemi görülmüştür.

Birleşik boyuna-enine titreşim pervanede meydana gelen eksenel kuvvetlerin sonucu olarak ortaya çıkar ve şaftın eksen kaçıklığına sebep olur. Birleşik burulma-boyuna titreşimleri için sistemin sayısal modeli oluşturulurken Enerji metodundan yararlanarak hareket denklemleri çıkarılmıştır. Sayısal modellemede denklemler kompleks olup kütle- yay modeline getirilirken matris formuna dönüştürmek ve birleşik titreşim katsayısına indirgemek oldukça zor olduğu için Ansys programı yardımı ile kütle-yay sistemi ile modellenerek sayısal olarak zamana bağlı hareket denklemleri çözülmüştür. Önerilen kütle-yay modelini doğrulamak için sonuçlar deney düzeneğinden elde edilen veri ile kıyaslanmıştır. Dönme hızının ve yükleme koşulunun değişimine bağlı olarak frekans tepkileri ve maksimum genliğin değişimi sunulmuştur. Birleşik boyuna-enine titreşimleri için sayısal metod da yer alan şaftın boyu, çapı, rijitlik katsayısı, sönümleme katsayısı gibi parametrelerin titreşime olan etkisi ayrıca incelenmiştir. Bu parametrelerin yanı sıra birleşik titreşim etkisi verilen şaftın ivme değerinin değişiminin titreşime etkisi ayrıca incelenmiştir.

Gerçekleştirilen üç farklı birleşik titreşim hesaplama ile; birleşik titreşim etkisi sistemin frekans tepkisi ve maksimum yer değiştirme değerleri incelenerek değerlendirilmiştir. Böylelikle birleşik titreşim etkisi göz ardı edildiğinde özellikle şaft da meydana gelen burulma açısı artışının da göz ardı edilerek yanlış sonuçlara varılabileceği ortaya konulmuştur. Bu çalışmada meydana gelen birleşik titreşim genlikleri DNV kuralları gereğince müsade edilen genliklerden oldukça düşük olduğu için titreşim sönümleyici bir öneride bulunulmamıştır.

1. INTRODUCTION

The main engine plays an important role in the reliability of safe cruising of a ship. For the movement of ships, the torque produced by the main engine is transmitted to the propeller via propulsion shaft system. Shaft is subjected to the harmonic forces and torques, as well as being stimulated in different ways by waves, winds and many other external forces during the course of the ship at the same time, and all these simulations lead to vibration response in the direction of the force. Unwanted vibration responses are observed in torsional, longitudinal, and lateral modes and their coupled forms in the shaft system. As a result, vibration responses occur in different directions at the same time instead of on a single axis. However, when the literature was examined, it was observed that excitation frequency and amplitudes that may occur with coupled vibration effect were ignored and these vibration forms are considered separately.

Ignoring the coupled vibration approach or pure uncoupled vibration The thesis aims to develop a comprehensive code simulating to analyze the behavior of coupled vibration characteristics on a typical marine propulsion chain consisting of main engine, shaft, and bearings, and propeller, as well as capable of model the uncoupled or singular vibration shapes and modes. For this purpose, the displacements about both coupled and uncoupled vibration were compared and the excitation frequency values were examined. Besides, the weights of the essential factors such as the ratio of the shaft length to diameter, damping, stiffness and the coupled vibration coefficient were also investigated numerically.

1.1 Purpose of Thesis

The thesis aims to develop a comprehensive code simulating to analyze the behavior of coupled vibration characteristics on a typical marine propulsion chain consisting of main engine, shaft and bearings, and propeller, as well as capable to model the uncoupled or singular vibration shapes and modes. For this purpose, the displacements about both coupled and uncoupled vibration were compared and the excitation frequency values were examined. Besides, the weights of the essential factors such as

the ratio of the shaft length to diameter, damping, stiffness and the coupled vibration coefficient were also investigated numerically.

1.2 Methodology

In order to investigate the coupled vibration types such as torsional-longitudinal, torsional-lateral and longitudinal-lateral for the experimental setup, the system was modeled as Euler-Bernoulli beam by considering the propeller side of the shaft can move and the main engine side of the shaft being fixed. Experimental setup for coupled torsional-longitudinal vibrations was modeled numerically as the mass-spring system, and the coupled vibration relationship was established with the specific coefficient well defined in the literature on coupled vibration since the experimental setup does not contain any propeller. For the coupled torsional-lateral vibration, a modified version of the Jeffcott Rotor model was used and the shafts were modeled whole instead of taking them as separate masses, and the numerical model was established with taking into account of the lateral displacement of system. For coupled longitudinal-lateral vibration, the equation of motion was derived according to the Energy method, but the mass-spring model of the system was created with the help of an Ansys-APDL program because it is quite difficult to simplify the equation of motion and bring it into matrix form. For all three numerical models; in order to verify numerical models, the experiment was carried out at different rotation speeds and different installations. Response amplitudes due to harmonic loads and different conditions are presented to find out the coupled vibration effect.

1.3 Literature Review

Single and coupled vibration induce fracture, fatigue, and tribological problems on the overall propeller shaft system. To avoid these structural problems, studies have been carried out especially on torsional vibration, yet studies on coupled longitudinal-torsional vibrations and coupled torsional-lateral vibrations are not sufficient to extend the typical vibration behavior. The majority of the studies about the equation of motion of the propulsion shaft system deal with the single-axis vibrations by ignoring the coupled vibrations, which causes the results obtained by the actual measurements to be quite different (Dai et al., 1989; Huang et al., 2019). Torsional vibration is the foremost dangerous vibration type for the crankshaft, the bearings, and the shaft lining,

and mainly studied in single-axis. (Brydum and Jakobsen, 1987). Murawski (2012) says that torsional vibration formulates for a system by torque output of the engine, propeller characteristics, elasticity, and damping of propeller shaft system. Huang and Horng (1999) use the transfer matrix method for torsional vibration analysis of damped systems. Wu et al. (1995) studied free and forced torsional vibration problems for the multi-degree of freedom system by using the transfer matrix method. Yang et al. (2011) used the transfer matrix method for creating an equation of motion of the shaft system for torsional vibration. Most recently, the finite element method was frequently applied for torsional vibration analysis (Senjanovića et al., 2019, Huang et al, 2016, Murawski and Charchalis, 2014). In addition, some of these studies on torsional vibration were evaluated by experiments (Xiang et al., 2012).

In the literature, longitudinal vibration has the second highest number of studies after torsional vibration for propulsion shaft system. The unbalanced propeller thrust causes the longitudinal vibration of the propulsion shafting. Longitudinal vibration issues can harm the propulsion system by increasing the wear of thrust bearings and flexible couplings due to increased relative motion between fixed and rotating parts. Zhang et al. (2014) declare that the longitudinal vibration occurs on the shaft system and the wear of the thrust bearings results from the motion between fixed bearings and rotating shafts when the propeller thrust is unsteady. Gan-bo and Yao (2012) used the reduced-order method but Zhang et al. (2014) preferred to use the finite element method to describe the dynamic behavior of marine propulsion shaft system and reduce longitudinal vibration. An experimental study shows that longitudinal vibrations can be only arose from the propeller and thrust bearing forces according to Pan et al. (2002). Chen et al. (2017) investigated longitudinal vibration by using the modal superposition method and analyzed the system with different dynamic parameters. Li et al. (2016) studied longitudinal vibration on the coupled system to isolate vibration. Zou et al. (2019) considered axial exciting force and vibration and their transmission mechanism to the hull via the optimal design of the propeller-shaft system.

The lateral vibration type is studied rarely than the first two types given above since it is easier to control with bearings. Warikoo and Haddara (1992) state that the lateral vibration is caused by imbalances of the rotating parts of the shaft system and because of the bending loads on the propeller in an unstable flow. When the studies on lateral

vibration are examined, it is observed that instead of examining the lateral vibration in a single axis, it is generally studied with coupled form. Nevertheless, the number of studies in lateral vibration of the shaft system field is limited in the shipbuilding industry and mainly has been carried out in the aero-engine field. The reliability of the shaft system is an important safety concern and the lateral-torsional vibration is another important topic and it is caused by unbalanced loads in the shaft system and results in rotor instability and damage on the bearings (Rao et al. , 2003; Murawski, 2005; Shi et al. 2010). As a result of this, the topic of coupled vibration has attracted a lot of attention lately in the shipbuilding industry (Chahr-Eddine and Yassine, 2014; Huang et al., 2017; Murawski, 2004; Qu et al., 2017; Yang et al., 2014; Zhang et al., 2014). Mohiuddin et al. (1999) and Al-Bedoor (2001) put forward the dynamic model of a rotor-bearing system by using the Lagrangian dynamics and their dynamic model includes gyroscopic effects as well as the inertia coupling between bending and twisting deformations. Han et al. (2017) and Hong et al. (2020) studied a rotor system with a dynamic model that the rotor disk is placed in the middle of a massless elastic shaft and the equation of motion is obtained by the Lagrangian dynamics. Han et al. (2019) derived the equation of motion similar to the prior study, assuming that the diesel engine drive system could be approached as a simple rotor model such as a Jeffcott rotor. Gayen (2017) presented a shaft with multiple cracks to study the transverse vibration effect on rotor-bearing systems with the finite element method. Moreover, Han and Lee (2019) and Yuan et al. (2007) have numerically modeled the vibration occurring as a result of the lateral and torsional forces by comparing the shaft system to the Jeffcott rotor system at three degrees of freedom. Besides, Das et al. (2011) have modeled a rotor shaft which subjected to external coupled lateral and torsional forces with a disk that is away from the midpoint of the shaft. Vlase et al. (2017) studied coupled lateral-torsional vibrations by calculating the eigenvalues and eigenvectors of the shaft system. Most recently, Huang et al. (2019) considered that the propeller shaft is equivalent to a cantilever beam and the non-linear model is numerically solved using high order Runga-Kutta method, which also is verified by experiments performed at different rotational speeds. As a result, it is seen that the Jeffcott rotor, the disc located at the midpoint of the massless shaft, is a common model for coupled transverse-torsional vibration.

There are also studies that deal with coupled vibration in addition to studies that consider longitudinal and torsional vibrations separately. The coupled torsional-longitudinal vibration is by far the most researched form of coupled vibration. The coupled torsional and longitudinal vibrations of propeller shaft systems are first investigated by Parsons (1983). His subsequent studies consider the coupling through added mass and hydrodynamic damping coefficients due to the propeller. Mao et al. (2016) used 2-D unsteady thin foil theory to predict the added mass and damping matrices of skewed propellers. Jang et al. (2004) created the equation of the motion with the finite element method and the coupling effect is included with the stiffness matrix by using the coefficient method for the coupled torsional-longitudinal vibrations. Firoizu et al. (2021) used the finite element method to define the equation of the motion of the shaft system and they mainly derived compatible equations for different blade characteristics. Huang et al. (2017) studied the problem both experimentally and numerically, using the lumped mass method. Unlike the studies which considered the coupling through added mass and hydrodynamic damping coefficients, they examined the response of the system by considering the coupling through a stiffness matrix by giving specific values to this coefficient.

The least common coupled vibration form in the literature is coupled longitudinal-lateral vibration. The reason for this is that the numerical model is quite complex. When the studies on coupled longitudinal-lateral vibration are examined, the governing equations which describe coupled longitudinal-lateral vibration of using Euler-Bernoulli theory are commonly used and solution for equations with boundary conditions are given with Arafat et. al. (1998). Morozov and Tovstik (2013) mentioned that coupled lateral-longitudinal vibrations of the Timoshenko beam which one side is fixed the other side free with lateral boundary conditions. Han and Benaroya (2000a) firstly searched free coupled longitudinal-lateral vibrations under only lateral forces and the study is expanded to forced vibration considering also longitudinal forces (Han and Benaroya (2000b)). Lenci and Rega (2016) are investigated the free Timoshenko beam analytically by using the asymptotic development method to see the interaction between axial-transverse vibration. Ghayesh et. al. (2012a) studied coupled longitudinal and lateral motions which were discretized via the Galerkin technique. Ghayesh et. al. (2012b) also investigated nonlinear coupled longitudinal-lateral vibrations of the beam which is supported by an intermediate spring and subjected to

harmonic external forces. Additionally; Ghayesh et. al. (2013) numerically modeled axially moving Timoshenko beam using Hamilton's principle considering stress-strain relations and equation of motion simplified to coupled longitudinal-lateral vibration via the Galerkin method. Ghayesh et. al. (2012c) studied the coupled longitudinal–lateral vibration of the axially accelerating beam and the axial speed is assumed as coupling effect to give interaction between axis. A coupled longitudinal-lateral model of marine propulsion is developed by Hamilton’s principle and discretized by the Galerkin method by Zou et al. (2015). Huang et al. (2015) used the Finite element method for coupled longitudinal-lateral vibration of complex ship structures. Huang et al. (2016) modeled shaft system with Euler-Bernoulli beam and equation of motion is obtained with Energy method and experimental analysis included to prove the validity of the numerical method. Chen et al. (2020) studied coupled longitudinal and transverse vibration characteristics of a submarine propeller-shaft-hull system and modeled using the finite element method. Kang et al. (2019) used the Timoshenko beam theory to analytically model considering longitudinal and transverse responses of the random vibration characteristics of the propeller-shaft system. Also, some experimental studies were conducted to see coupled longitudinal-transverse vibration. Sah et al. (2016) conduct experiments to see how a longitudinal hammer impact can cause transverse vibrations in a beam.

2. COUPLED TORSIONAL AND LONGITUDINAL VIBRATIONS

The propulsion shaft system can be modelled as a cantilever beam with assuming the propeller at free end and the main engine at the other but fixed end. The system will behave as a beam with a mass payload, where its mass center does not need be coincident with the centerline of the beam.

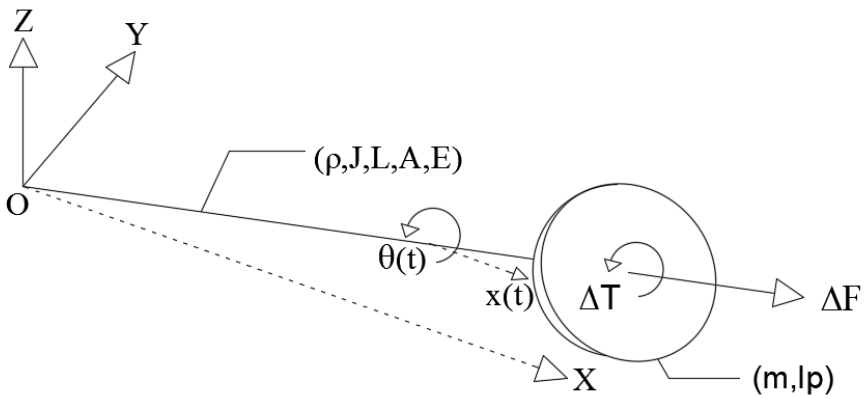

Figure 2.1 : Schematic of the beam with a mass payload (Hassan and Mehrdaad, 2006).

The shaft is excited by a harmonic torque forcing it a torsional stress, but during the rotational movement, longitudinal vibration also occurs whenever any shrinkage or eccentricity are along the shaft. So the torsional angle affect the longitudinal deformation positively and negatively and two axes in an interaction simultaneously (Song et al., 1989; Du et al., 1992).

The equivalent coupled longitudinal force ΔF caused by torsional angle and equivalent coupled torsional torque ΔT can be described as given:

$$\Delta F = k_{xt}\theta(t) \qquad \Delta T = k_{tx}x(t) \tag{2.1}$$

where $\theta(t)$ is the rotational angle, k_{xt} is the coupled longitudinal-torsional stiffness, and $x(t)$ is the longitudinal deformation, k_{tx} is the coupled torsional-longitudinal stiffness. Equivalent force ΔF and torque ΔT are used to express excitation of the system. Forcing torque and axial load are $T\sin(\omega_t t)$ and $F\sin(\omega_t t)$, respectively.

Hence, the numerical formula of coupled torsional and longitudinal vibrations are expressed as (Du et al., 1992);

$$\begin{aligned} J\ddot{\theta} + d_t\dot{\theta} + k_t\theta - k_{tx}x &= T\sin(\omega_t t) \\ m\ddot{x} + d_x\dot{x} + k_x x - k_{xt}\theta &= F\sin(\omega_t t) \end{aligned} \tag{2.2}$$

where k_{tx} and k_{xt} are the coupling stiffness which are defined as $k_{tx} = \delta k_t$, $k_{xt} = \delta k_x$ where δ is the coupling stiffness coefficient which determines the longitudinal deformation induced by torsional angle $\theta(t)$. The δ is defined as (Parson, 1983; Huang, 2017);

$$\delta = m_c^{\ 2} / mJ \tag{2.3}$$

The value of δ has only been investigated by Parsons based on a series of experiments. It reports that the coefficient δ is less than 0.10 for propeller shafts values while 0.008, 0.02, and 0.06 were also examined by Li and Sun (2003). However, detailed explanation on the δ selection has not been provided. Huang et all; δ=0.02 was considered as an initial value in the numerical analysis. Therefore, δ value is taken as 0.02 for coupled torsional-longitudinal vibration (Parson, 1983; Huang, 2017).

2.1 Numerical Model for the Coupled Torsional and Longitudinal Vibrations

The structural characteristics of the propulsion system which is a combination of multiple shafts are considered in this section to investigate the coupled torsional-longitudinal vibration of the system in detail with utilizing the lump-mass method which is also widely used in engineering research. Main principle of this approximation is to concentrate the distribution of each structural element into a specific location according to the predefined rules in literature so that the overall quality of the structure is discrete into a series of quality points, and the rest are considered to have no quality but have elastic properties.

Inertial force and interaction of the mass points defines the degree of freedom of the equation of motion of the discrete system in terms of the displacement of these particles, and so help to simplify the infinite degree of freedom to a finite degree of freedom system. The model is shown in Figure 2.2. Where m_j and x_j for the mass and displacement of each mass point, k_j and d_j for the stiffness and damping values of the connection mass point.

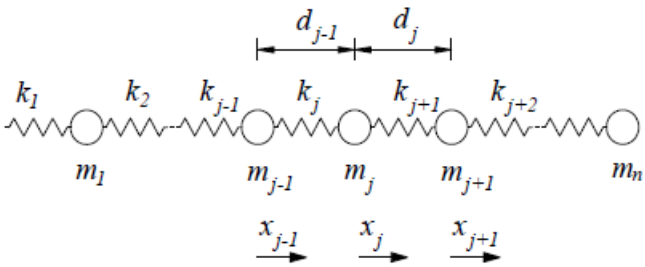

Figure 2.2 : Schematic of lumped-mass model of the shaft (Huang, 2017).

The coupled motion of a vibrating shaft system is modeled with lumped mass and given by Eq. 2.2 ;where $\boldsymbol{J}$ is the matrix of moment of inertia, $\boldsymbol{M}$ is the matrix of mass. $\boldsymbol{D_T}$ and $\boldsymbol{D_X}$ are the matrix of torsional and longitudinal damping. $\boldsymbol{K_T}$ and $\boldsymbol{K_X}$ are the matrix of torsional and longitudinal stiffness. $\boldsymbol{K_{TX}}$ and $\boldsymbol{K_{XT}}$ are the coupled torsional and coupled longitudinal stiffness matrices.

According to the shaft torsional-longitudinal coupled vibration which is given with Eq. 2.2; combined with the above-mentioned lump-mass method and the actual connection of the shaft system, the shaft system coupled vibration model can be obtained after discrete as (Kouroussis and Verlinden, 2015);

$$\begin{bmatrix} \boldsymbol{M} & 0 \\ 0 & \boldsymbol{J} \end{bmatrix}\begin{bmatrix} \ddot{\boldsymbol{x}} \\ \ddot{\boldsymbol{\theta}} \end{bmatrix}+\begin{bmatrix} \boldsymbol{D}_x & 0 \\ 0 & \boldsymbol{D}_t \end{bmatrix}\begin{bmatrix} \dot{\boldsymbol{x}} \\ \dot{\boldsymbol{\theta}} \end{bmatrix}+\begin{bmatrix} \boldsymbol{K}_x & \boldsymbol{-K}_{xt} \\ \boldsymbol{-K}_{tx} & \boldsymbol{K}_t \end{bmatrix}\begin{bmatrix} \boldsymbol{x} \\ \boldsymbol{\theta} \end{bmatrix}=\begin{bmatrix} \boldsymbol{F} \\ \boldsymbol{T} \end{bmatrix} \tag{2.4}$$

The test platform used in this chapter is a comprehensive performance test bench for the ship shaft system which promotes 2 intermediate shaft and a tail shaft composition, defining the above centralized quality model (j = 4). As can be seen from the installation diagram, given in Fig. 2.3, it consists of 4 different shaft parts.

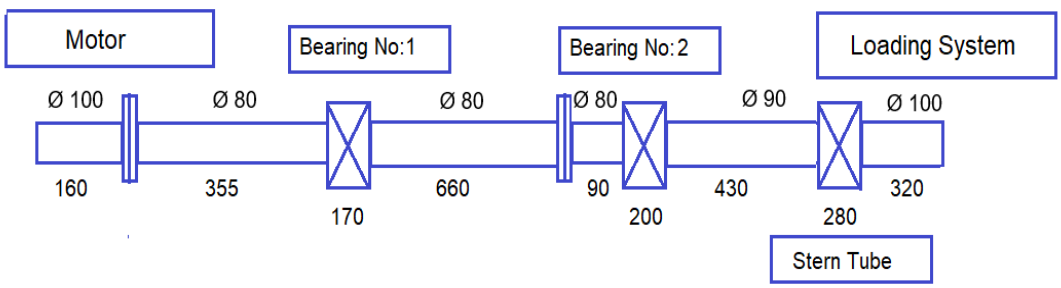

Figure 2.3 : Details of the shaft system.

Therefore, the system of torsional mass matrix $\boldsymbol{M}$ and inertia matrix $\boldsymbol{J}$ can be expressed as follows:

$$\boldsymbol{M} = \begin{bmatrix} m_1 & 0 & 0 & 0 \\ 0 & m_2 & 0 & 0 \\ 0 & 0 & m_3 & 0 \\ 0 & 0 & 0 & m_4 \end{bmatrix}, \qquad \boldsymbol{J} = \begin{bmatrix} J_1 & 0 & 0 & 0 \\ 0 & J_2 & 0 & 0 \\ 0 & 0 & J_3 & 0 \\ 0 & 0 & 0 & J_4 \end{bmatrix}, \tag{2.5}$$

the torsional damping and longitudinal damping matrices are defined as

$$\boldsymbol{D_x} = \begin{bmatrix} d_{x_1} & -d_{x_1} & 0 & 0 \\ -d_{x_1} & d_{x_1}+d_{x_2} & -d_{x_2} & 0 \\ 0 & -d_{x_2} & d_{x_2}+d_{x_3} & -d_{x_3} \\ 0 & 0 & -d_{x_3} & d_{x_3}+d_{x_4} \end{bmatrix}, \tag{2.6 a}$$

$$\boldsymbol{D_t} = \begin{bmatrix} d_{t_1} & -d_{t_1} & 0 & 0 \\ -d_{t_1} & d_{t_1}+d_{t_2} & -d_{t_2} & 0 \\ 0 & -d_{t_2} & d_{t_2}+d_{t_3} & -d_{t_3} \\ 0 & 0 & -d_{t_3} & d_{t_3}+d_{t_4} \end{bmatrix}, \tag{2.6 b}$$

Where d_{t_j} and d_{x_j} (j=1, 2 ,3 or 4) are the torsional and longitudinal damping coefficients for each part of shaft, which can be defined as Eq. 2.7 (Li and Sun, 2003);

$$\begin{aligned} d_{t_j} &= 0.08 J_j \omega_j \\ d_{x_j} &= 0.05 m_j \omega_j \end{aligned} \tag{2.7}$$

where m_j is the mass and J_j is the moment of inertia of each part of shaft, ω_j is the rotational speed. Similarly, the matrix of torsional stiffness $\boldsymbol{K_t}$ and longitudinal stiffness $\boldsymbol{K_x}$ are defined as Eq. 2.8.

$$\boldsymbol{K_x} = \begin{bmatrix} k_{x_1} & -k_{x_1} & 0 & 0 \\ -k_{x_1} & k_{x_1}+k_{x_2} & -k_{x_2} & 0 \\ 0 & -k_{x_2} & k_{x_2}+k_{x_3} & -k_{x_3} \\ 0 & 0 & -k_{x_3} & k_{x_3}+k_{x_4} \end{bmatrix}, \tag{2.8 a}$$

$$\boldsymbol{K_t} = \begin{bmatrix} k_{t_1} & -k_{t_1} & 0 & 0 \\ -k_{t_1} & k_{t_1}+k_{t_2} & -k_{t_2} & 0 \\ 0 & -k_{t_2} & k_{t_2}+k_{t_3} & -k_{t_3} \\ 0 & 0 & -k_{t_3} & k_{t_3}+k_{t_4} \end{bmatrix}, \tag{2.8 b}$$

where k_{t_j} and k_{x_j} (j=1, 2,3 or 4) are the torsional and longitudinal stiffness of each part of shaft. For the cylindrical section of the shaft, the torsional stiffness k_{tj} and longitudinal stiffness k_{xj} can be expressed with Eq. 2.9;

$$\begin{aligned} k_{t_j} &= GJ_j / L_j \\ k_{x_j} &= EA_j / L_j \end{aligned} \tag{2.9}$$

The matrix of coupled torsional $\boldsymbol{K_{TX}}$ and longitudinal stiffness $\boldsymbol{K_{XT}}$ can be expressed with Eq.2.10:

$$\begin{aligned} \boldsymbol{K_{TX}} &= \delta \boldsymbol{K_T} \\ \boldsymbol{K_{XT}} &= \delta \boldsymbol{K_X} \end{aligned} \tag{2.10}$$

The value of δ has only been investigated in Parsons (1983) based on a series of experiments. However, detailed explanation on the δ selection has not been provided. Huang et al. (2017) considered $\delta = 0.02$ in the numerical analysis. Therefore in this study, the coupled vibration coefficient was taken as 0.02 (Parson, 1983; Huang et al., 2017).

The matrix of torsional angle $\boldsymbol{\theta}$ and longitudinal deformation $\boldsymbol{x}$ are given with Eq. 2.11:

$$\begin{aligned} \boldsymbol{\theta} &= \begin{bmatrix} \theta_1 & \theta_2 & \theta_3 & \theta_4 \end{bmatrix}^T \\ \boldsymbol{x} &= \begin{bmatrix} x_1 & x_2 & x_3 & x_4 \end{bmatrix}^T \end{aligned} \tag{2.11}$$

where θ_j is the torsional angle and x_j is the longitudinal deformation of each part of shaft (j=1, 2, 3 or 4).

2.2 Experimental Setup

The propulsion shaft system is one of the main sources of ship vibrations. This experiment uses a small-scale shafting test rig to study the influence of coupled

vibrations on shaft system. The results are compared with simulation calculations to verify the reliability of the model.

This experiment is mainly to measure the torsional vibration, longitudinal vibration, lateral vibration and power flow of the shafting under different working conditions. The different working conditions mainly include the rotation speed, different external forces, and the direction and size of the deformation.

The diagram of shaft experimental system which consists of propeller shafts driven by a motor, a thrust with support bearings, foundation and a base is shown in Fig. 2.4

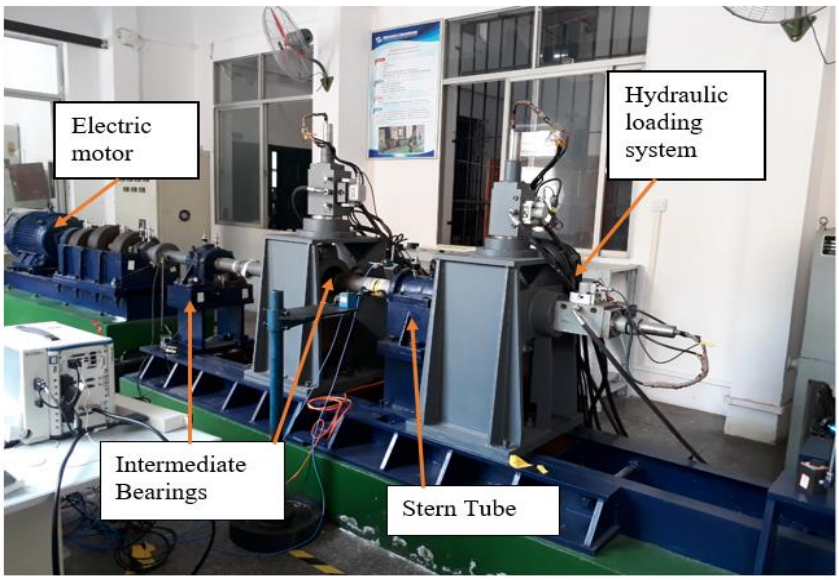

Figure 2.4 : Propulsion shaft system test plan.

The base was mounted on the foundation, with the propulsion shafts and bearings fixed on it. The propulsion shaft system has two intermediate shafts and a tail shaft, with a hydraulic couplings connecting each two shafts. The two intermediate shafts were supported by an intermediate bearing, while the tail shaft was supported by a stern bearing. The dimensions are shown in Table 2.1 with Young's modulus $E = 206\ GPa$, shear modulus $G = 77\ GPa$ and density $\rho = 7850\ kg/m^3$.

Table 2.1: Geometrical properties of the shaft segments.

Shaft No.	**1**	**2**	**3**	**4**
Length (m)	0.6	0.935	0.67	0.46
Diameters (m)	0.08	0.08	0.09	0.1

Fig. 2.5 shows measurement points of different sensors and they are converted into corresponding digital signals and stored by the system.

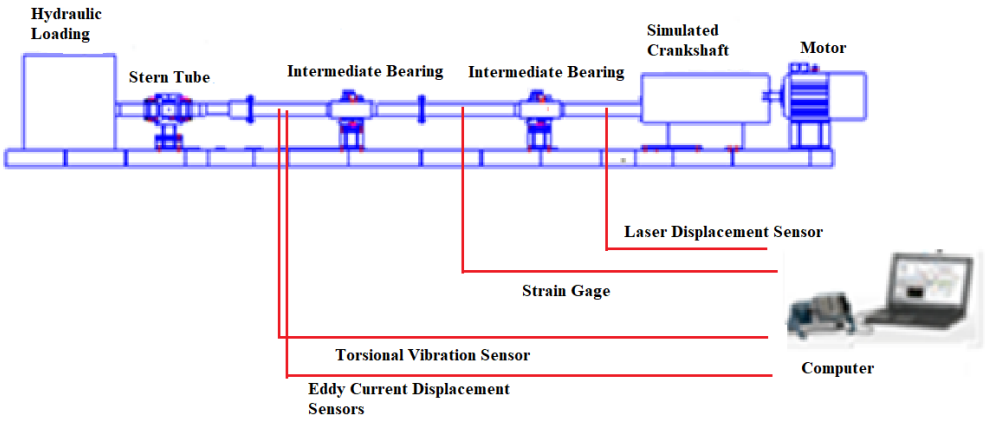

Figure 2.5 : Vibration measurement points layout.

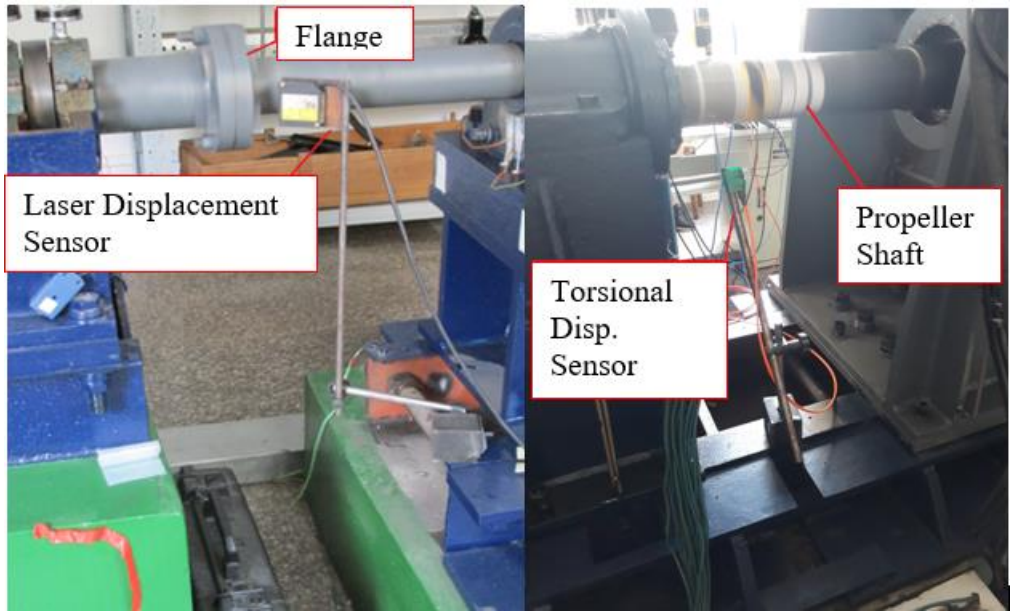

Figure 2.6 : Longitudinal and torsional vibration measurement points layout.

During the torsional vibration test, the laser torsional vibration meter (B&K MM0071 sensor and 2523 laser) is used to measure the torsional vibration signal of the tail shaft and check the shaft speed as given in Figure 2.6. The laser's measurement frequency range is 0.5 to 3000 Hz, and its sensitivity is 100 mV/g. Figure 2.6 also shows the flange surface of the longitudinal vibration selected by the laser displacement sensor (OPTEX CD33) which takes the longitudinal vibration signal corresponding to the position of the shaft system, and test the flange at the intermediate shaft as the

measuring point. Repeat accuracy is also 2 μm*, and high-accuracy displacement measurement is supported. The sensor position is fixed to reduce the test error caused by its vibration.

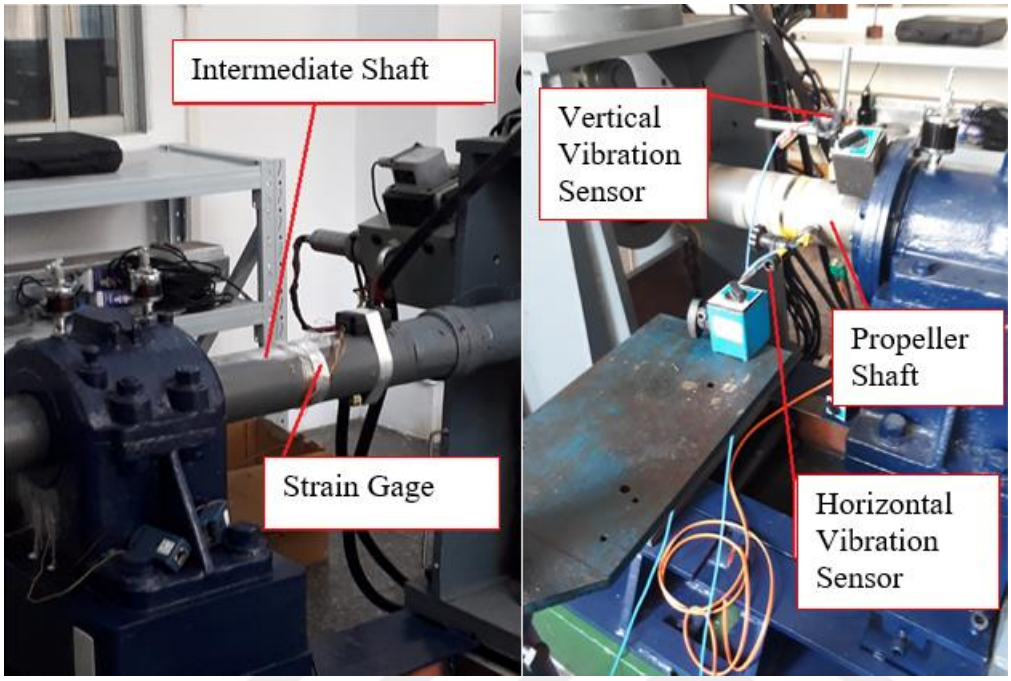

Figure 2.7 : Vibration measurement points layout.

Figure 2.7 shows the strain gage which is used for the measure of torque occured at intermediate shaft and the measurement of the point at tail shaft by arranging the eddy current sensors (ZA- 210803) in the vertical and horizontal vibrations. The sensor's standart sensitivity is 3.33 V mm^{-1} with a sensitivity error of 0.5%. In this case, the test selects the two positions of the tail shaft as the measuring points for testing.

Figure 2.8 : The signal acquisition and analysis system.

Figure 2.8 shows the signal acquisition and analysis system (type: PXIe-6358 and 16-Bit, 1.25 MS/s/ch). During the above-mentioned torsional, longitudinal and lateral vibration test, the optical and electrical signals obtained by different sensors are converted into corresponding digital signals and stored by the system. Different types of vibration signals are recorded in the shafting, and the test data of each group of working conditions are recorded separately, and finally the results of different vibration forms under different working conditions are obtained.

2.3 Application and Discussion

The vibration response of the structure mainly describes the dynamic characteristics of the system and has an important influence on the control method and operational reliability of the system. Dynamic applications including harmonic analysis and transient analysis can not only determine the natural frequency of the system to reduce or avoid resonance, but also calculate the law of displacement of the system in the time domain. Therefore, this chapter is based on the above-mentioned lump-mass method to analyze the frequency responses and transient amplitude of the torsional-longitudinal coupled vibration of the ship shafting.

The experimental setup allowed the propulsion shaft to rotate at various speeds. The maximum rotational speed was 190 rpm. The experiment system is so arranged that the shaft speed varies 100 to 190 rpm with an increase of 30 rpm. The frequency response and ultimate amplitude of the coupled vibrations were measured at the above mentioned four rotational speeds. Only the axial and lateral loading system is available in the test apparatus but the torsional stress could not be applied. The longitudinal stresses were defined as 0.6, 0.9, 1.2 and 1.5 mm for loading system while the frequency of the excitations is chosen as 2 Hz with increasing revolution. Table 2.2 shows the axial force and torque that correspond to these loading values for each rotational speed.

Table 2.2: Loadings for each rotational speed.

Rotational speed (rpm)	**100**	**130**	**160**	**190**
Displacement (mm)	0.6	0.9	1.2	1.5
Axial force (kN)	85.904	87.129	88.359	89.586
Torque (Nm)	0.055	0.125	0.275	0.325

The loading system only allows loading longitudinal and lateral external forces. As a result, the torque is measured as a response under external forces. It is seen in Fig. 2.9 that maximum longitudinal displacement value is 2.45×10^{-5} m for numeric method, 2.78×10^{-5} m for the experiment, and with Fig. 2.11 maximum torsional angle value is 5.23×10^{-7} rad for the experiment while 5.23×10^{-7} rad for the numeric method. As might be expected, test results are found to be higher than the numerical predictions owing to the imperfection of theoretical models but the margin of error is low and numerical method is very compatible with experiment results.

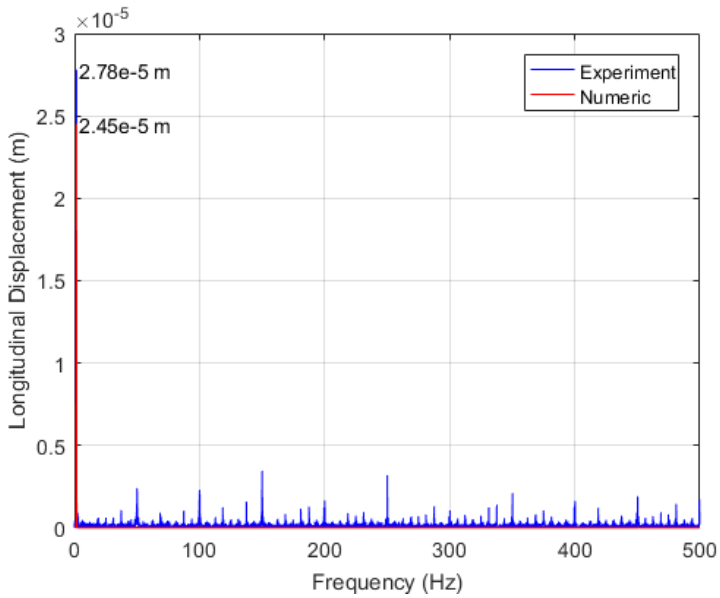

Figure 2.9 : Experimental and numerical coupled longitudinal vibration results.

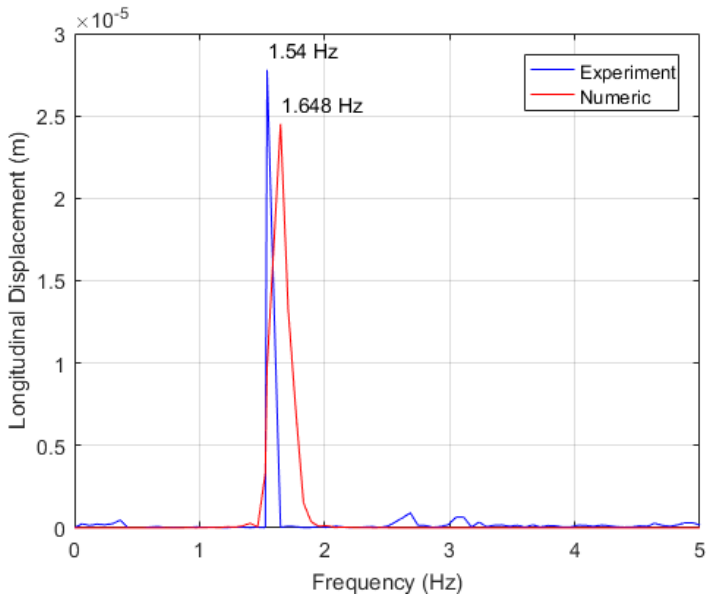

Figure 2.10 : Experimental and numerical coupled longitudinal vibration results.

In order to see the frequency values more clearly, the displacement and frequency values are given for Fig. 2.10 and Fig. 2.12 for the first 5 Hz. Looking at Fig. 2.10 and Fig. 2.12 for longitudinal and torsional vibration, it is seen that the excitation frequency for the numeric model occurs in the excitation frequency corresponding to 100 rpm and takes the value of 1.66, while the experiment data shows that it is at 1.54 Hz. It was observed that the numeric model yielded a higher value compared to the experiment with a low margin of error for the excitation frequency.

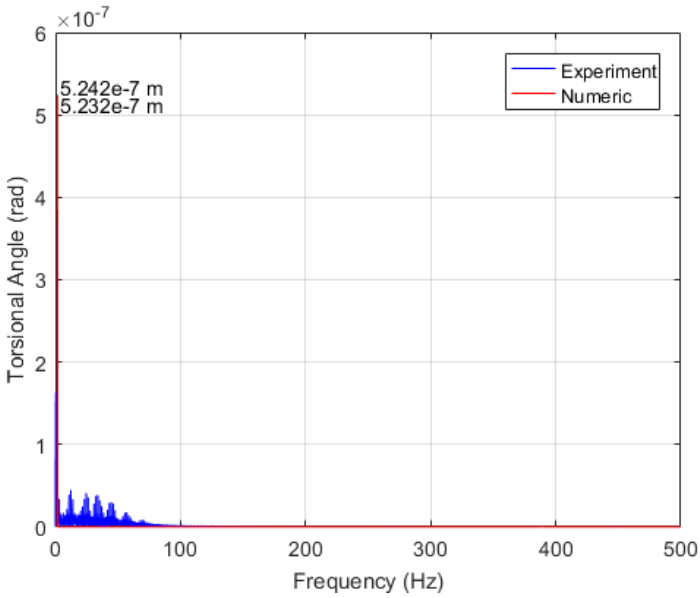

Figure 2.11 : Experimental and numerical coupled torsional vibration results.

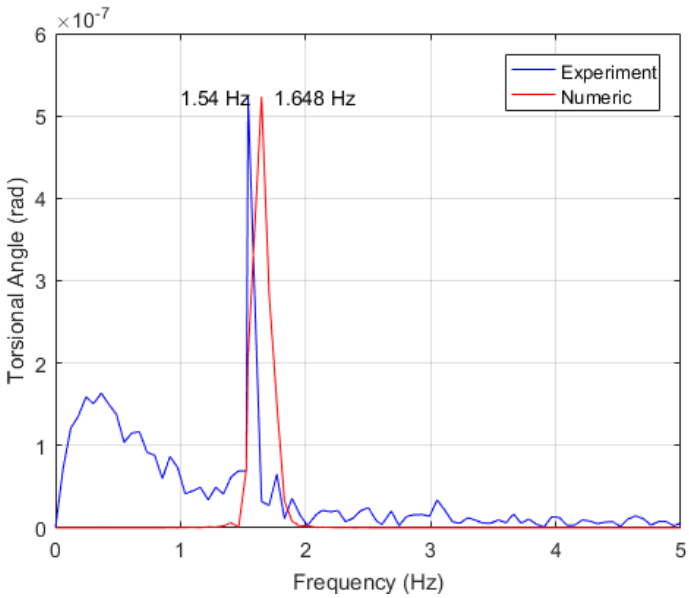

Figure 2.12 : Experimental and numerical coupled torsional vibration results.

After the validity of the numeric method was proved as explained above, the results were obtained for the coupled and the uncoupled vibration and shown in Fig. 2.13 and 2.14. The coupled and uncoupled vibration amplitudes for longitudinal vibration, are shown in Figure 2.13, are 2.45×10^{-5} m. With Figure 2.14, the coupled and uncoupled vibration amplitudes for torsional vibration are 5.23×10^{-7} rad and 3.35×10^{-8} rad, according to the order. For longitudinal vibration, the effect of coupled vibration is too low to be seen in the chart, but it is seen that the effect is more dominant at torsional vibration. As a result; it is proved that torsional and longitudinal vibration interact with each other during the movement of the shaft.

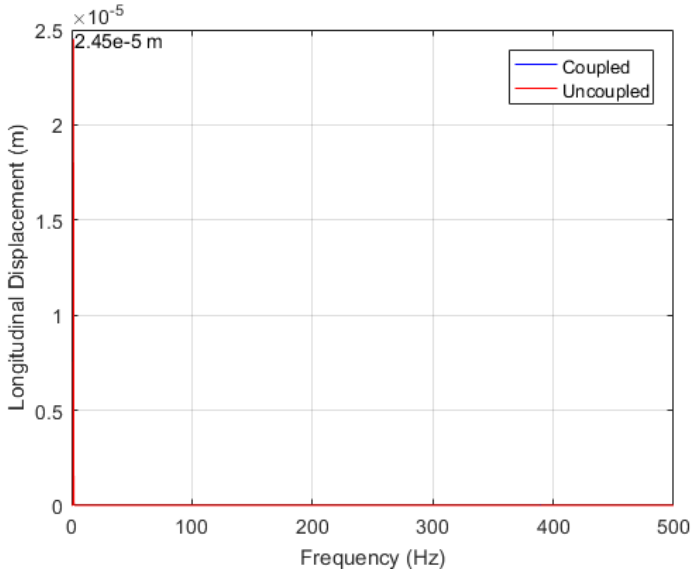

Figure 2.13 : Longitudinal displacement for coupled and uncoupled form.

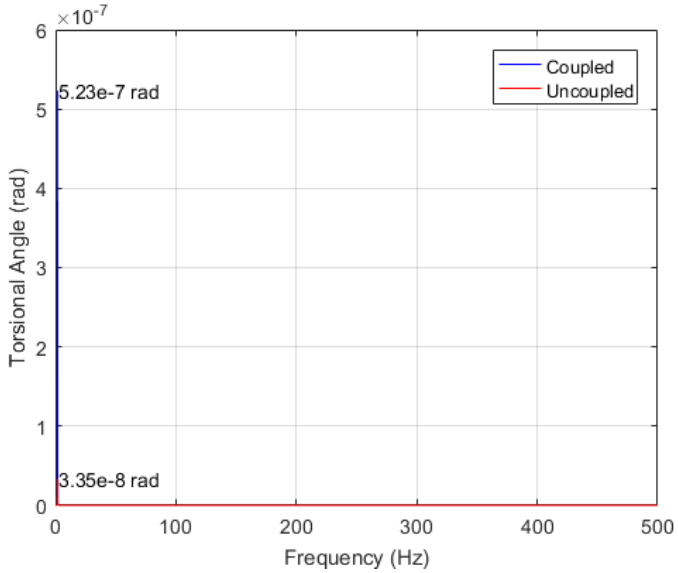

Figure 2.14 : Torsional angle for coupled and uncoupled form.

Tablo 2.3 shows the natural frequency values of the system for coupled and uncoupled vibration. It can be considered that the natural frequency of system remains unchanged at coupled or uncoupled form and at any rotational speeds. As a result natural frequencies are independent of the rotational speed and coupling effect.

Table 2.3: Natural frequencies predicted by the coupled and uncoupled form (Hz).

Coupled	Uncoupled
452	452
592	592
1266	1267
1513	1512
1867	1868
2275	2274
2386	2388
2808	2807

The first natural frequency of torsional vibration is 1867 Hz, the second one is 2275 Hz, the third one is 2386, and the fourth one is 2808, whereas the first natural frequency of longitudinal vibration is 452 Hz, 592 Hz, 1266 Hz, and 1513 Hz, respectively.

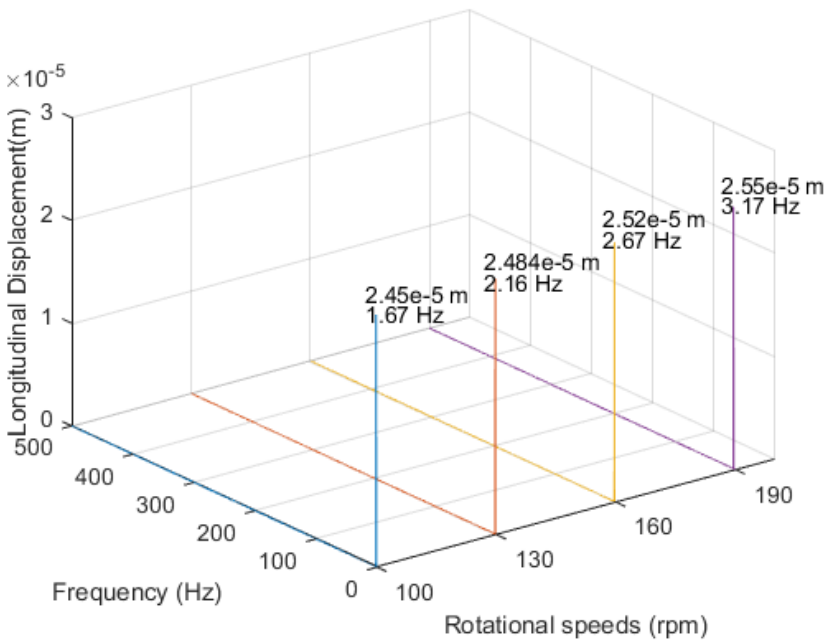

Figure 2.15 : Numerical method results for 100–190 rpm in the longitudinal direction.

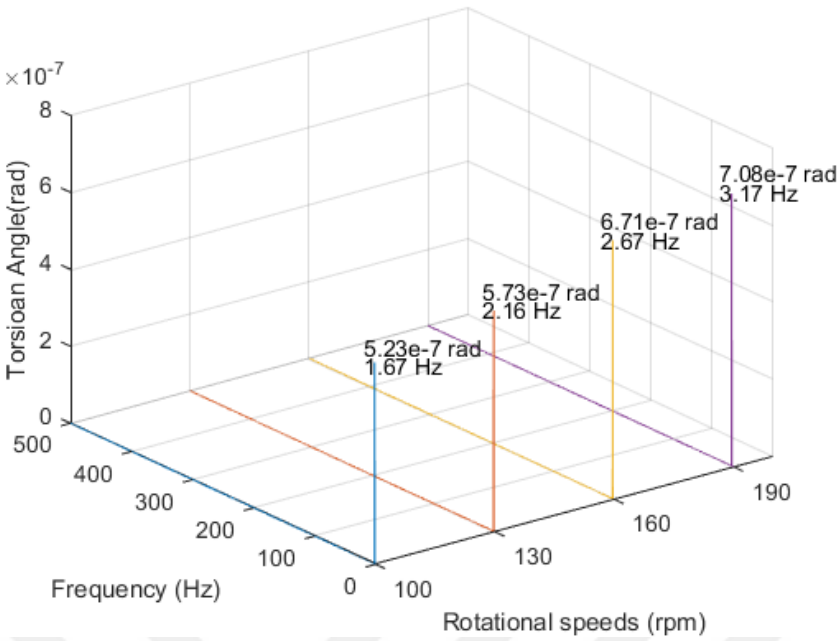

Figure 2.16 : Numerical method results for 100–190 rpm in the torsional direction.

In the analysis of the influence of the rotational speed on the coupled vibration in Figure 2.15,2.16 show the numerical results of the torsional-longitudinal coupled vibration harmonic response of the shaft system at a rotational speed of 100-190 rpm. It can be seen that when the shaft speed increases, the frequency response of torsional and longitudinal vibration changes very slightly. The specific data are: torsional direction 1.67 Hz, 2.16 Hz, 2.67 Hz to 3.17 Hz; longitudinal direction 1.67 Hz, 2.16 Hz, 2.67 Hz to 3.17 Hz. Besides, it can be found that the peak value at the driving frequency becomes larger as the rotation speed increases. Figure 2.17, 2.18 show the numerical results of the torsional-longitudinal coupled vibration transient response of the shaft system at a speed of 100-190 rpm. It can be seen that the transient amplitudes of torsion and longitudinal direction increase with the increase of speed.The specific data are: torsion direction 5.23×10^{-7} rad, 5.73×10^{-7} rad, 6.71×10^{-7} rad to 7.08×10^{-7} rad; longitudinal direction 2.45×10^{-5} m, 2.484×10^{-5} m, 2.52×10^{-5} m to 2.55×10^{-5} m.

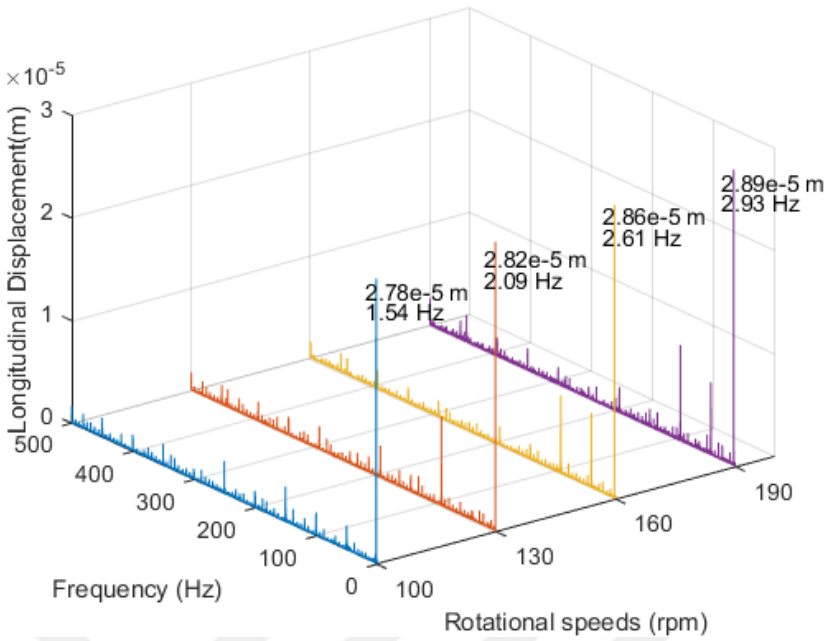

Figure 2.17 : Experiment results for 100–190 rpm in the longitudinal direction.

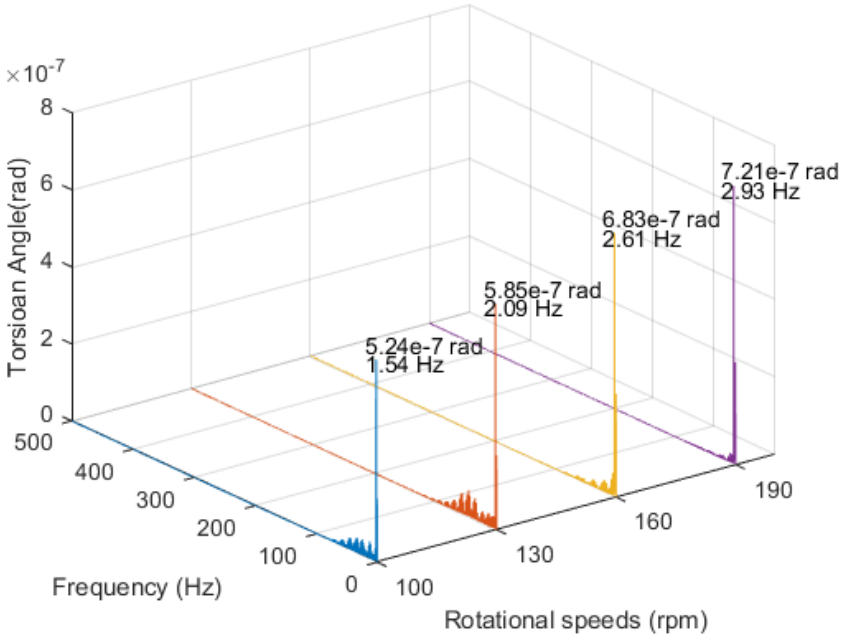

Figure 2.18 : Experiment results for 100–190 rpm in torsional direction.

In the actual measurement process of the test, the ship shafting will be affected by oil film damping, friction, main engine noise, and instrument accuracy, making the error rate high and the process repeated at different shaft speed to see validity of the experiment. These interference factors are not considered in the numerical model, so the errors in the measurement process are acceptable. In order to study the error

generated in the test process, the numerical solution of the vibration result and the test value are analyzed and compared, and the test error of each set of data is given with Table 2.4. Eq. 2.12 was used to investigate the error rate for each group of numerical and experimental values.

$$error_i = \frac{100 * a_{\exp_i}}{a_{num_i}} \tag{2.12}$$

$a_{\exp_i}$ and a_{num_i} are the experimental and numerical results of the coupled vibrations, the $_i$ denotes the each rotational speeds.

Table 2.4: Error margin for each rotational speed.

Speed (rpm)	Torsional angle (%)	Longitudinal disp.(%)
100	13	0.2
130	14	2
160	13	3
190	13	2

As given in Table 2.4, the error margin is higher on torsional vibration, but it is similar against increasing values of shaft speed and external forces in both axes. Similar error margin rates at different shaft speed values prove that the experiment is valid.

2.4 Different Parameter Effects to Coupled Torsional-Longitudinal Vibration

It has been proven by the previous study that the numerical model is applicable for the coupled torsional-longitudinal vibrations of the shaft. The numerical model was mainly developed by focusing on the length-to-diameter ratio of the shaft, the damping coefficient, the stiffness coefficient, and the coupling coefficient. The results were compared by changing certain proportions to observe the effects of the change of these parameters on the vibration behavior of the model. While examining each parameter, other parameters were kept constant and the studied parameter was examined for 5 different situations with 20%, 10% increase, and decrease rates.

2.4.1 Effect of diameter and length ratio of the shaft

To examine the effect of shaft length on coupled torsional-longitudinal vibrations, the shaft diameter was kept constant, while shaft length was examined with 10% increases

and decreases, and 5 different conditions were determined and the results were obtained with Figure 2.19.

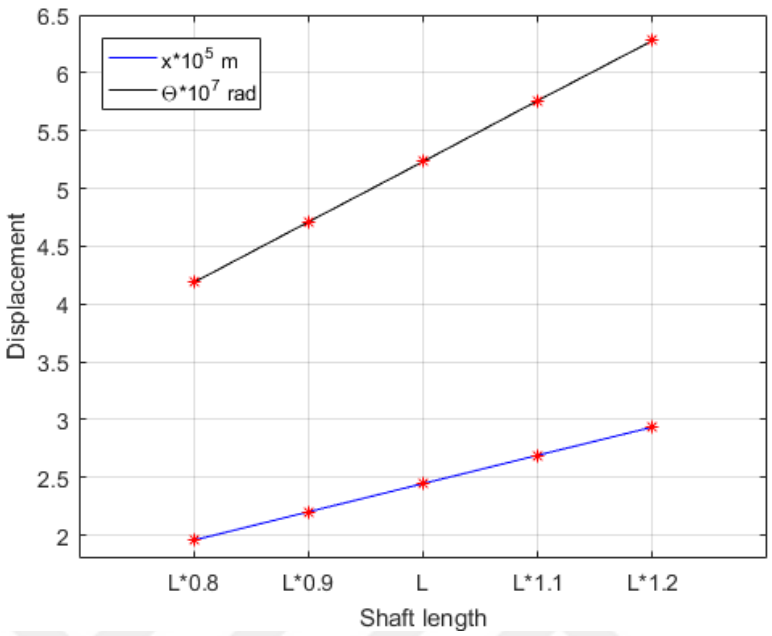

Figure 2.19 : The effect of the shaft length.

As shown in Figure 2.19, the displacement values in both axes are directly proportional to the shaft length change. The displacement values on both axes increased by 10% while the shaft length increased by the same rate.

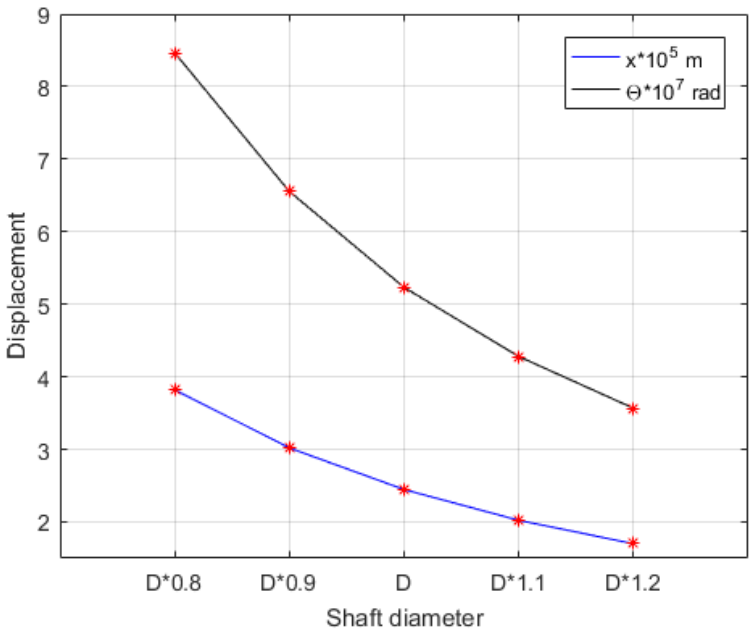

Figure 2.20 : The effect of the shaft diameter.

As given by Figure 2.20, the displacement values on both axes are inversely proportional to the shaft diameter change. The longitudinal vibration was reduced by approximately 18% and the torsional vibration was reduced by 21% while the shaft diameter increased by 10%. The increase in shaft diameter is more dominant on the torsional angle due to the fact that coupled vibration is more effective on the torsional angle. As a result, displacement values has been seen that they cannot be directly associated with the diameter change ratio. These parameters help to identify the location of the bearings.

2.4.2 Effect of damping coefficient and stiffness coefficient of the shaft

Stiffness and damping coefficients are the factors having major importance in the optimization of the shaft system. In this thesis, these two values were calculated primarily depending on the parameters of the shaft. First, the stiffness coefficient and other parameters were kept constant, while the damping coefficient was examined for 5 situations with 10% increases and decreases.

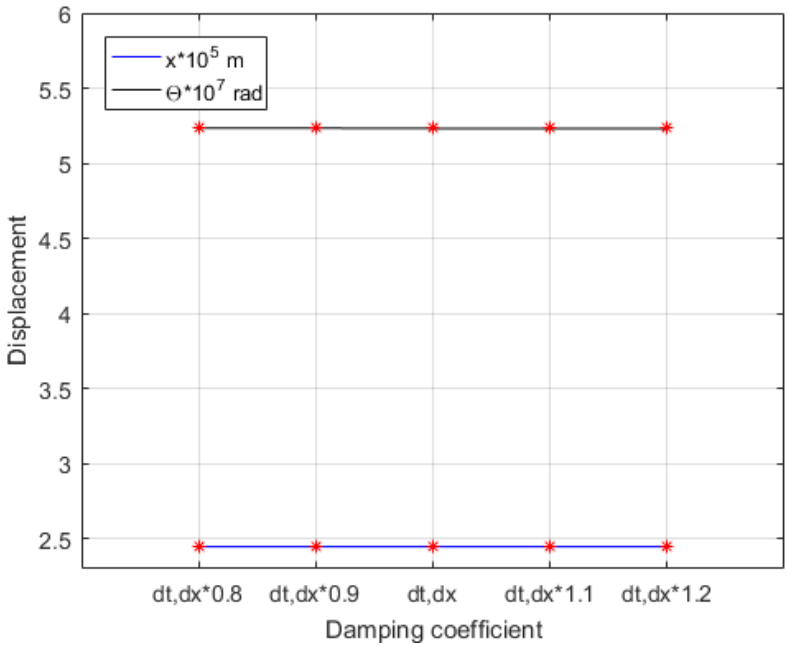

Figure 2.21 : The effect of damping coefficient.

As given in Figure 2.21, it was observed that the increase or decrease in damping coefficients due to shaft parameters occurring on x and θ axes had no effect on vibration amplitudes. The reason for the lack of change in vibration amplitudes is that the damping coefficient values are too small to have an effect.

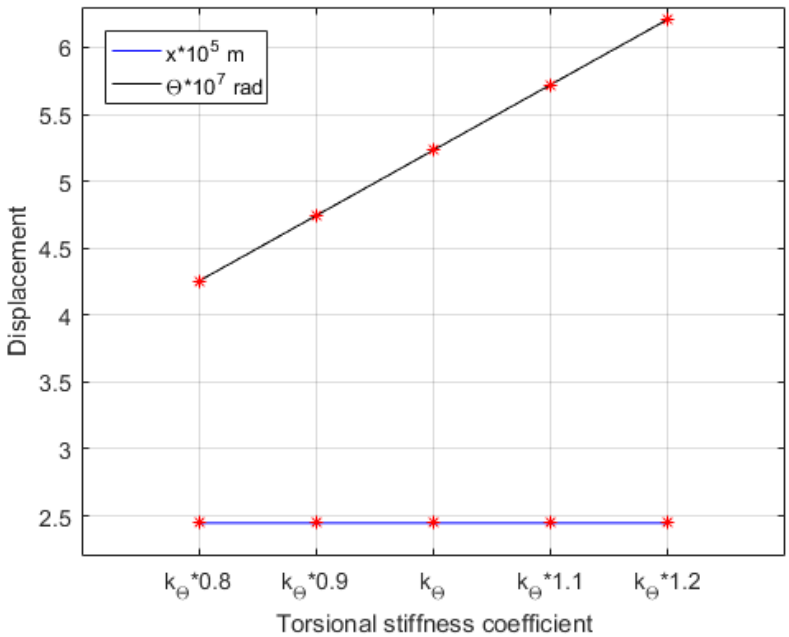

Figure 2.22 : The effect of torsional stiffness coefficient.

As shown in Figure 2.22, the displacements amplitudes are given for the coefficient value of torsional stiffness is changed in different proportions. While the torsional angle increased with the increase of torsional stiffness, it was observed that there was small change enough to be ignored in the longitudinal displacement value.

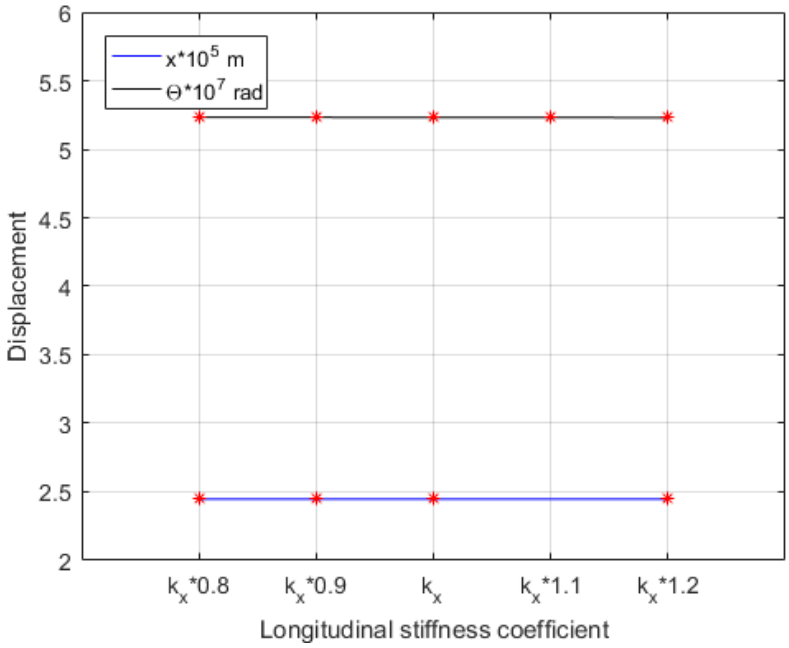

Figure 2.23 : The effect of longitudinal stiffness coefficient.

As given in Figure 2.23, when the longitudinal stiffness coefficient value is changed in different proportions, vibration amplitudes that interfere with these values are given. With the increase of the coefficient of longitudinal stiffness, it was observed that there was no change in the torsional angle and longitudinal displacement values.

According to the results obtained shown in Figure 2.22 and Figure 2.23, it was observed that while the change in torsional stiffness affect torsional angle, its effect on the longitudinal displacement is so small that cannot be seen on the figure and the change in longitudinal stiffness has almost no effect on both axes. As a result, coupled vibration coefficient was examined to determine why torsional stiffness affects two axes at different rates.

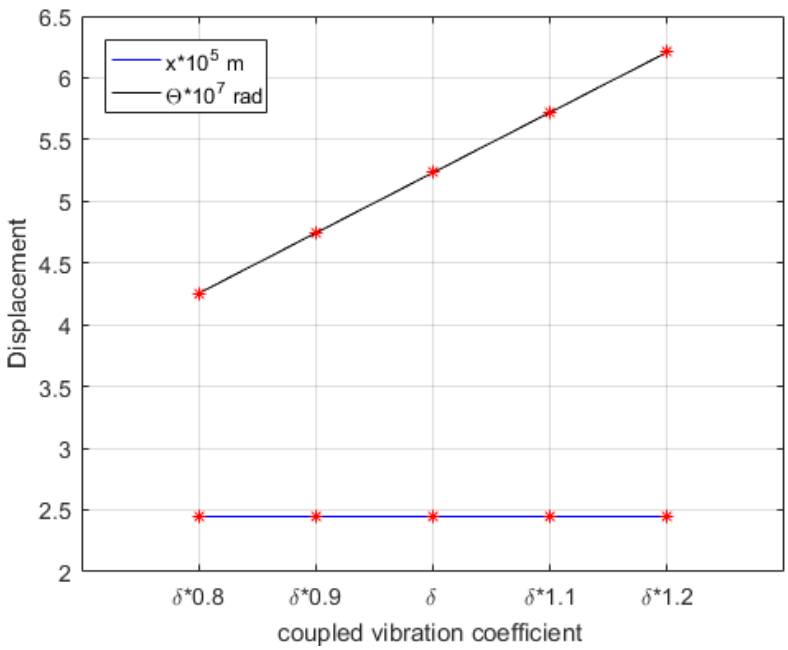

Figure 2.24 : The effect of coupled vibration coefficient.

As shown in Figure 2.24, when coupled vibration coefficient value is changed in different proportions, vibration amplitudes are shown that correspond to these values. The amount of increase in longitudinal displacement changes in 10^{-8} and it is difficult to see the change in the chart. However, the effect on the torsional angle is clearly seen. As a result, the coupled vibration effect is predominantly effective on the torsional angle.

2.5 Permissible Torsional Vibration Stresses

According to DNV rules, variable torsional vibration stress in any part of the shaft equipment should not exceed their value in continuous work specified below. The study given above was carried out continuously at constant speed values. In this case, maximum vibration stress allowed to occur in the shaft at 100 rpm is obtained by Equation 2.13;

$$\tau_c = \frac{\sigma_B + 160}{18} C_K C_D \left(3 - 2\lambda^2\right) \qquad \text{for} \quad \lambda < 0.9 \tag{2.13}$$

On the equation σ_B specified minimum tensile strength (MPa) of shaft meterial, $\lambda = n / n_0$ is the speed ratio,and λ for the shaft is 1/1.84. C_K is factor for the particular shaft design features (C_K =1.0);and C_D is size factor with $C_D = 0.35 + 0.93d^{-0.2}$. With equation 2.14, the maximum vibration stress value was obtained as 27.3 MPa.

The torque caused by 5.23× 10^{-7} rad displacement for 100 rpm shaft speed as shown in Figure 2.16 is obtained with ;

$$T = \frac{\theta JG}{L} \tag{2.14}$$

In the equation $T =$ Torque (Nm) , $L =$ Legth of the shaft (m) , $J =$ cross section's polar moment of inertia (m^4), $G =$ Modules of rigidity (GPa) and the torque value has been obtained with the Eq. 2.14 is 2.6690× 10^{-4} Nm.

$$\tau = \frac{Tr}{J} \tag{2.15}$$

With the equation 2.16 when τ is the shear stress (Pa) value ; T is the twisting moment (Nm), J Polar Moment of Inertia of Area (m^4), r distance from center to stressed surface in the given position (m) and shear stress is obtained as 2.66 Pa and the stress given by Eq. 2.13 is quite low from the shear stress. As a result, the torsional stress occured on the system quite low compared to permitted shear stress and the operating range is safe.

2.6 Results

The dynamic behavior of coupled torsional-longitudinal vibration for propulsion shaft system subjected to exciting torque and longitudinal force is modeled. The dynamic response of displacements and frequency response for the system with single and coupled vibration respectively are discussed in detail. Some conclusions are obtained as follows:

When the coupling effect is as small as neglectable on the axial displacement, it is highly effective on the torsional angle. This inference leads to obtain the result that torsional and longitudinal vibration are mutually coupled with each other. In the linear system, maximum longitudinal displacement and torsional angle were observed at the excitation frequency. While frequency responses were compared with the experiment; the margin of error was found to be low and frequency responses well-matched with each other. The displacement amplitudes increase in both directions with the increase in length of the shaft and decrease with an increase in diameter. The displacements are directly proportional and vary at the same rate as the shaft's length change. The longitudinal vibration was reduced by approximately 18% and the torsional vibration was reduced by 21% while the shaft diameter increased by 10%. The effect of the diameter rate is larger and it has been seen that it cannot be directly associated with the displacement ratio. The change of damping coefficient value has been shown to have no effect on the system as a result of the damping value is quite small. When the stiffness coefficient value is changed and the variation in displacement values are examined, it is discovered that while changes in longitudinal stiffness values have no effect on the torsional angle and longitudinal displacement, changes in torsional stiffness values have a dominant effect on the torsional angle. Finally, the coupled vibration coefficient was investigated, and it was discovered that the coupled vibration coefficient is dominant on the torsional angle while having little effect on longitudinal displacement. This finding also explains why torsional stiffness has such a strong influence on the torsional angle. Furthermore, the coupled vibration has no effect on the system's natural frequencies.

3. COUPLED TORSIONAL AND LATERAL VIBRATIONS

The marine propeller shaft is equivalent to a cantilever beam with fixed end (the main engine) and free end (the propeller), which can be considered as a beam, as shown in Fig. 3.1. The parameters ρ, J, L, A and E denotes the density, the moment of inertia, the length, the cross-sectional area, and the Young's modulus, respectively, ,in the shaft schematic.. And the m, e and I denotes the mass, the eccentricity of cross section and the second axial moment of area. The $x(t), y(t)$ and $\theta(t)$ are the deformations in X-lateral, Y-lateral and torsional directions, and the external excitations F_x, F_y and M_θ are the lateral force and torsional torque on the shaft in respective directions.

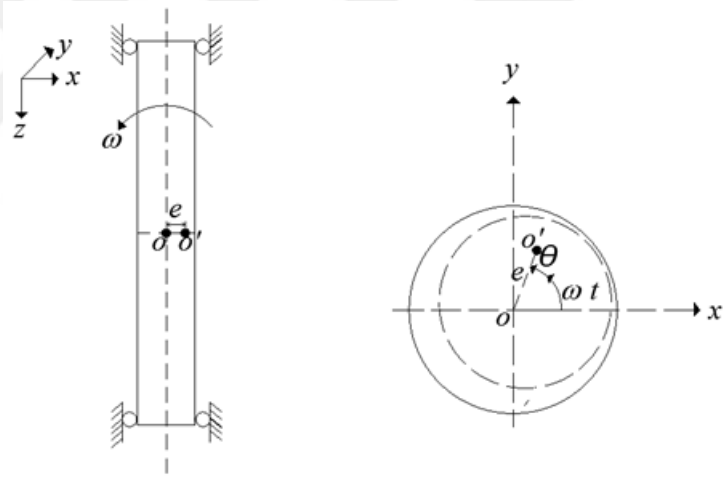

Figure 3.1 : Unbalanced shaft model.

As a result of external forces, the center of mass relocated to the $0'$ point, and x_c and y_c are the new coordinates in X-lateral and Y-lateral axis, respectively. The eccentricity e is the distance between the 0 point and $0'$. The ω and θ are the rotational speed and angle of the shaft, respectively. The initial positions for deformation and torsional angle can be presented by the parameters x_0, y_0 and θ_0. The torsional angle is produced during the shaft rotation, and the lateral deformation will be caused as the effect of the eccentricity.

3.1 Numerical Model for Coupled Torsional and Lateral Vibrations

The shaft can be subjected to both lateral and torsional deformations in which lateral motions are x_c and y_c ,and the torsional motion is θ due to the acting forces. Figure 3.1 shows the deformed configuration in a particular state. The governing equation of the system is obtained by Lagrangian dynamics. The kinetic energy of the shaft is given with Equation 3.1:

$$T = \frac{1}{2} m(\dot{x}_c^2 + \dot{y}_c^2) + \frac{1}{2} J(\omega + \dot{\theta})^2 \tag{3.1}$$

where x_c and y_c are the new position of the mass centre and their relationship with x, y;

$$\begin{aligned} x_c &= x + e\cos\varphi \\ y_c &= y + e\sin\varphi \\ \varphi &= \theta + \omega t \end{aligned} \tag{3.2}$$

e is the eccentricity of cross section appeared on the system due to the external forces. Using the expressions of x_c and y_c by substituting Eq. (3.2) into Eq. (3.1), the expression of shaft kinetic energy becomes:

$$T = \frac{1}{2} m(\dot{x} - e(\omega + \dot{\theta})\sin(\omega t + \theta))^2 + \frac{1}{2} m(\dot{y} + e(\omega + \dot{\theta})\cos(\omega t + \theta))^2 + \frac{1}{2} J(\omega + \dot{\theta})^2 \tag{3.3}$$

In addition, the potential energy of the system is defined as:

$$V = \frac{1}{2} k_x x^2 + \frac{1}{2} k_y y^2 + \frac{1}{2} k_\theta \theta^2 \tag{3.4}$$

Similarly, the dissipation energy of the shaft system is presented as:

$$D = \frac{1}{2} c_x \dot{x}^2 + \frac{1}{2} c_y \dot{y}^2 + \frac{1}{2} c_\theta \dot{\theta}^2 \tag{3.5}$$

where k_x, k_y and k_θ are the stiffness coefficients and c_x, c_y and c_θ are the damping coefficients in the lateral and torsional directions, respectively. The equations of motion for the shaft system is obtained by substituting the expressions of kinetic energy , potential energy and dissipation energy in Lagrange equations :

$$\frac{d}{dt}\left(\frac{\partial T}{\partial \dot{\boldsymbol{q}}}\right) - \frac{\partial T}{\partial \boldsymbol{q}} + \frac{\partial V}{\partial \boldsymbol{q}} + \frac{\partial D}{\partial \dot{\boldsymbol{q}}} = \boldsymbol{Q} \tag{3.6}$$

where $\boldsymbol{Q}$ stands for the non-conservative forces, and $\boldsymbol{q}$ stands for the generalized coordinates with $\boldsymbol{q} = \begin{bmatrix} x & y & \theta \end{bmatrix}^T$. In order to obtain the equations of motion for the lateral-torsional coupled vibration of the system, the following equation is used:

$$\begin{cases} m\ddot{x} - me\ddot{\theta}\sin(\omega t + \theta) + c_x\dot{x} + k_x x = me(\omega + \dot{\theta})^2 \cos(\omega t + \theta) \\ m\ddot{y} + me\ddot{\theta}\cos(\omega t + \theta) + c_y\dot{y} + k_y y = me(\omega + \dot{\theta})^2 \sin(\omega t + \theta) \\ (J + me^2)\ddot{\theta} - me\ddot{x}\sin(\omega t + \theta) + me\ddot{y}\cos(\omega t + \theta) + c_\theta\dot{\theta} + k_\theta\theta = 0 \end{cases} \tag{3.7}$$

It ought to be noticed that,in Eq. 3.7, the torsional acceleration terms $me\ddot{\theta}\sin(\omega t + \theta)$ and $me\ddot{\theta}\cos(\omega t + \theta)$ are also found in the equations of lateral motions, while the lateral acceleration terms $me\ddot{x}\sin(\omega t + \theta)$ and $me\ddot{y}\cos(\omega t + \theta)$ are found in the equation of torsional motion. As a result, the lateral vibration couples with torsional vibration through the inertia terms of the equations, which are brought about by the mass of the unbalance. Moreover, the equations of motion of the unbalanced rotor system end up being nonlinear when the coupling of lateral vibration and torsional vibration is taken into account.

Usually, the torsional displacements in most rotor systems is small permitting and to be approximated by the main term of their particular developments. Under this supposition, the accompanying relations are utilized. By and large, the amplitude of torsional vibration in most rotor systems is little, permitting $\sin\theta$ and $\cos\theta$ to be approximated by the first term of their respective Taylor Series expansions. Assuming this, the relations below are utilized (Hong et al. 2020).

$$\begin{cases} \cos(\omega t + \theta) = \cos(\omega t)\cos\theta - \sin(\omega t)\sin\theta \approx \cos\omega t - \theta\sin\omega t \\ \sin(\omega t + \theta) = \sin(\omega t)\cos\theta + \cos(\omega t)\sin\theta \approx \sin\omega t + \theta\cos\omega t \end{cases} \tag{3.8}$$

Eq. 3.9 is obtained by ignoring the unknown higher order terms in Eq. 3.7 with the assumtions in Eq. 3.8;

$$\begin{cases} m\ddot{x} - me\ddot{\theta}\sin\omega t + c\dot{x} - 2me\omega\dot{\theta}\cos\omega t + kx + me\omega^2\theta\sin\omega t = me\omega^2\cos\omega t \\ m\ddot{y} + me\ddot{\theta}\cos\omega t + c\dot{y} - 2me\omega\dot{\theta}\sin\omega t + ky - me\omega^2\theta\cos\omega t = me\omega^2\sin\omega t \\ (J + me^2)\ddot{\theta} - me\ddot{x}\sin\omega t + me\ddot{y}\cos\omega t + c_\theta\dot{\theta} + k_\theta = 0 \end{cases} \tag{3.9}$$

Coupled torsional-lateral equation of motion presented in Eq. 3.9 can be rewritten in the matrix form as shown in Eq. 3.10:

$$\begin{bmatrix} m & 0 & -me\sin(\omega t) \\ 0 & m & me\cos(\omega t) \\ -me\sin(\omega t) & me\cos(\omega t) & J+me^2 \end{bmatrix}\begin{bmatrix} \ddot{x} \\ \ddot{y} \\ \ddot{\theta} \end{bmatrix}+\begin{bmatrix} c_x & 0 & -2me\omega\cos(\omega t) \\ 0 & c_y & -2me\omega\sin(\omega t) \\ 0 & 0 & c_\theta \end{bmatrix}\begin{bmatrix} \dot{x} \\ \dot{y} \\ \dot{\theta} \end{bmatrix}+$$
$$\begin{bmatrix} k_x & 0 & me\omega^2\sin(\omega t) \\ 0 & k_y & -me\omega^2\cos(\omega t) \\ 0 & 0 & k_\theta \end{bmatrix}\begin{bmatrix} x \\ y \\ \theta \end{bmatrix}=\begin{bmatrix} me\omega^2\cos(\omega t)+F_x(t) \\ me\omega^2\sin(\omega t)+F_y(t) \\ M_\theta(t) \end{bmatrix} \tag{3.10}$$

It is demonstrated by Eq. 3.10 that the eccentricity of cross section is the cause and therefore a fundamental element of the coupled lateral-torsional vibrations. The vertical and horizontal vibrations are observed to be unconnected to the torsional vibration with the case of $e=0$. In order to continue the coupled vibration calculations, the eccentricity of cross section is taken as 0.001 (Huang et al., 2017; Jie et al.,2020).

The coefficients c_x, c_y and c_θ defining the vertical, horizontal and torsional damping for each shaft, are given by $c_x = c_y = \xi_{x,y} m\omega, c_\theta = \xi_\theta J\omega$ where, the ξ_x, ξ_y and ξ_θ are the lateral and torsional damping coefficients with the value of $\xi_x = \xi_y = 0.05$ and $\xi_\theta =$ 0.08, which are considered on the basis of the mechanical properties of actual materials. The stiffness coefficients k_x, k_y and k_θ defining vertical, horizontal and torsional stiffness are given by $k_x = k_y = 3EI / L^3, k_\theta = GI_P / L$ where L is the length of shaft and it is 2.665 m (Huang et al., 2019). E and G are the Young's modulus and the shear modulus and I and I_P are the second axial moment of area and the second polar moment of area with the $I = \pi D^4 / 64, I_P = \pi D^4 / 32$ expression also diameter of the shaft is 0.086 m. External forces and torsional torque on the shaft are given with $F_x(t) = F_{x_0}\sin(\omega t), F_y(t) = F_{y_0}\sin(\omega t)$ and $M_\theta(t) = M_{\theta_0}\sin(\omega t)$. $F_{x_0}, F_{y_0}, M_{\theta_0}$ are external forces measured from tail shaft and they have different amplitude at different rotational speeds.

3.2 Experimental Setup

Figure 2.4 presents how the experimental setup is installed. Details of the experimental setup are given in Section 2 and therefore they will not be repeated in this section. Fig. 3.2 presents measurement points, where the sensors transmitting the analog signals are located.

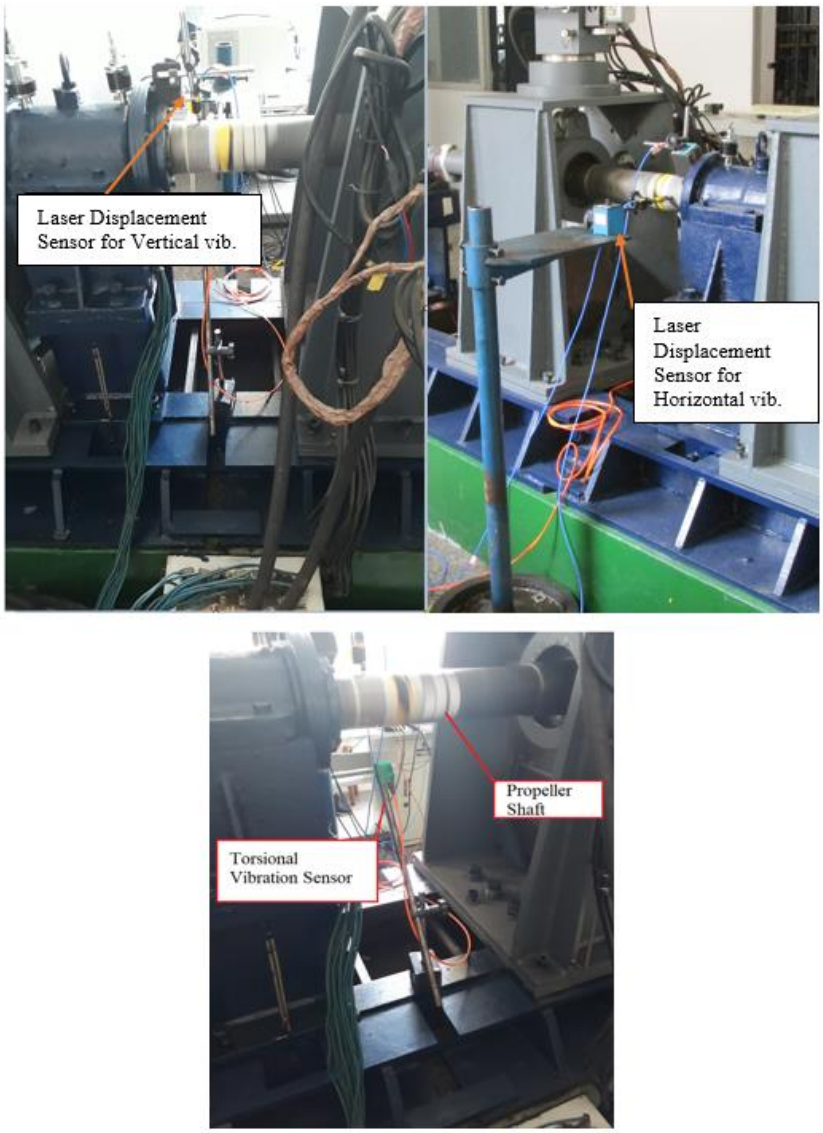

Figure 3.2 : Measurement points layout for the shaft lateral and torsional vibrations.

Recordings of torsional and lateral vibration signals are made simultaneously along the shaft. The signal of the tail shaft is measured and shaft speed is checked by using the laser torsional vibration meter (B&K MM0071 sensor and 2523 laser; sensivity 100 mV/g.) as can be seen in Fig. 3.3. Additionally, measurements for vertical and horizontal displacements of the tail shaft are made by using the eddy current sensors (ZA- 210803 and sensitivity 3.33 V mm^{-1}). In this particular case, the test selects the two measuring points of the tail shaft for lateral vibration. Possible errors due to the vibration are reduced by fixing the sensor position.

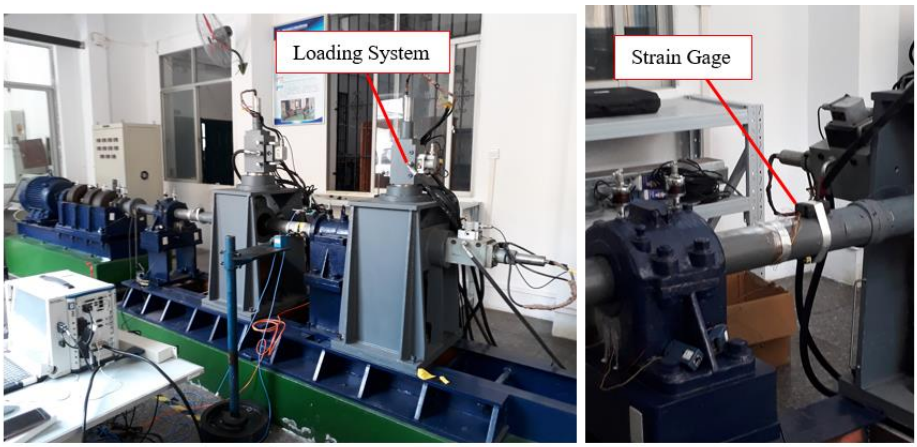

Figure 3.3 : Hydraulic loading system and torque measurement point.

Lateral loads are exposed to a hydraulic system. A strain gage positioned on the tail shaft is used to measure the torque produced by the lateral forces (Fig. 3.3). Although shaft speed values are determined from 100 to 190 in 30 increments and frequencies and amplitudes for the shaft coupled vibrations are recorded for each speed—the measurements and results presented in Section 3.4 are only for 100 rpm. The amplitudes of each lateral force applied and corresponding torque are 300 kN and 0.06 Nm, correspondingly, for 100 rpm. Due to the fact that the test apparatus only permits axial and lateral loadings, the torsional stress could not be obtained directly, nevertheless torque values are obtained from the measured lateral stresses. The lateral stresses are collected for the lateral forces applied with regard to the displacements of the loading system. Applied displacements and measured torque and lateral force amplitudes are provided in Table 3.1.

Table 3.1: Loadings for each rotational speed.

Rotational speed (rpm)	**100**	**130**	**160**	**190**
Displacement (mm)	0.6	0.9	1.2	1.5
Vertical Force(N)	300	320	330	350
Horizontal Force(N)	300	320	330	350
Torque (Nm) under lateral forces	0.06	0.065	0.07	0.075

3.3 Application and Discussion

In order to obtain steady results, for each speed, the simulation time is taken as 1 minute for the experiment. The initial conditions are taken as $x_0 = y_0 = \theta_0 = 0$,

simulation time is applied as 10 s, and the results tend to be steady in this period. The second half of the simulation's time interval was used to show the numerical results.

3.4 Verification

Lateral displacements and torsional angles are calculated by numerical model and compared with the experimental results in Figure 3.4-3.8, and Excitation frequency are compared with the experiment in three direction.

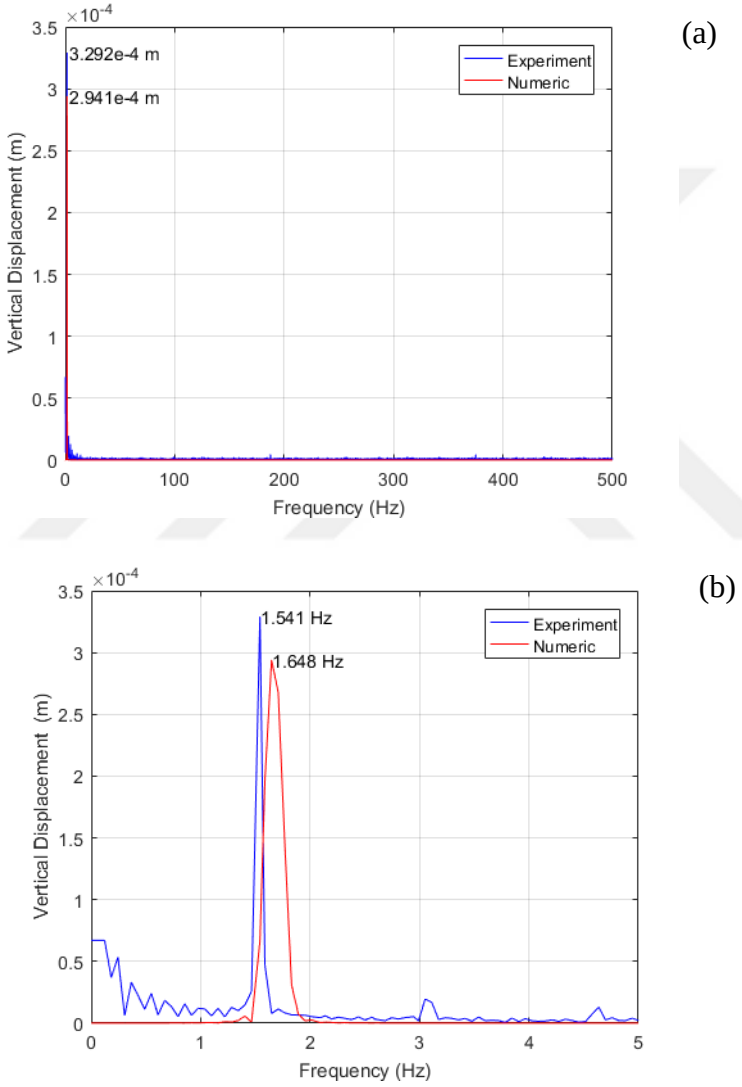

Figure 3.4 : Vertical displacements results (a) at 100 rpm (b) between 0-5 Hz.

Figure 3.4 indicates the displacements in vertical vibration of experiment and numerical model at 100 rpm. While the vertical displacement is 3.292×10^{-4} m at 1.541 Hz for experiment, the numerical result is 2.941×10^{-4} m at 1.648 Hz. In the graph given with Figure 3.4 (a), the time step was kept the same with the experiment data in order

to avoid errors in the comparisons with the experiment, so even though the maximum displacements are seen before 5 Hz, the frequency range continues up to 500 Hz. It is found that the vertical displacement of the numerical model is lower than the experimental data. Despite the margin of error, the frequency value corresponding to the maximum displacement is similar, indicating that the numerical model yields similar results to the experimental data.

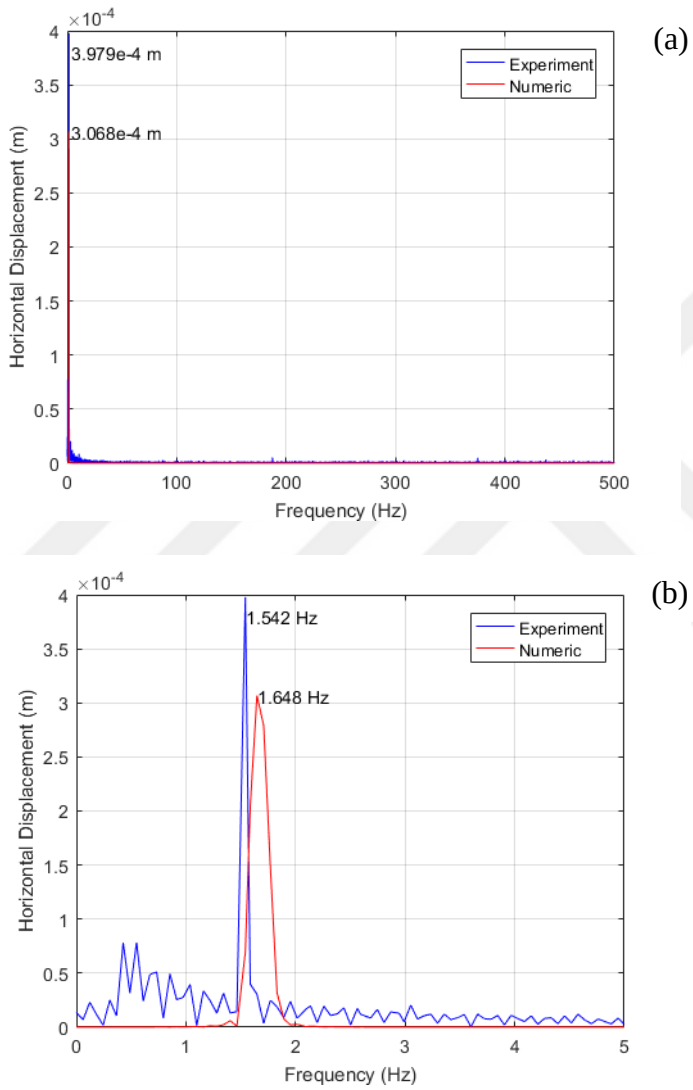

Figure 3.5 : Horizontal displacements results (a) at 100 rpm (b) between 0-5 Hz.

Figure 3.5 shows the displacements in horizontal vibration of experiment and numerical model at 100 rpm. While the vertical displacement is 3.979×10^{-4} m at 1.542 Hz for experiment, the numerical result is 3.068×10^{-4} m at 1.648 Hz.

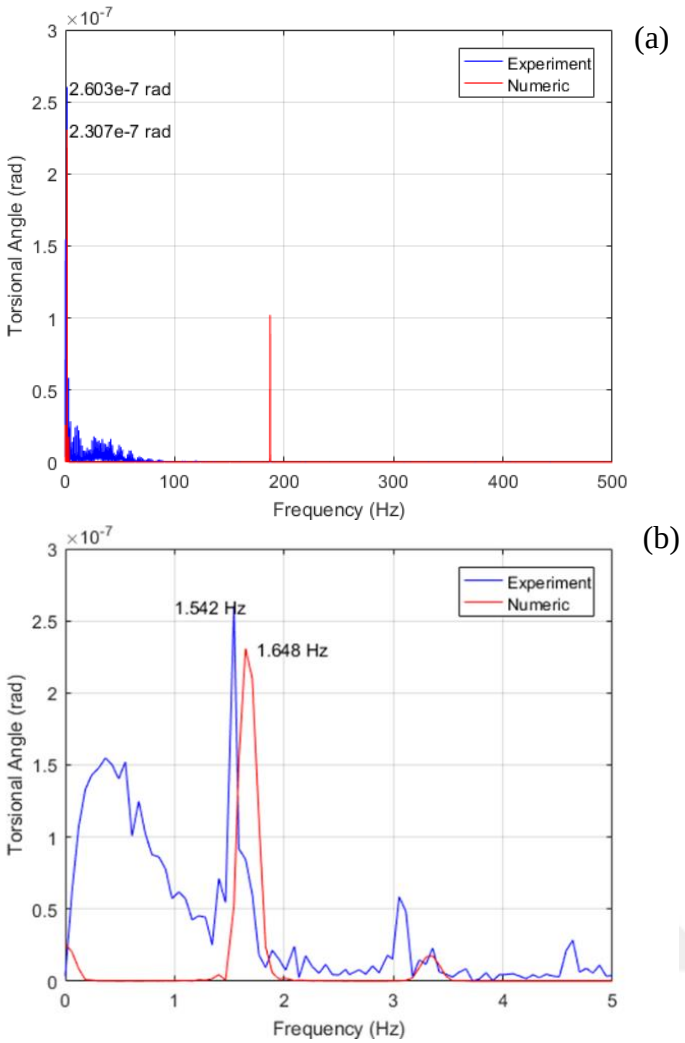

Figure 3.6 : Torsional angles results (a) at 100 rpm (b) between 0-5 Hz

Figure 3.6 shows the displacements in torsional vibration of experiment and numerical model at 100 rpm. While the torsional angle is 2.603×10^{-7} rad at 1.542 Hz for experiment, the numerical result is 2.307×10^{-7} rad at 1.648 Hz. As might be expected, test results are higher than numerical predictions owing to the imperfection of theoretical models.

3.5 Verification at Various Speed Range

Figure 3.7 and Figure 3.8 indicate the difference in coupled torsional-lateral vibration of experiment and numerical models by increasing rotational speed. In this section, the aim is to observe the validity of the numerical method by looking at the error margins of the experiment at different speed values.

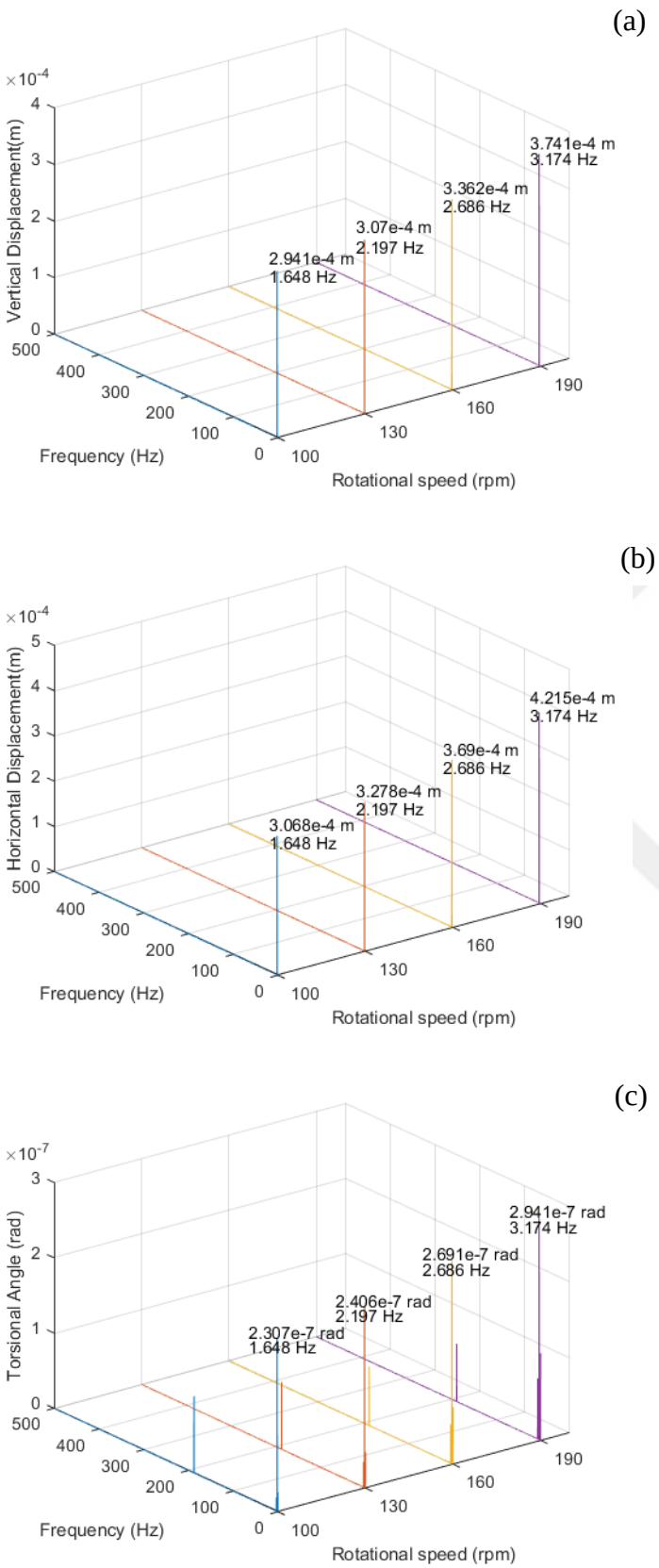

Figure 3.7 : Numerical results between 100-190 rpm (a) vertical (b) horizontal (c) torsional.

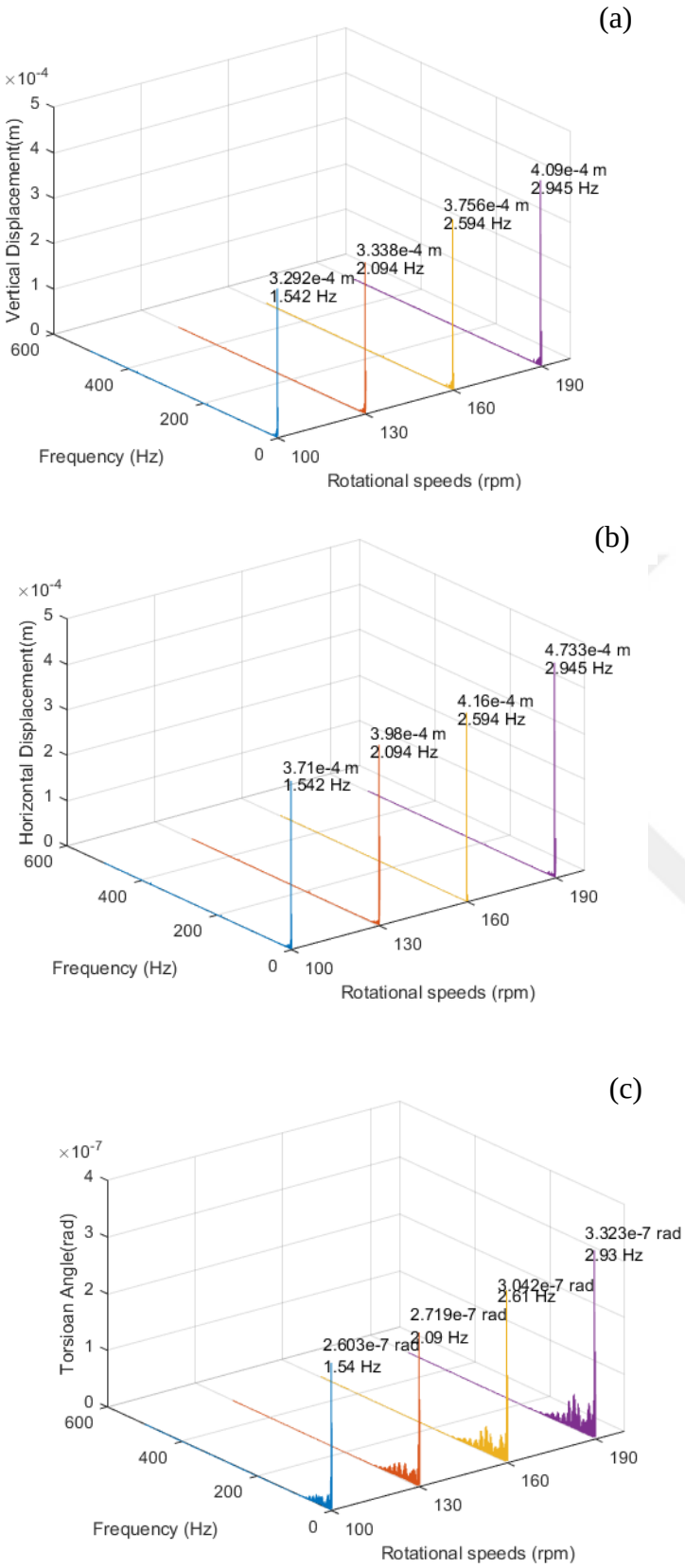

Figure 3.8 : Experimental results between 100-190 rpm (a) vertical (b) horizontal (c) torsional.

It is found that the lateral displacement and torsional angle of all numerical models is lower than the experimental data and the error margin is similar for each rotational speeds which is given with Table 3.2. However, the fact that the slope of curves in the graphic are similar despite the margin of error indicates that the numerical models yield good correlation with the experimental data.

Table 3.2: Error margin for each rotational speed.

Speed (rpm)	Vertical disp.(%)	Horizontal disp.(%)	Torsional angle (%)
100	13	12	19
130	12	9	20
160	13	11	12
190	13	8	13

After the numerical model's validity was established, the natural frequency values for coupled and uncoupled vibration were investigated. Although the shaft experimental platform has four shafts, numerical simulations treated them as if they were a single shaft. The error rate would obviously increase as a result of operating state differences. With the study given above, by proving the validity of the numerical model with different conditions such as shaft speed and external forces, the coupling effect on naturel frequencies also is investigated with Table 3.3.

Table 3.3: Natural frequencies predicted by the coupled and uncoupled form (Hz).

Coupled	Uncoupled
208	208
13	13
13	13

The system's natural frequency remains constant in coupled or uncoupled form and at all rotational speeds. As a result, rotational speed and the coupling effect do not effect on natural frequencies. The natural frequencies are 13 hertz (Hz) in the vertical direction, 13 hertz (Hz) in the horizontal direction, and 208 hertz (Hz) in the torsional direction.

3.6 Different Parameter Effects to the Coupled Torsional-Lateral Vibration

The numerical model was primarily developed by focusing on the shaft's length-to-diameter ratio, damping coefficient, stiffness coefficient, and coupling coefficient. The

results were compared by varying certain proportions and observing the effects of these changes on the model's vibration behavior.

3.6.1 Coupling effect

In Table 3.4, lateral and torsional vibration amplitudes are given for coupled and uncoupled vibration forms. When examining differences between three directions, it is seen that the coupling effect has an impact only on lateral displacements. Comparing vertical and horizontal direction; the coupling has an impact approximately 0.1% and 4.4%, respectively. As a result, it has been observed that the coupled vibration is more effective in the horizontal axis.

Table 3.4: Coupled effect on three axis.

Direction	coupled	uncoupled
x (m)	2.941×10^{-4}	2.938×10^{-4}
y (m)	3.068×10^{-4}	2.938×10^{-4}
θ (rad)	2.307×10^{-7}	2.307×10^{-7}

3.6.2 Effect of diameter and length ratio of the shaft

In order to examine the effect of the length of the shaft on the coupled torsional-lateral vibrations in the shaft system, the length value of the shaft was changed at 10% intervals while other parameters constant as shown in Figure 3.9.

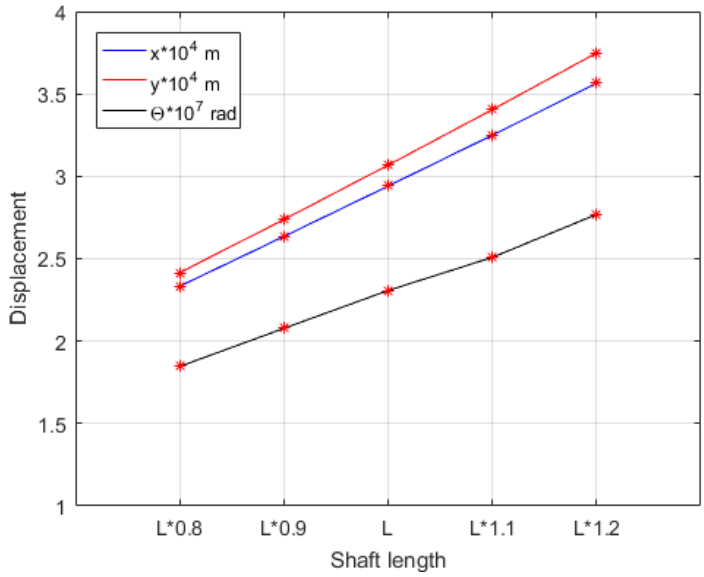

Figure 3.9 : Displacements for different shaft length.

As shown in Figure 3.9, the lateral and torsional displacement results vary in trend with the length ratio, and all three axes were similarly affected.

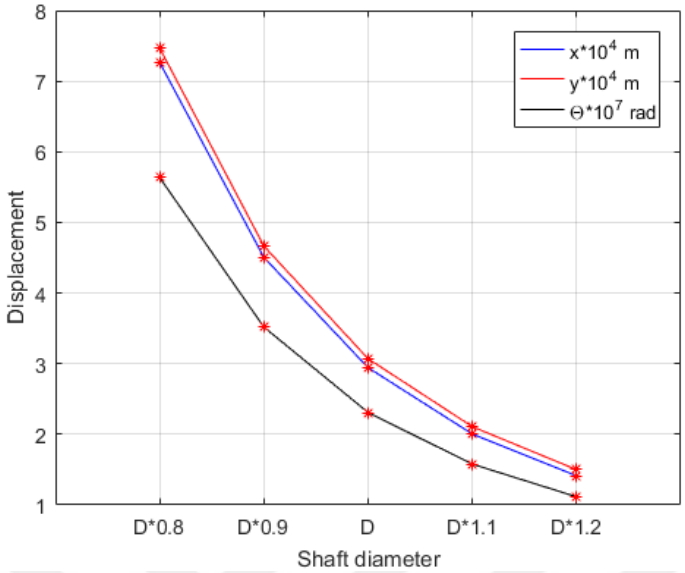

Figure 3.10 : Displacements for different shaft diameter.

To investigate the effect of shaft diameter, the diameter of the shaft was varied in 10% increments while holding the length constant, and the results are shown in Figure 3.10. The vibration amplitudes changed proportionally to the length ratio of the shaft, while they changed inversely to the diameter change of the shaft. As predicted, changes in diameter have an effect on lateral and torsional stiffness, so shaft diameter has a greater effect on displacement values than shaft length, and it has been discovered that it is not directly related to shaft diameter rate. The lateral vibration was increased by 50%, and the torsional vibration was increased by approximately 40%, while the shaft diameter was decreased by 10%. When it comes to lateral displacement, coupled vibration is more effective, and increasing shaft diameter has a bigger impact.

3.6.3 Effect of stiffness and damping coefficient ratio of the shaft

Stiffness and damping coefficients are important factors for the optimization of the shaft system. In this study, these two values are firstly calculated depending on the parameters of the shaft. However, in order to observe the effect of these factors on the coupled torsional-lateral vibrations, the stiffness and damping coefficient are changed at a certain ratio, the other values kept constant.

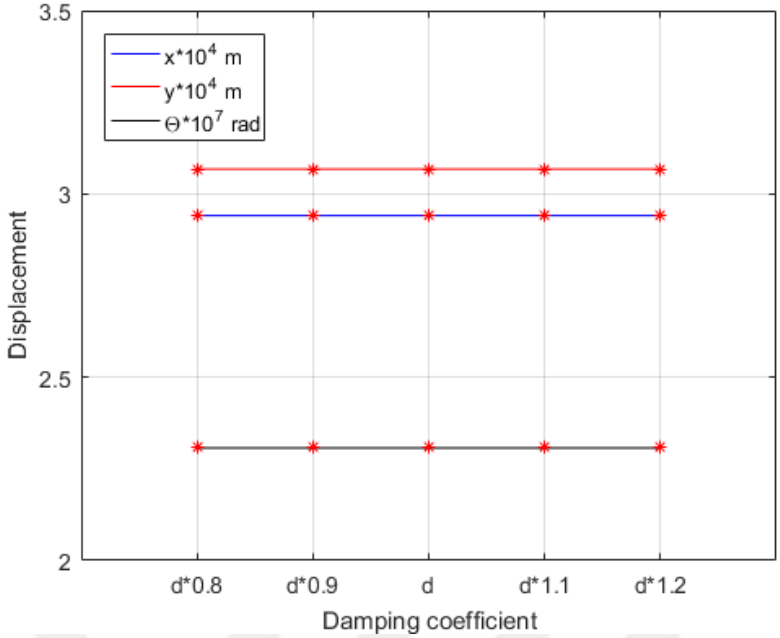

Figure 3.11 : Displacements for different damping coefficients.

In Figure 3.11, while the stiffness values were kept constant, the damping coefficient values were changed at different rates for 100 rpm shaft speed and its effect on the system was examined. The change in the damping coefficient has no effect on the system, because the damping coefficient values are very low and they are obtained from the bearing parameters. Since the damping coefficient in all 3 axes has no effect on the system, all damping coefficients are symbolized by d on the figure.

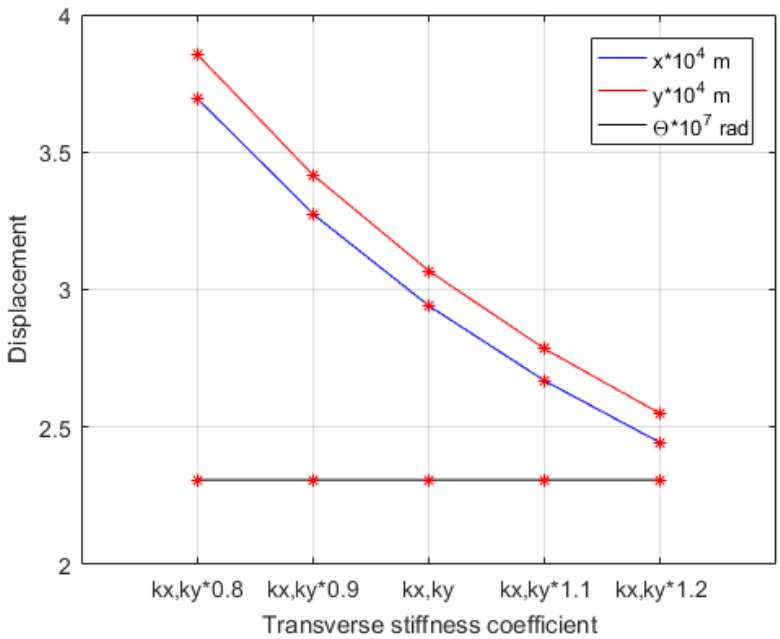

Figure 3.12 : Displacements for different lateral stiffness coefficients.

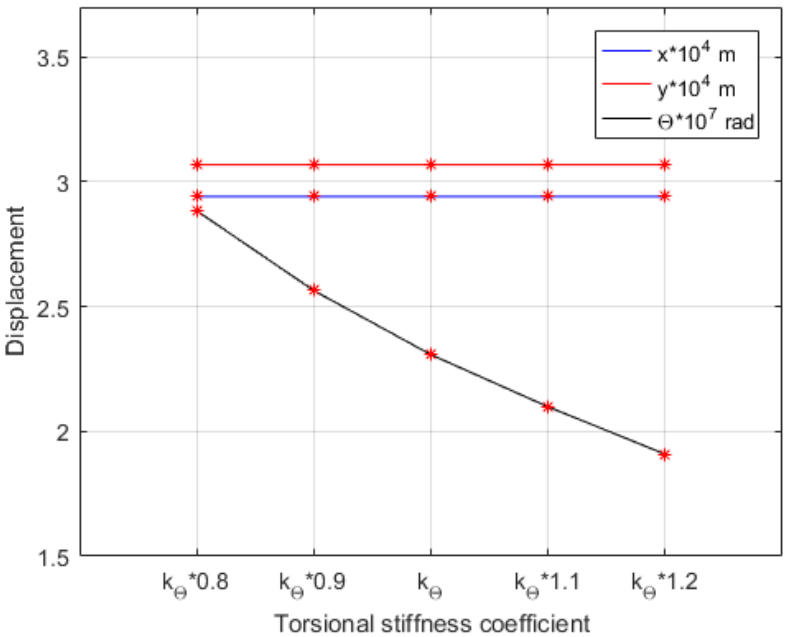

Figure 3.13 : Displacements for different torsional stiffness coefficients

In Figure 3.12, the vibration occurring when the k_x, k_y lateral stiffness coefficients are changed at 100 rpm shaft speed value at different rates were given and it was observed that while a decrease is seen in lateral displacement with the increase of coefficients, there is no change in the torsional angle value. Figure 3.13 shows the displacement values for when k_θ torsional stiffness value is changed at different rates for 100 rpm shaft speed and it was observed that while the torsional angle decreased with the increase of coefficients, there was no change in the value of lateral displacement. According to the results obtained, lateral displacement and torsional angle did not couple with each other, as shown in Figures 3.12 and 3.13, and in order to reveal the causes of this, displacements at different eccentricity of cross sections were investigated and presented in Figure 3.14.

3.6.4 Effect of eccentricity of cross section ratio

Fig. 3.14 presents the displacement values for all three axes at different eccentricity of cross section values. It was observed that the coupled vibration effect disappears with a decrease in the value accepted in the first stage of numerical calculations which is given with e=0.001. While the eccentricity of cross section ratio increased, the displacements increased significantly in all three axes through more interaction between them.

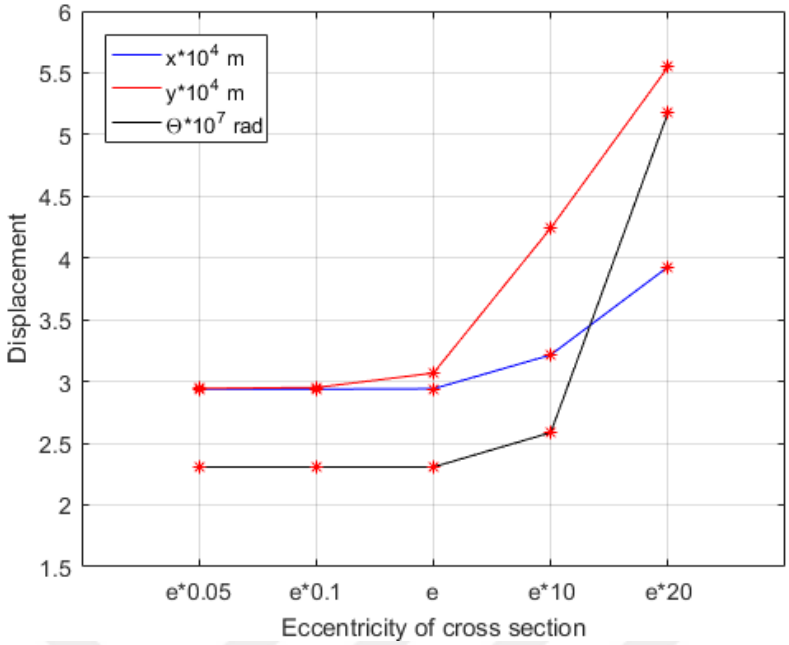

Figure 3.14 : Displacements at different eccentricity of cross sections.

As shown in Figure 3.14, with coupled vibration effect x and y axes are seen to affect each other at $e = 0.001$ value. However, the coupling impact on the torsional angle is almost neglectable. Moreover, it is clearly seen that although the e (which is 0.001) value decreases, x and y axes continue to affect each other while torsional angle does not affected. The value of $e = 0.005$ (symbolized by $e*5$ in the figure) has a displacement value of 3.009×10^{-4} m on the x axis and 3.59×10^{-4} m on the y axis and θ has a value of 2.409×10^{-7} rad and these values are compared to the results obtained at $e = 0.001$. The displacement values increased with a decreased margin of error which is given with Table 3.5 on all three directions, also the numerical results closer to the results of the experiment. Additionally, the effect of coupled vibration between three directions is seen more clearly. As a result of this, the coupled vibration effect cannot be seen between lateral and torsional direction at any e value selected from the references and it is important to determine the eccentricity of cross section coefficient value correctly in the design stage.

3.7 Permissible Torsional Vibration Stresses

According to DNV rules, torsional vibration stress in any part of the shaft equipment should not exceed specified stress which is given with Eq. 3.11 "τ_c" below in continuous work. The study given was carried out continuously at constant speed value

instead of speed range. In this case, maximum vibration stress is searched for only certain shaft speed and the stress occured in the shaft at 100 rpm is obtained with Equation 3.11;

$$\tau_c = \frac{\sigma_B + 160}{18} C_K C_D \left(3 - 2\lambda^2\right) \qquad \text{for} \quad \lambda < 0.9 \tag{3.11}$$

On the equation σ_B specified minimum tensine strength (MPa) of shaft meterial, $\lambda = n / n_0$ is the speed ratio, λ for the shaft is 1/1.84 'dür. C_K is factor for the particular shaft design features (C_K =1.0); C_D is size factor and $C_D = 0.35 + 0.93d^{-0.2}$ 'dir. With Equation 3.11, the maximum vibration stress value was obtained as 27.3 MPa.

The torque caused by 2.307e-7 rad displacement for 100 rpm shaft speed as shown in Figure 3.7 is obtained with ;

$$T = \frac{\theta JG}{L} \tag{3.12}$$

In the equation $T =$ Torque (Nm) , $L =$ Legth of the shaft (m) , $J =$ cross section's polar moment of inertia (m^4), $G =$ Modules of rigidity (GPa) and the torque value has been obtained with the Eq. 3.12 is 560.74 Nm.

$$\tau = \frac{Tr}{J} \tag{3.13}$$

With the equation 3.13 when τ is the shear stress (Pa) value ; T is the twisting moment (Nm), J Polar Moment of Inertia of Area (m^4), r distance from center to stressed surface in the given position (m) and shear stress is obtained as 266.74 Pa and the stress given by Eq. 3.11 is quite low from the shear stress. As a result, the torsional stress occured on the system quite low compared to permitted shear stress and the operating range is safe.

3.8 Results

In the present study, the shaft model is subjected to torque and lateral excitation forces and the dynamic behavior of the system is observed via implementing coupled torsional-lateral vibration. The displacements and frequency response of the system

for single and coupled vibration respectively have been discussed in detail. Major conclusions obtained as a result of the study are as follows:

Table 3.5: The relative errors of numerical results compared to experimental results.

	Torsional angle	Vertical displacement	Horizontal displacement
$e = 0.001$	10	20	11
$e = 0.005$	8	11	8

For the $e = 0.001$, the coupling effect is not observed on the torsional angle, it is mostly effective on the horizontal displacement compare to vertical; however, with an increase in $e = 0.005$ value, the coupling effect was observed more clearly and 3 direction coupled with each other, additionally, the margin of error with the experiment has decreased. The displacement amplitudes increase in three direction with the increase in length of the shaft, it decreases with an increase in diameter. Moreover, the coupled vibration effect has no impact on the natural frequencies of the system. The displacement values in both axes increased by 10% when the shaft's length was increased by 10%. However, a 10% increase in the diameter value reduced lateral vibration by 50% while torsional vibration decreased by 40%. As a result, it has been discovered that diameter change is dominant over lateral vibration. The change of damping coefficient value has been shown to have no effect on the system which stems from the fact that the damping value is quite small. When the change in the stiffness coefficient value and the changes in the displacements have been investigated, it was observed that while the change in lateral stiffness values did not affect the torsional angle, the change in torsion stiffness value did not affect the lateral displacement values. As a result, while there is an interaction between horizontal and vertical axes with the $e = 0.001$ value determined in the first stage of the study but it has no effect on the torsion angle. With the increase of $e = 0.001$ value, the interaction between lateral and torsional vibration was observed. In addition, while the rate of increase in displacement values is in direct proportion to an increase in "e" and cannot be associated directly, with a decrease in "e" value, the vibration effect occurs between x and y axes instead of torsional vibration. As a result, the importance of accurately defining the eccentricity of cross-section coefficient value was seen.

4. COUPLED LONGITUDINAL AND LATERAL VIBRATIONS OF SHAFT SYSTEM

The propulsion shaft system is equivalent to a cantilever beam with taking the propeller free end and the main engine fixed end. The propulsion shaft system can be modelded as a beam with a mass payload, where its mass center does not need be coincident with the centerline of the beam.

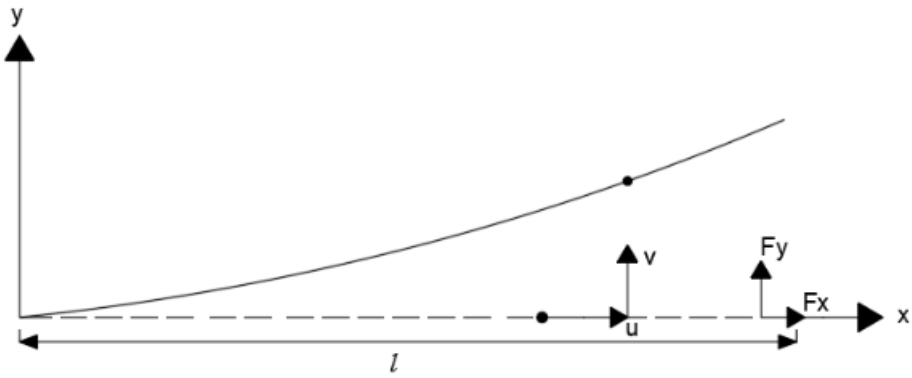

Figure 4.1 : Schematic of the beam with a mass payload.

The $u(x,t)$ and $v(x,t)$ are the deformations in longitudinal and vertical directions and $w(x,t)$ is the horizontal direction which is perpendicular to the uv plane. And the external excitation F_x is the longitudinal external force and F_y vertical external force on the shaft are shown with Figure 4.1.

4.1 Numerical Model for Coupled Longitudinal and Lateral Vibrations

The displacements are investigated for coupled longitudinal-lateral vibrations according to the theory of material mechanics and displacement of all directions can be written as (Huang et al.,2015);

$$\begin{aligned} U(x,y,t) &= u(x,t) - y\frac{\partial v}{\partial x}(x,t) \\ V(x,t) &= v(x,t) \\ W(x,t) &= 0 \end{aligned} \tag{4.1}$$

the relationship between shear strain and normal strain can be defined according to the strain tensor in elastic mechanics as follows:

$$\varepsilon_x = \frac{\partial U}{\partial x} + \frac{1}{2}\left(\frac{\partial V}{\partial x}\right)^2 \quad \varepsilon_y = \frac{\partial U}{\partial y} \quad \varepsilon_z = 0 \tag{4.2}$$

$$\gamma_{xy} = \frac{1}{2}\left(\frac{\partial V}{\partial x} + \frac{\partial U}{\partial y}\right) \quad \gamma_{yz} = 0 \quad \gamma_{zx} = 0 \tag{4.3}$$

Taking the definition of displacement in the normal strain, the direction located normal strain of the main stress can be expressed as follows:

$$\varepsilon_x = \frac{\partial U}{\partial x} + \frac{1}{2}\left(\frac{\partial V}{\partial x}\right)^2 = \frac{\partial U}{\partial x} - y\frac{\partial^2 v}{\partial x^2} + \frac{1}{2}\left(\frac{\partial v}{\partial x}\right)^2 \tag{4.4}$$

the stress of main stress direction can be defined according to the Hooke's law, the strain energy (PE) of the system can be defined as:

$$PE = \frac{1}{2}\int_V \sigma_{ij}\varepsilon_{ij} dV \tag{4.5}$$

the strain energy can be rewritten by taking the main strain expression to the strain energy theory;

$$PE = \frac{E}{2}\int_x \int_A \left[\frac{\partial u}{\partial x} - y\frac{\partial^2 v}{\partial x^2} + \frac{1}{2}\left(\frac{\partial v}{\partial x}\right)^2\right]^2 dAdx \tag{4.6}$$

with the moment of inertia of the beam with circular cross-section is $I_x = \int_A y^2 dA$,the Eq. 4.6 can be rewritten:

$$PE = \frac{1}{2}\int_l \left[EA\left(\frac{\partial u}{\partial x} + \frac{1}{2}\frac{\partial^2 v}{\partial x^2}\right)^2 + EI\left(\frac{\partial v}{\partial x}\right)^4\right]dx \tag{4.7}$$

The kinetic energy of the system can be expressed according to the theorem of kinetic energy $E_k = mv^2/2$:

$$KE = \frac{E}{2}\int_l \int_A \left\{\rho\left[\left(\frac{\partial U}{\partial t}\right)^2 + \left(\frac{\partial V}{\partial t}\right)^2\right]\right\}dAdx \tag{4.8}$$

The Eq. 4.9 defines kinetic energy of the system it is more general defination by adding the displacement expression to Eq. 4.8:

$$KE = \frac{1}{2}\int_l \left\{ p\left[\left(\frac{\partial u}{\partial t}\right)^2 + \left(\frac{\partial v}{\partial t}\right)^2 \right] + \rho I \left(\frac{\partial^2 v}{\partial x \partial t} \right)^2 \right\} dx \qquad (4.9)$$

The Lagrange equation of the system is time dependent and it is obtained by combining the strain energy Eq. 4.6 and the kinetic energy Eq. 4.9:

$$\begin{aligned} &\int_1^f L dt = \int_1^f (KE - PE) dt = \\ &\int_1^f \left\{ \int_l \left[\rho A\left(\dot{u} + \dot{v}^2\right) + \rho I \dot{v}'^2 - EA\left(u' + \frac{1}{2} v'^2 \right)^2 - EIv''^2 \right] dx \right\} dt \end{aligned} \qquad (4.10)$$

The Eq. 4.10 can be determined according to the virtual displacement formula as:

$$\begin{aligned} &\delta \int_1^f L dt = \int_1^f \left\{ \int_l \left[\rho A\left(\dot{u}\delta\dot{u} + \dot{v}\delta\dot{v}\right) + \rho I \dot{v}'\delta\dot{v}' - \right.\right. \\ &\left.\left. EA\left(u' + \frac{1}{2} v'^2 \right)\left(\delta u' + v'\delta v'\right) - EIv''\,\delta v'' \right] dx \right\} dt \end{aligned} \qquad (4.11)$$

When the beam is under the effect of external forces, the work is done by external forces is defined with $W = F.s$. As a result, the work is done by the external force acting in the longitudinal direction $N_x \sin \omega t$ is determined as:

$$U_u = \frac{1}{2}\int_l N_x \sin \omega_u t du = \frac{1}{2}\int_l \frac{\left(N_x \sin \omega_u t\right)^2}{GI_P} dx = \frac{1}{2}\int_l EA\left(\frac{du}{dx}\right)^2 dx \qquad (4.12)$$

The work is done by the external force acting in the lateral direction $F_z \sin \omega t$ can determined as:

$$U_v = \frac{1}{2}\int_l F_z \sin \omega_v t dv = \frac{1}{2}\int_l \frac{\left(F_z \sin \omega_v t.l\right)^2}{EI} dx = \frac{1}{2}\int_l EI\left(\frac{dv}{dx}\right)^2 dx \qquad (4.13)$$

When the work done by the longitudinal and lateral force is combined:

$$\int_1^f W dt = \int_1^f \left(U_u + U_v\right) dt = \int_1^f \left[\int_l EAu'^2 dx + \int_l EIv'^2 dx \right] dt \qquad (4.14)$$

The Eq. 4.15 can be determined with the virtual displacement formula,

$$\delta \int_1^f W dt = \int_1^f \int_l \left(EAu'\delta u' + EIv'\delta v' \right) dx dt \qquad (4.15)$$

According to the Hamilton's principle: $\delta\int_1^f (W-L)dt = 0$, Eq. 4.11 and Eq. 4.15 are combined and the Lagrange equation of motion dependent on time:

$$\begin{aligned}&\int_1^f (W-L)dt = \int_1^f \Big\{\int_l \big(EAu'\delta u' + EIv'\delta v'\big)dx - \\ &\int_l \Big[\rho A\big(\dot{u}\delta\dot{u} + \dot{v}\delta\dot{v}\big) + \rho I\dot{v}'\delta\dot{v}' - \\ &EA\left(u' + \frac{1}{2}v'^2\right)\big(\delta u' + v'\delta v'\big) - EIv''\,\delta v''\Big]dx\Big\}\,dt\end{aligned} \tag{4.16}$$

Adopting a subsection integral method, the above function can determined as:

$$\begin{aligned}&\delta\int_1^f (W-L)dt = \delta\int_l^f \Big\{\int_l \big(-EAu''\delta u dx - EIv''\delta v dx\big) - \\ &\Big[-pA\big(\ddot{u}\delta u dx + \ddot{v}\delta v dx\big) + \rho I\ddot{v}''\delta v dx + \\ &EA\left(u' + \frac{1}{2}v'^2\right)'\big(\delta u dx + v'\delta v dx\big) - \big(EIv''\big)''\,\delta v dx\Big]\Big\}\,dt\end{aligned} \tag{4.17}$$

According to the principle of Hamilton's principle, the above function can be given by:

$$\begin{cases}-\rho A\ddot{u} + EA\left(u' + \frac{1}{2}v'^2\right)' = -EAu'' \\ -\rho A\ddot{v} - \big(EIv''\big)'' + \rho I\ddot{v}'' + \left[EA\left(u' + \frac{1}{2}v'^2\right)'\right]v' = -EIv''\end{cases} \tag{4.18}$$

When the beam is modeled for the free coupled longitudinal and lateral vibration, the above formula can be rewritten:

$$\begin{cases}\rho A\dfrac{\partial^2 u}{\partial t^2} - EA\left(\dfrac{\partial^2 u}{\partial x^2} + \dfrac{1}{2}\dfrac{\partial v}{\partial x}\dfrac{\partial^2 v}{\partial x^2}\right) = 0 \\ \rho A\dfrac{\partial^2 v}{\partial t^2} + EI\dfrac{\partial^4 v}{\partial x^4} - EA\left[\dfrac{\partial^2 u}{\partial x^2}\dfrac{\partial v}{\partial x} + \dfrac{\partial u}{\partial x}\dfrac{\partial^2 v}{\partial x^2} + \dfrac{3}{2}\left(\dfrac{\partial v}{\partial x}\right)^2\dfrac{\partial^2 v}{\partial x^2}\right] = 0\end{cases} \tag{4.19}$$

4.2 Experimental Setup

Figure 2.4 presents how the experimental set-up is installed. Details of the experimental setup are given in Section 2 and therefore they will not be repeated in

this section. Fig. 4.2 presents measurement points, where the sensors transmitting the analog signals are located.

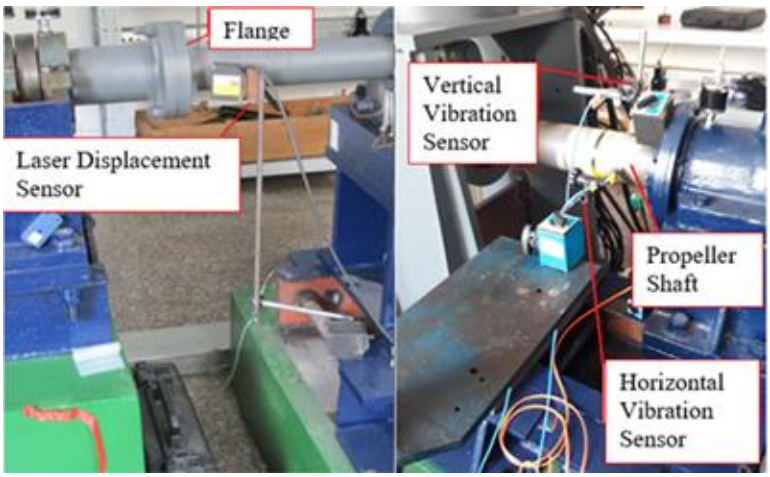

Figure 4.2 : Measurement points layout for the shaft longitudinal and lateral vibrations.

Fig. 4.2 shows the flange surface which is used to measure the longitudinal vibration selected by the laser displacement sensor (OPTEX CD33 with sensitivity; 3.33 V mm^{-1}) which takes the longitudinal vibration signal corresponding to the position of the shaft system. The measurement point for lateral vibration is located at the tail shaft and horizontal displacements of the tail shaft are made by using the eddy current sensors (ZA- 210803 with sensitivity; 3.33 V mm^{-1}). Possible errors due to the vibration are reduced by fixing the sensor position. Although shaft speed values are determined from 100 to 190 in 30 increments and frequencies and amplitudes for the shaft coupled vibrations are recorded for each speed—the measurements and results presented in Section 3.3 are only for 100 rpm.

Table 4.1 : Loadings for each rotational speed.

Rotational speed (rpm)	**100**	**130**	**160**	**190**
Longitudinal Force (N)	86	87	88.5	90
Vertical Force (N)	300	320	330	350
Horizontal Force (N)	300	320	330	350

The longitudinal and lateral stresses are collected for the external forces applied with regard to the displacements of the loading system. Applied displacements and measured longitudinal and lateral forces amplitudes are provided in Table 4.1.

4.3 Application and Discussion

The shaft system is modeled with a mass spring system with the help of Ansys APDL program. It is very difficult to solve the equation of motion by bringing it into matrix form and simplified with coupled vibration coefficient as given in Chapter 2 and Chapter 3. The geometrical properties of each part is given with Table 4.2. However, the shaft is modeled as a whole with the length L=2.66 m and diameter D=0.086 m.

Table 4.2 : The geometrical properties of the shaft segments.

Shaft No.	**1**	**2**	**3**	**4**
Length (m)	0.6	0.935	0.67	0.46
Diameters (m)	0.08	0.08	0.09	0.1

The coefficients c_x, c_y and c_z defining the longitudinal and lateral damping for each shaft are 60 Nm/s and 0.08 Nms/rad considered on the basis of the bearing properties. The stiffness coefficients k_x , k_y and k_z defining longitudinal and lateral stiffness are defined by 7×10^5 N/m and 1.7×10^5 N/m the help of bearing data. External forces on the shaft are given with $F_x(t) = F_{x_0}\sin(\omega t)$, $F_y(t) = F_{y_0}\sin(\omega t)$, $F_z(t) = F_{z_0}\sin(\omega t)$. $F_{x_0}, F_{y_0}, F_{z_0}$ are external forces measured from tail shaft and they have different amplitude at different rotational speeds. The properties of the propulsion shaft used during modeling with Ansys Apdl is given in Table 4.3.

Table 4.3 : Properties of the propulsion shaft.

Property	Value
Length	2.665 m
Diameters	0.083 m
Density , ρ	7850 kg/m^3
Elastic modulus , E	210 GPa
Shear modulus , G	77 GPa
Poisson's ratio, ν	0.3
Rotational speed	100-190 rpm

4.4 Numerical Simulation

The finite element is universally used in the design and analysis of complex ship structures (Tian Ran et al.,2009). The FEA software ANSYS APDL was used to

simulate the coupled longitudinal-lateral vibration of the experimental setup. The external forces and rotational speed of numerical simulation were defined the same as in the experiment. The simulation was performed at 0.001-second intervals for 10 seconds since data acquisition from the experimental setup was performed at intervals of 0.001 seconds.

The experiment data is obtained for only time-dependent displacements at different rotational speeds and external loads therefore the simulation results were obtained for transient analysis. In this study, the propulsion shaft system consists of 4 different shafts. But in numerical modeling, the shafts are considered as a whole, and the system is modeled with one end fixed and the other end free. The vibration behavior of the shaft system given in Table 4.3 has been investigated. The finite element model of the shaft system was constructed by using Beam 188 and Combine 214 element was used to define bearings. The propeller was simulated by external forces at the end of the tail shaft and the value of the external forces for each speed are given in Table 4.1.

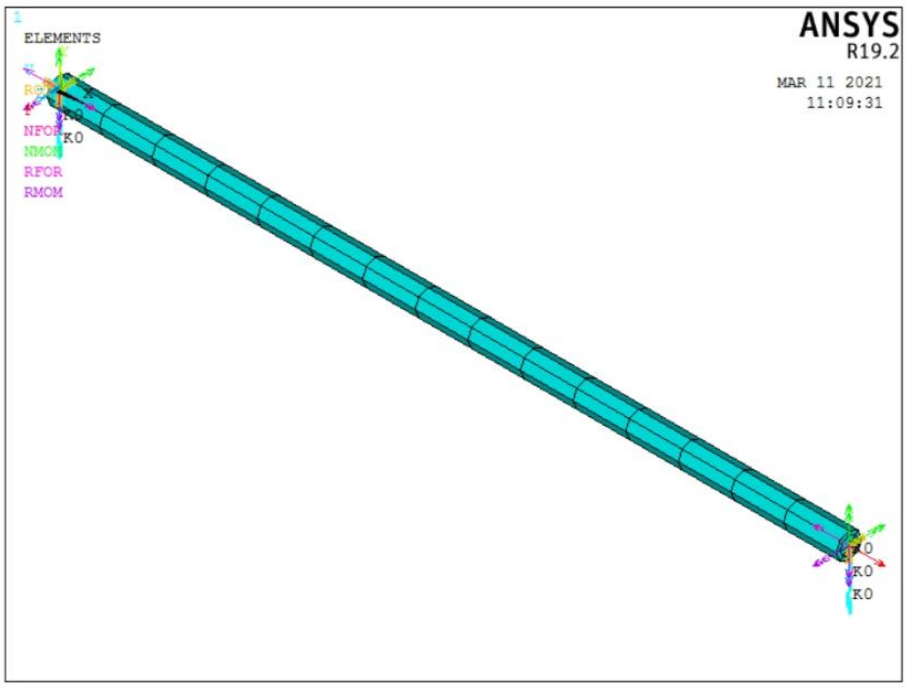

Figure 4.3 : Finite element model with boundary conditions.

The acceleration value for the shaft is defined to give the coupled vibration effect in the Ansys-Apdl program (Huang et al.,2015). The acceleration values are calculated with the help of each shaft speed which is defined during the experiment. Transient analysis is used to determine the dynamic response of a shaft under a time-varying load.

4.5 Verification

Figure 4.4 , Figure 4.5, and Figure 4.6 indicate the difference in coupled longitudinal-lateral vibration of the numerical model with the experiment at 100 rpm shaft speed. In this section, the aim is to observe the validity of the numerical method by looking at the error margins with the experiment. Besides, excitation frequency are compared with the experiment in three directions.

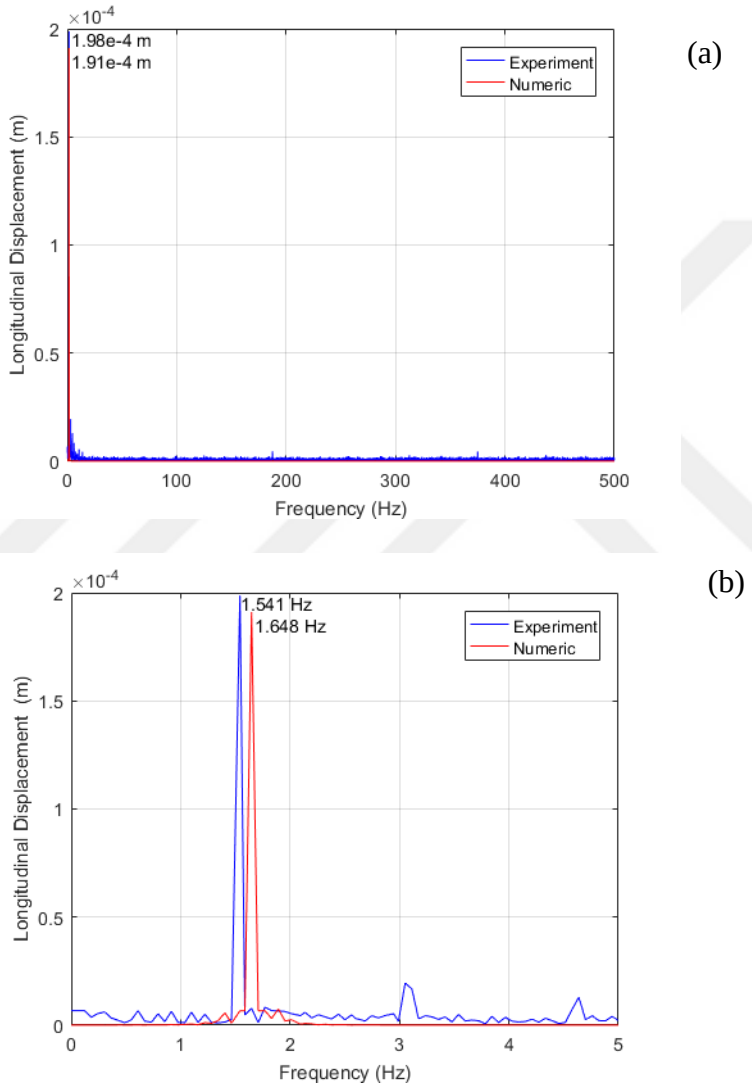

Figure 4.4 : Longitudinal displacements results (a) at 100 rpm (b) between 0-5 Hz.

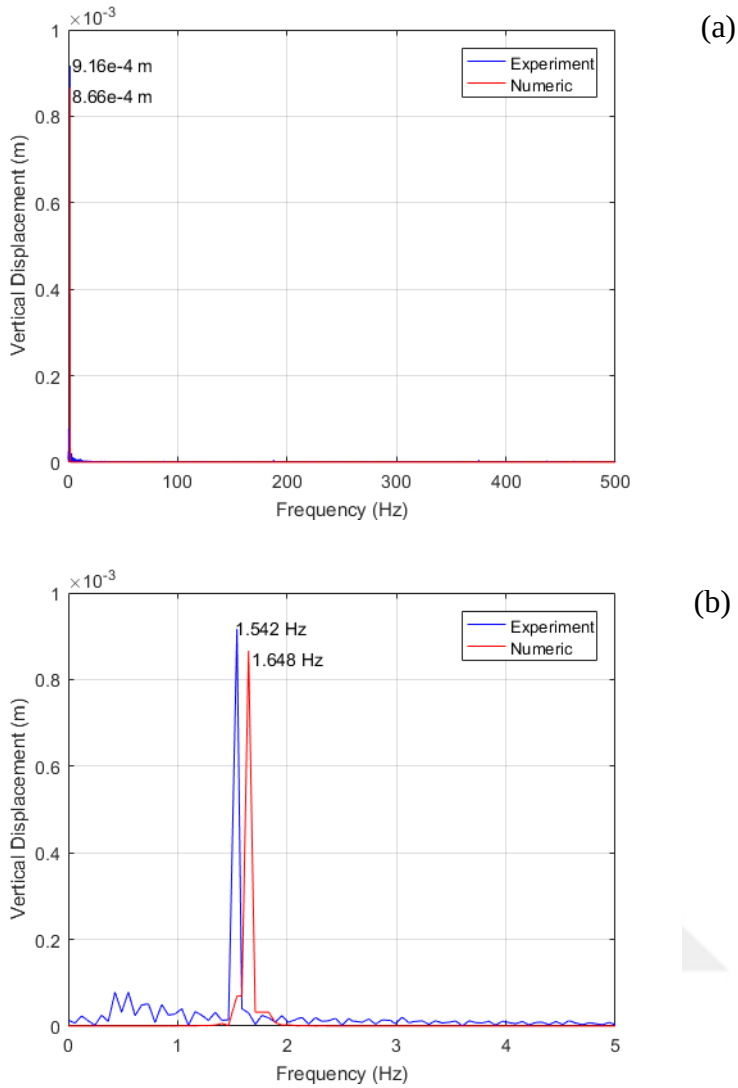

Figure 4.5 : Vertical displacements results (a) at 100 rpm (b) between 0-5 Hz.

Figure 4.4 indicates the displacements in longitudinal direction of experiment and numerical model at 100 rpm. While the longitudinal displacement is 1.98×10^{-4} m at 1.541 Hz for experiment, the numerical result is 1.91×10^{-4} m at 1.648 Hz. The time step was kept the same with the experiment data in the graph shown in Fig.4.4 (a) to avoid errors in comparisons with the experiment, so even though the maximum displacements are seen before 5 Hz, the frequency range continues up to 500 Hz. Figures 4.5 and 4.6 show the vertical and horizontal displacements of the experiment and numerical model at 100 rpm. While the vertical displacement for the experiment is 9.16×10^{-4} m at 1.542 Hz, the numerical result is 8.66×10^{-4} m at 1.648 Hz, and the horizontal displacement is 9.16×10^{-4} m at 1.542 Hz, the numerical result is 8.66×10^{-4} m at 1.648 Hz.

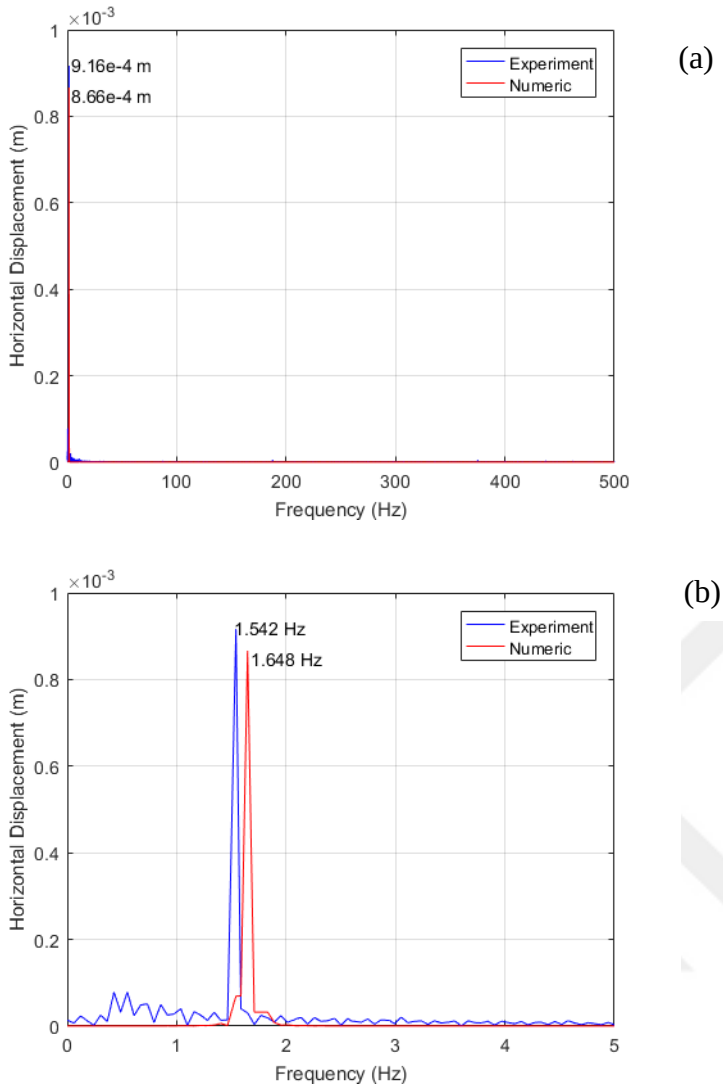

Figure 4.6 : Horizontal displacements results (a) at 100 rpm (b) between 0-5 Hz.

It is discovered that the numerical model's displacements in all three directions are lower than the experimental data. Despite the margin of error, the frequency values corresponding to the maximum displacement are similar, indicating that the numerical model produces a similar result to the experimental data.

4.6 Verification at Various Speed Range

Figures 4.7, 4.8, and 4.9 show the difference in coupled longitudinal-lateral vibration of experiment and numerical models as rotational speed increases. The goal of this section is to examine the error margins of the experiment at various shaft speeds to determine the validity of the numerical method. Figure 4.7 indicates that the maximum displacement values are 1.91×10^{-4} m, 1.93×10^{-4} m, 1.96×10^{-4} m to 1.99×10^{-4} m for

longitudinal direction and 8.66×10^{-4} m, 9.29×10^{-4} m, 9.62×10^{-4} m to 1.02×10^{-3} m for lateral direction.

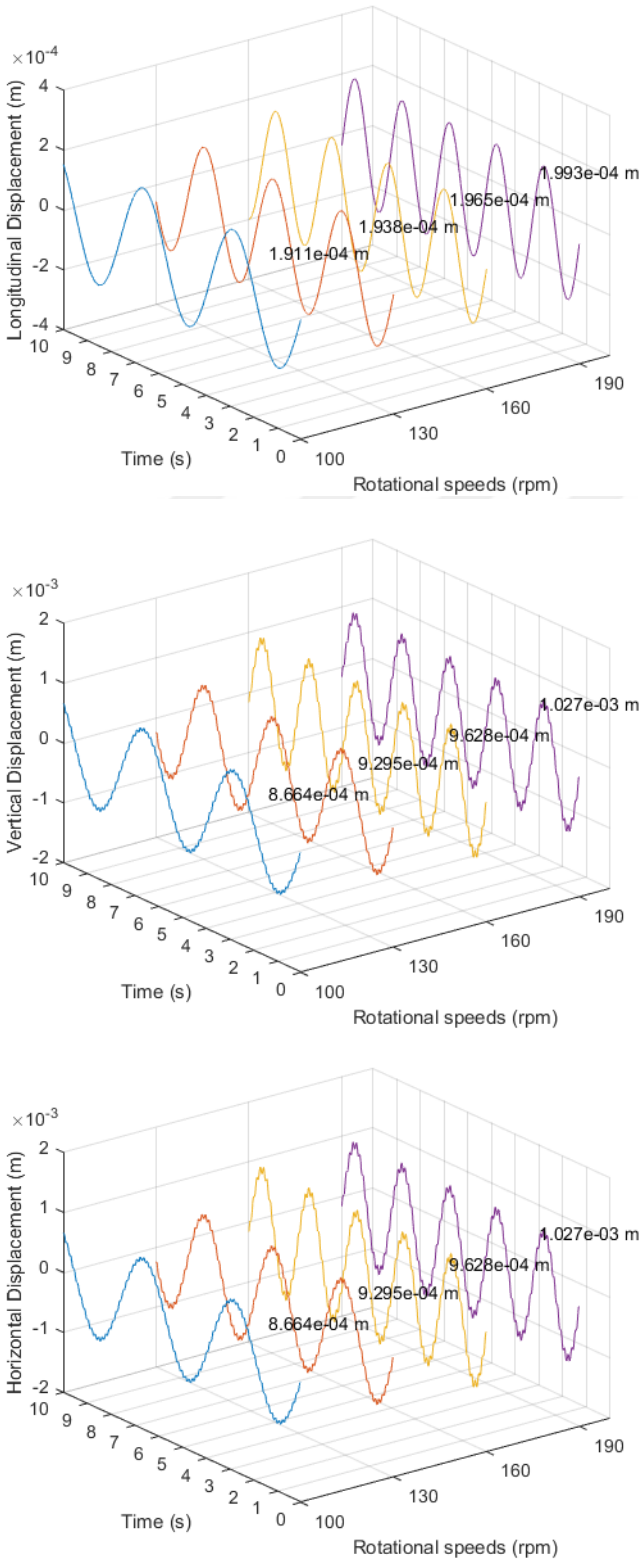

Figure 4.7 : Numerical results between 100-190 rpm (a) longitudinal (b) vertical (c) horizontal

(a)

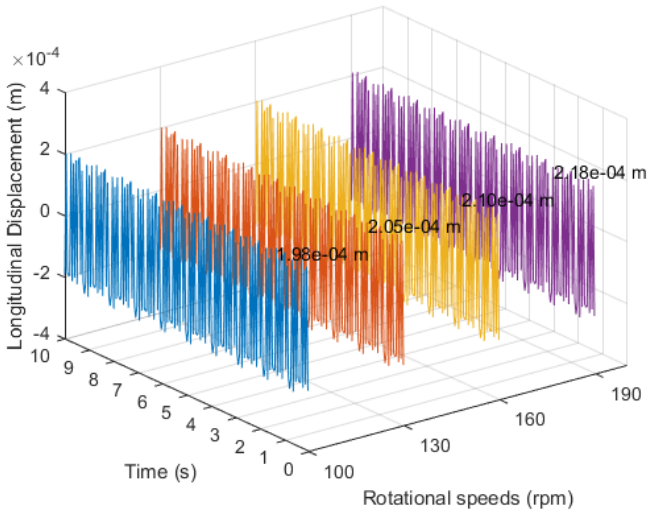

(b)

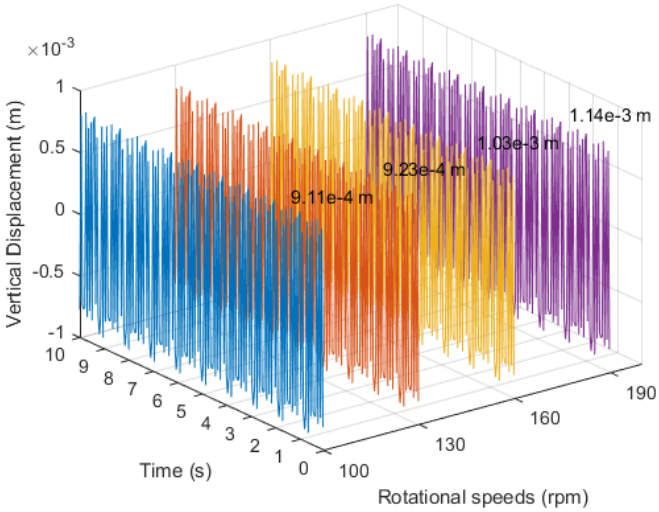

(c)

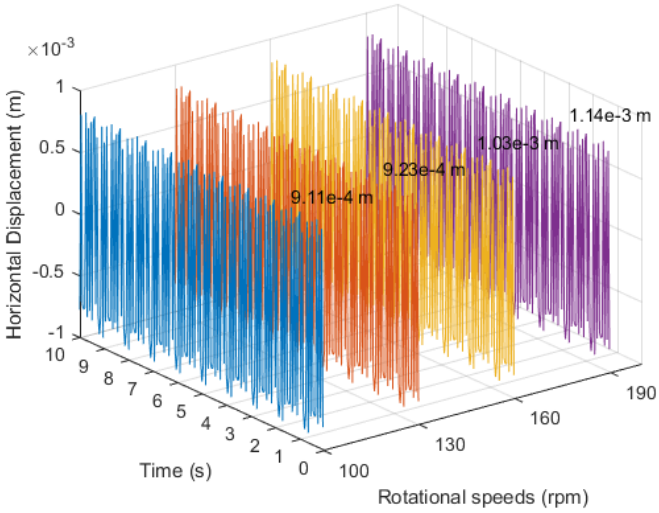

Figure 4.8 : Experimental results between 100–190 rpm (a) longitudinal (b) vertical (c) horizontal.

Figure 4.8 shows that the maximum displacement values are 1.98×10^{-4} m, 2.05×10^{-4} m, 2.10×10^{-4} m to 2.18×10^{-4} m for longitudinal direction and 9.11×10^{-4} m, 9.23×10^{-4} m, 1.03×10^{-3} m to 1.14×10^{-3} m for lateral direction. Since the results are the same for vertical and horizontal direction, they are given with lateral direction title. Additionally, with an increase of the rotational speed and external force; the displacement values in both axes increased at a similar rate. To investigate the error generated during the testing process, the numerical solution of the vibration result and the test value are analyzed and compared, and the test error of each set of test data is provided in Table 4.4. Despite the fact that the shaft experimental platform has four shafts, numerical simulations treated them as if they were one. Also, the experimental setup includes three bearings, but the numerical model only takes into account two of them. These distinctions increase the error rate between the numerical model and the experiment.

Table 4.4 : Error margin for each rotational speed.

Speed (rpm)	Longitudinal disp.(%)	Lateral disp.(%)
100	4	5
130	6	2
160	7	6
190	10	11

Table 4.5 : Naturel frequencies predicted by the coupled and uncoupled form (Hz).

Coupled	Uncoupled
76	76
14	14
14	14

Table 4.5 shows that the natural frequencies are 14 hertz (Hz) in the vertical direction, 14 hertz (Hz) in the horizontal direction, and 76 hertz (Hz) in the longitudinal direction. Previous research has shown that the numerical model is applicable to the coupled longitudinal-lateral vibrations of the shaft. The natural frequency values of the system were obtained with Modal analysis by selecting 3 modes and scanning the range of 0.5-500 Hz. Table 4.5 displays the system's natural frequencies in both coupled and uncoupled forms, and it is clear that the coupling effect has no impact on the natural frequency.

4.7 Different Parameter Efffects to the Coupled Longitudinal-Lateral Vibration

The numerical model was primarily developed by focusing on the shaft's length-to-diameter ratio, damping coefficient, stiffness coefficient, and angular velocity. The results were compared by varying certain proportions and observing the effects of these changes on the model's vibration behavior. Other parameters were held constant while each parameter was examined, and the studied parameter was examined for 5 different scenarios.

4.7.1 Coupling effect

With the study given above, after proving the validity of the numerical model under different shaft speeds and external forces, the coupled vibration effect is investigated in three axes. In Figure 4.9; longitudinal vibration amplitudes are given for coupled and uncoupled vibration forms at 100 rpm shaft speed. It is seen that the coupling effect has no impact on longitudinal displacement.

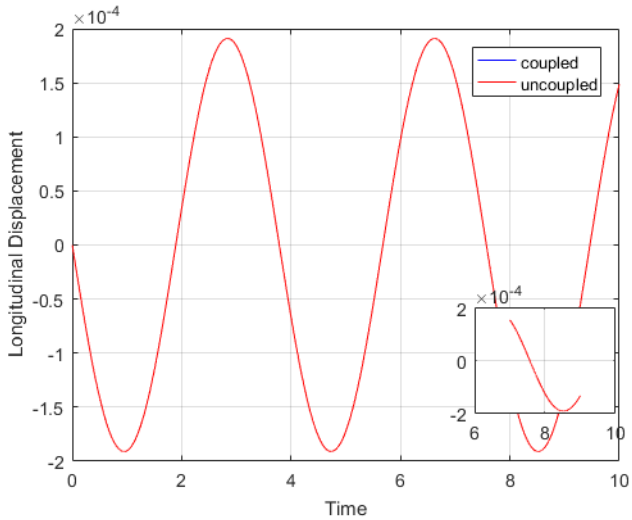

Figure 4.9 : Longitudinal displacement for coupled and uncoupled form.

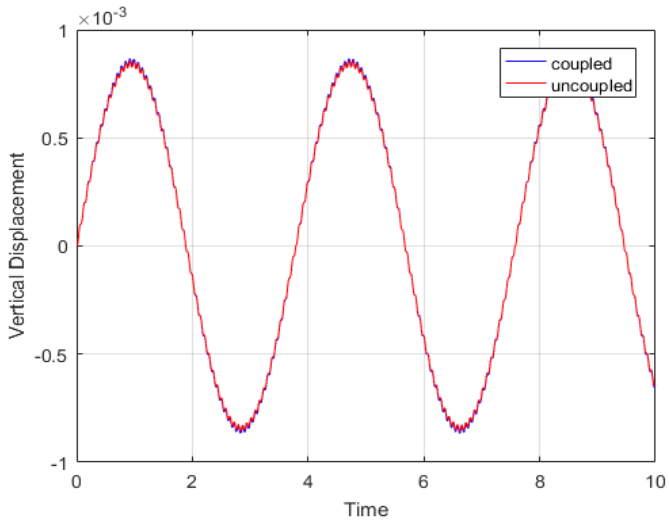

(a)

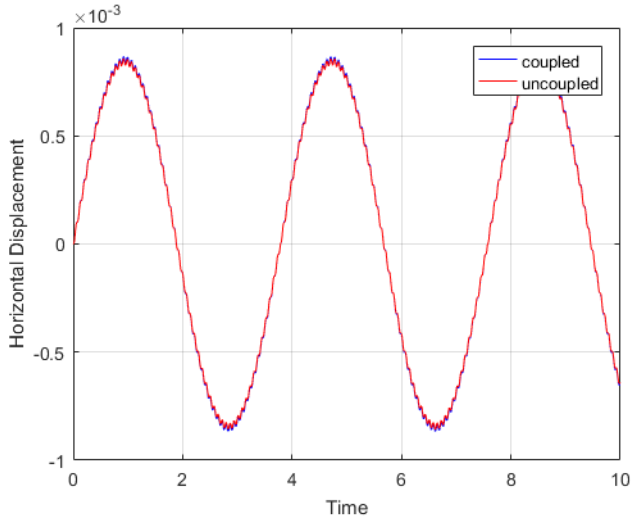

(b)

Figure 4.10 : Lateral displacement for coupled and uncoupled form (a) vertical (b) horizontal.

The coupled vibration effect resulted in an increase of approximately 0.2 percent in the vertical and horizontal axes, but had no effect on the longitudinal vibration.

4.7.2 Effect of the diameter and length ratio of the shaft

The diameter of the shaft was kept constant to observe the effect of the shaft length parameter, varying by %10 as given in Figure 4.11, on the coupled longitudinal-lateral vibration. Since the horizontal and vertical axes give the same result, they are represented by “y” and longitudinal vibration is represented by “x” in this section.

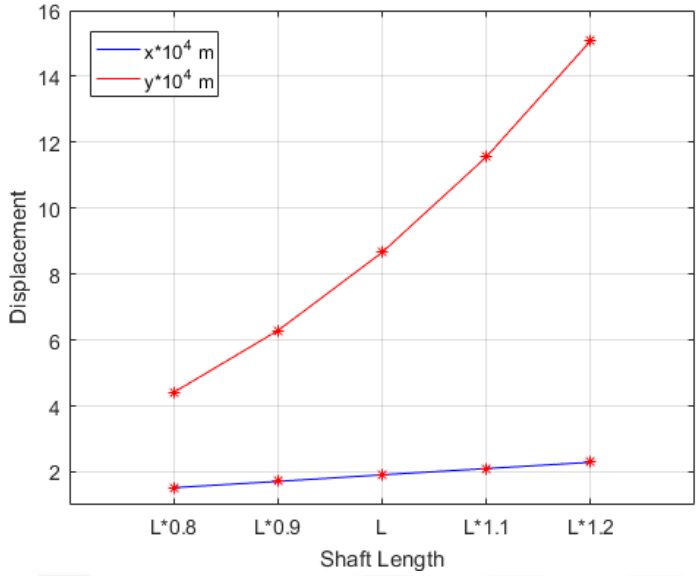

Figure 4.11 : Displacements for different shaft length.

The longitudinal vibration was increased by 10%, and the lateral vibration was increased by approximately 25%, while the shaft length was increased by 10%. Because coupled vibration is more effective on lateral displacement, increasing shaft length has a greater influence on lateral vibration. As a result, the length change ratio cannot be directly related to lateral displacement.

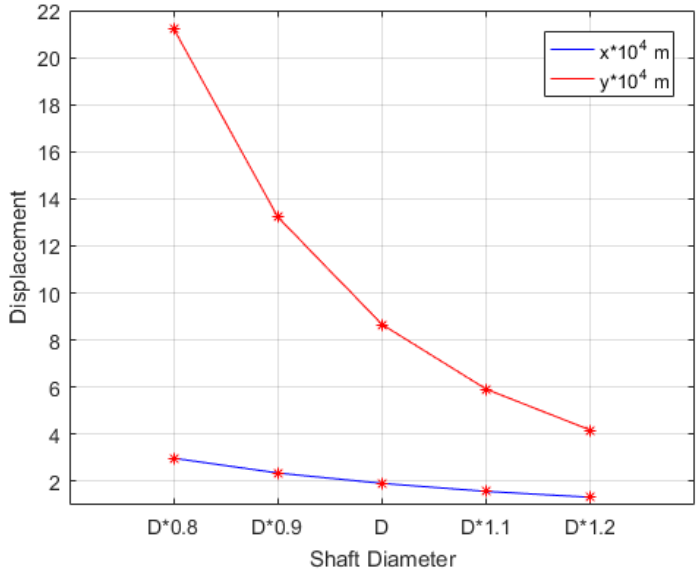

Figure 4.12 : Displacements for different shaft diameter.

Figure 4.12 elaborates the vibration amplitudes in three axes with varying diameters. It is observed that the vibration amplitudes changed proportional to the length ratio of the shaft, while they changed in inverse to diameter change of the shaft. The

longitudinal vibration was reduced by approximately 25%, and the lateral vibration was reduced by 50%, while the shaft diameter increased by 10%. Because coupled vibration is more effective on the lateral axis, an increase in shaft diameter has a greater influence on lateral displacement. As a result, displacement values on both axes are not directly related to the diameter change ratio.

4.7.3 Effect of stiffness and damping coefficient ratio

Stiffness and damping coefficients are important factors in the optimization of the shaft system. In this study, these two values are defined with the help of the bearing parameters of the shaft. However, in order to observe the effect of these factors on the coupled longitudinal-lateral vibrations, the stiffness and damping coefficient are changed at a certain ratio, the other values kept constant.

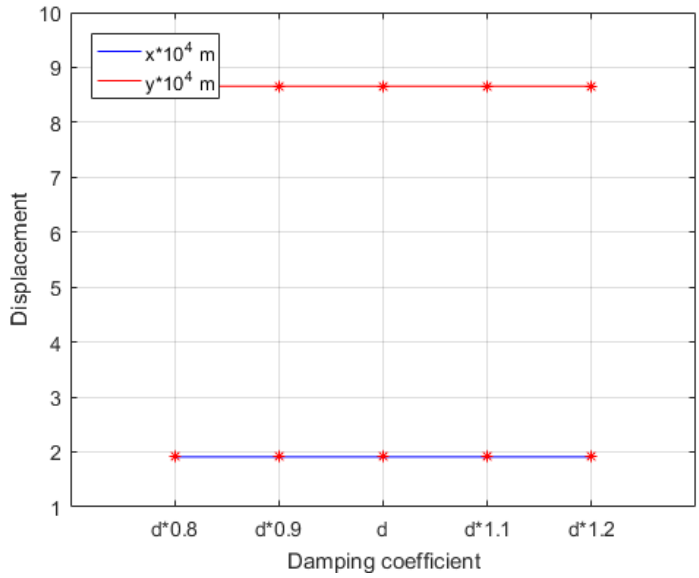

Figure 4.13 : Displacements for different damping coefficients.

In Figure 4.13, while the stiffness values were kept constant, the damping coefficient values were changed at different rates for 100 rpm shaft speed and its effect on the system was examined. The change in the damping coefficient has no effect on the system, because the damping coefficient values are very low due to they are obtained from the shaft parameters. Since the damping coefficient in all axes "d_x, d_y, d_z" has no effect on the system, all damping coefficients are symbolized by d on the figure.

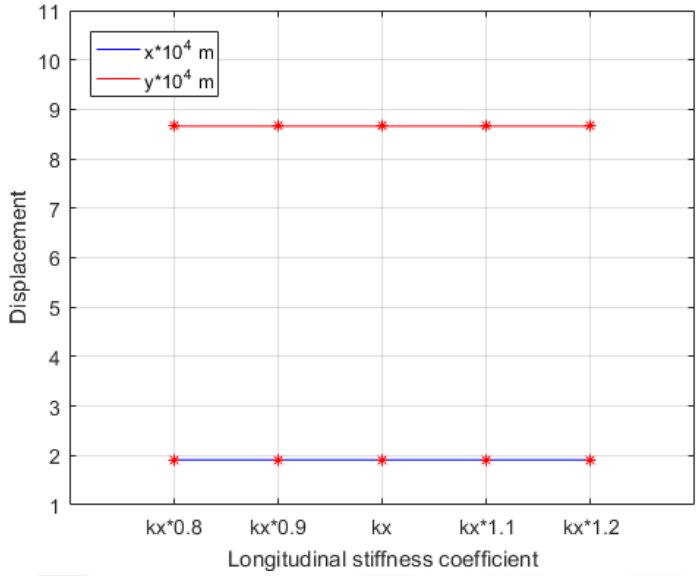

Figure 4.14 : Displacements for different longitudinal stiffness coefficients.

In Figure 4.14, vibration amplitudes occurring when the "k_x" longitudinal stiffness coefficient value is changed at 100 rpm speed value at different rates were given and it was observed that there is no change in the longitudinal and lateral displacement value.

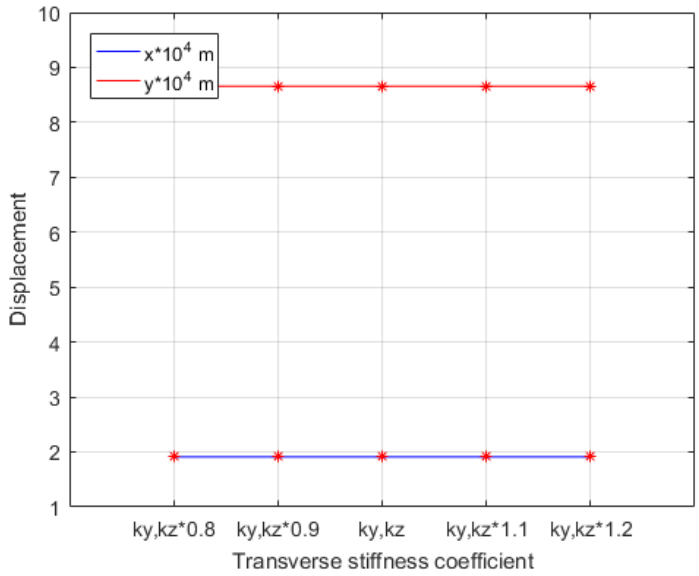

Figure 4.15 : Displacements for different lateral stiffness coefficients.

In Figure 4.15, the vibration occurring when the k_y, k_z lateral stiffness coefficients are changed at 100 rpm speed value at different rates were given and it was observed that results are stable for all three direction with the increase of coefficient. The longitudinal and lateral displacements did not change with the stiffness ratio, as shown

in Figures 4.14 and 4.15. As a result, the change in the stiffness value provided from the bearings data was insignificant.

4.7.4 The effect of the coupling coefficient

The angular velocity values are defined with the help of each shaft speed and they are 10.47 s^{-1}, 13.61 s^{-1}, 16.75 s^{-1} and 19.89 s^{-1} . In Figure 4.16, each acceleration value is symbolized with $\omega_1, \omega_2, \omega_3$ and ω_4 , respectively.

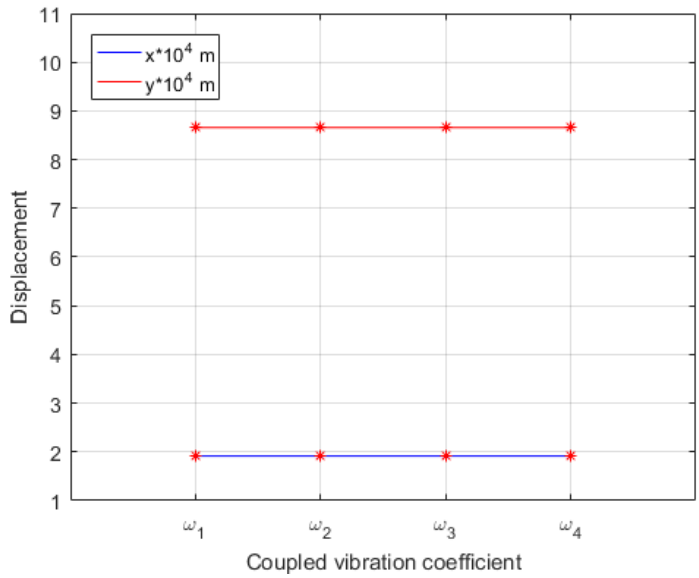

Figure 4.16 : Displacements for different coupled vibration coefficient.

As shown by Figure 4.16, when coupled vibration coefficient value is changed in different proportions, there is no change in the displacement values. While the coupled longitudinal and lateral vibration was modeled with the Ansys Apdl program, the coupled vibration effect was provided by angular velocity. However, the change in acceleration value does no effect the coupled longitudinal-lateral vibration. As a result, the coupled vibration effect which is numerically modeled without considering torsional angle is very low in the system. The torsional angle provides the interaction between all three axes.

4.8 Results

The dynamic behaviors of coupled longitudinal-lateral vibration for propulsion shaft systems subjected to longitudinal and lateral forces are modeled. The dynamic

response of the system with displacements for different shaft speed are discussed in detail. Some conclusions are obtained as fallow:

The equation of motion of the system has not been sufficiently simplified and reduced to a coupled vibration coefficient and brought into matrix form. As a result, a numerical model has been obtained with the help of the Ansys Apdl program, and coupled vibration effect is given with angular velocity. The maximum displacement values and frequency response of the numerical model are firstly compared with the experiment at 100 rpm shaft speed. The validity of the numerical model at 100 rpm was proved. The process was repeated at different shaft speeds to show the validity of the numerical model and similar error margins showed the validity of the numerical model. When the coupling effect is investigated, the coupled vibration effects on lateral vibration and longitudinal direction are too small to be ignored. The displacement amplitudes increase in both directions with the increase in length of the shaft, it decreases with an increase in diameter. The displacements are directly proportional to the length change rate of the shaft and change at an equivalent rate and while it changes in inverse proportion to the diameter rate. The effect of the diameter rate is larger and it has been seen that it cannot be directly associated with the displacement rate. The change of damping and stiffness coefficient value has been shown to not affect the system which stems from the fact that the values are quite small.

5. CONCLUSION

In this thesis, torsional, longitudinal, and lateral vibrations and their coupled forms occurring in a marine propulsion and shaft system are comprehensively investigated. It is very difficult to model numerically the vibrations occurring in 3 axes and the error percentages also increase because of the coupling requirements. For this reason, it is decided the coupled vibration analysis to be modeled numerically taking into account the interaction of the two axes with each other. Therefore; the coupled torsional-longitudinal, torsional-lateral, and longitudinal-lateral vibrations of the shaft system are presented, respectively. The numerical model's accuracy for the coupled vibrations of the torsional-longitudinal, torsional-lateral, and longitudinal-lateral types was validated and tested by comparing the findings with those of an experimental setup that is a smaller representative model of a marine propulsion shaft system. Using the experimental opportunity at the Wuhan University of Technology, numerical findings were compared using time-dependent displacement values at different shaft speeds. The only shortcoming in the experimental setup is that any scaled propeller could not be mounted at the free end of the propulsion shaft. However, a loading system was used in place of it to obtain the inertia forces created by the propeller.

In Chapter 2, the coupled torsional-longitudinal vibrations were subjected. At first, the numerical model was needed to be proven valid by comparing the experimental results according to the maximum displacement and the frequency response at different shaft speeds and so done. For this purpose, uncoupled and coupled torsional and longitudinal vibrations were studied and the coupling effect was then investigated. It is observed that the effect of the coupled vibration on the torsional angle to be dominant with comparing to the longitudinal displacement. In addition, the change in stiffness coefficient, damping coefficient, coupling coefficient, and the length-diameter ratio of the shaft on the vibration amplitudes was also examined in the case of the coupled torsional-longitudinal vibration. The torsional and longitudinal stiffness coefficients are calculated by the parameters of the propulsion shaft and are inversely proportional to the length of the shaft. It is noticed that the vibration amplitudes are increased with

an increase in the torsional stiffness value but in longitudinal vibration, the effect is too small to be seen on the graph. Normally, the vibration amplitudes are expected to decrease with the increase in the stiffness value, but it is accepted that the shaft length is shortened in order to increase the stiffness coefficient. As the shaft length decreased, the moment of inertia and mass value of each shaft segment decreased, and they were more dominant than the stiffness coefficient. Thus, the vibration amplitudes increased contrary to expectations. The change in the longitudinal stiffness coefficient did not affect both axes. The reason is that the longitudinal stiffness coefficient is approximately a hundred times smaller than the torsional stiffness. As a result, the effect on the system is so small as to be negligible. After that, it is noticed that there is a directly proportional relationship between the vibration amplitudes and the changes at the shaft length while it is inversely proportional between the amplitudes and the diameter changes. Furthermore, when the calculated vibration amplitudes are examined, it is observed that the effects of the changings in the shaft diameter on the vibration amplitudes at both axes are highly more than those of length changings. It is caused by; while the moment of inertia has the shaft diameter to the power of four, the mass value includes the square of the shaft diameter value. Also, the length of the shaft is not as effective as the diameter value. As a result, the change in the diameter of the shaft is a more effective parameter on the variation of the coupled vibration amplitudes compared to the change in shaft length. Besides, the diameter change of the shaft is more effective on the torsional vibration for the same reason. Classification societies publish some essential requirements and resolutions about torsional vibration, in special. For example, DNV is a leading classification society and also a member of the IACS-International Association of Classification Societies. Since the allowable torsional vibration stress under DNV rules is greater than the torsional stress experienced by the system, no anti-vibration measures are recommended in the system.

Chapter 3 examines the coupled torsional-lateral vibrations. Coupled torsional-lateral vibrations cause the axial displacement between the center of mass and the center of the lateral section of the shaft as a result of the axial forces affecting the shaft and imbalances during rotational movement. The equation of motion is based on the Energy Method by considering a misalignment occurring in the shaft system. Equation of motion can be represented in matrix form by utilizing the coefficients for coupled vibration. Those coefficients are given in detail in the literature for the coupled

torsional-lateral vibration. Firstly, the validity of the numerical model was proved by comparing the experimental results with using the maximum displacement and excitation frequency at different speed values. The uncoupled/singular and coupled torsional and lateral vibrations were examined and the effect of coupled vibration given in detail and the effect was seen to dominate on torsional vibration. In addition, in order to examine the effect of factors such as eccentricity of cross-section, damping coefficient, stiffness coefficient, and the length-diameter ratio of the shaft in the numerical model, the displacement values in all three axes are given by changing them at different rates. With the increase in the length of the shaft, vibration amplitudes increase on all three axes, while the shaft diameter decreases as it increases. The displacements are directly proportional to the length change of the shaft and vary in the equivalent proportion, but the diameter ratio has a higher effect when changing inversely with the diameter change and cannot be directly associated with the displacement values. The reason is; the impact ratio of the shaft diameter is higher than shaft length in the equations of motion. It has been observed that the change of damping coefficient does not affect the system, which is due to the fact that the damping coefficient values are quite small. When the effect of the change in the value of the stiffness coefficient was examined, it was observed that the change in horizontal-vertical stiffness values did not affect the torsional angle, while the change in the torsional stiffness value did not affect horizontal-vertical displacement values. As a result of this finding, it was determined that the eccentricity of the cross-section value used in the numerical method and obtained from the literature is not sufficient to capture the coupled vibration effect and will vary in each shaft system. A new eccentricity of cross-section value has been proposed for the experimental setup, which both reduces the error rate and shows the coupled vibration effect. Consequently, the importance of accurately defining the eccentric coefficient value was observed. Also, the solution is not recommended to reduce the torsional vibration amplitudes while they are much smaller than the maximum values allowed by DNV.

Chapter 4 the coupled longitudinal-lateral vibration was subjected. In longitudinal-lateral vibration, the equation of motion was created with the Energy Method based on axial displacement occurring in the propeller shaft system as a result of axial forces that act on the propeller shaft system. However, the equation of motion is too complex to be simplified to coupled vibration coefficient. As a result, a numeric model was

created using the Finite element method and numerically modeled with the help of the Ansys APDL program, and coupled vibration effect is defined with angular velocity. Firstly, the validity of the numerical model was proved by comparing the experimental results with using the maximum displacement and excitation frequency at different speed values. The maximum displacement results under the external force were obtained with the transient solution depending on the shaft speed and time. The effect of parameters such as the length, diameter of the shaft and stiffness coefficient, damping coefficient of the bearings in the numerical method for coupled longitudinal-lateral vibrations were also examined. The effect of the coupled vibration on the lateral vibration to be dominant with comparing to the longitudinal displacement. The effect of the change in the stiffness and damping coefficients in both direction were examined. Since; the stiffness values are obtained from bearing data and they are to small to have an impact, it was observed that there was no difference in the maximum displacement values. There is a directly proportional relationship between the vibration amplitudes and the changes at the shaft length while it is inversely proportional between the amplitudes and the diameter changes. Additionally, when the calculated amplitudes are examined, it is observed that the effects of the changings in the shaft diameter on the longitudinal vibration at both axes are highly more than those of length changings. Finally, with the increase, angular velocity was examined, and it was discovered that angular velocity was also too small to have an impact.

The damping and stiffness coefficient has been attempted to be calculated in the numerical model by taking into account the impact variables during the experimental calculation. Equations of motion for coupled vibration cases were derived using specific coefficients defined in the literature on coupled vibration analysis. Furthermore, the shaft experimental platform has four shafts, but numerical simulations treated them as a single shaft. The mean-variance would increase as a result of differences in the operating state, the method of acquiring the displacement values, and the structural properties. Despite these issues, the amount of variance for all coupled vibration forms is less than 20%. Deviations should be accepted, and any numerical method's applicability should be accepted.

The most dangerous vibration form for a propulsion shaft system is torsional vibration, so measurement of torsional vibration amplitudes is recommended by classification societies. However, it was discovered that coupled torsional-longitudinal vibrations

increased torsional angle values by 56%, while torsional-lateral vibrations increased by 4%. Furthermore, coupled vibration has the greatest impact on torsion angle vibration. It was established that examining torsional vibration in the shaft system alone would be insufficient and that the torsional angle values would vary due to the coupled vibration effect. Furthermore, for all coupled vibration types that occur on the system, the coupled vibration does not affect the system's natural frequencies.

REFERENCES

Al-Bedoor, B.O. (2001). Modeling the coupled torsional and lateral vibrations of unbalanced rotors. *Computer Methods in Applied Mechanics and Engineering, 190* (45):5999-6008.

Arafat, H.N., Nayfeh, A.H., Chin, C. (1998). Nonlinear nonplanar dynamics of parametrically excited cantilever beams. *Nonlinear Dyn. 15*:31-61.

Benham, P., Crawford, R., Armstrrong, C. (1996). *Mechanics of Engineering Materials.*

Brydum, L., Jakobsen, S.B. (1987). Vibration characteristics of two-stroke, low speed diesel engines. *MAN B&W Diesel a/s, Copenhagen pp*. 1-16.

Chahr-Eddine, K., Yassine, A. (2014). Forced axial and torsional vibrations of a shaft line using the transfer matrix method related to solution coefficients. *Journal of Marine Science and Application 13*(2):200-205.

Chen, F., Chen, Y., Hua, H. (2020). Coupled vibration characteristics of a submarine propeller-shaft-hull system at low frequency. *J. Low Freq. Noise Vib. Act. Control. 39*(2):258–279.

Chen, Y., Wang, L., Hua, H.X. (2017). Longitudinal vibration of marine propeller-shafting system induced by inflow turbulence, *J. Fluids Struct. 68*:264–278.

Dai, L., Zhang, Z., Sun, D. (1989). A study on axial, later and torsional coupled vibration of marine propulsion system with transfer matrices method (in Chinese). *Ship Build. China, 04*:98–106.

Das, A.S., Dutt, J.K., Ray, K. (2011). Active control of coupled flexural-torsional vibration in a flexible rotor–bearing system using electromagnetic actuator. *International Journal of Non-Linear Mechanics, 46*:1093–1109.

Du, H., Chen, Z., Jing, B. (1992). The mathematical model for the coupled torsional-axial vibration of internal combustion engine shaft system (in Chinese). *Chin. Intern. Combust. Engine Eng. 13*(2): 66–74.

DNV Rules For Classification Ships Edition. (2015). Part 4 Systems and components Chapter 2 Rotating machinery, General, Available from: https://rules.dnvgl.com/docs/pdf/DNVGL/RU-SHIP/2015-10/DNVGL-RU-SHIP-Pt4Ch2.pdf)

Firouzi, J., Ghassemi, H., Shadmani, M. (2021). Analytical model for coupled torsional-longitudinal vibrations of marine propeller shafting system considering blade characteristics. *Applied Mathematical Modelling, 94*:737-756.

Gan-bo, Z., Yao, Z. (2012). Reduced-order Modeling Method for Longitudinal Vibration Control of Propulsion Shafting. *2'nd International Conference on Mechanical, Industrial, and Manufacturing Engineering. IERI Procedia, 1*:73 – 80.

Gayen, D., Chakraborty, D., Tiwari, R. (2017). Finite element analysis for a functionally graded rotating shaft with multiple breathing cracks. *International Journal of Mechanical Sciences, 134*:411–423.

Ghayesh, M.H., Kazemirad, S., Amabili, M. (2012a). Coupled longitudinal-transverse dynamics of an axially moving beam with an internal resonance. *Mechanismand Machine Theory, 52*:18–34.

Ghayesh, M.H., Amabili, M., Paidoussis, M. (2012b). Nonlinear vibrations and stability of an axially moving beam with an intermediate spring support: two-dimensional analysis. *Nonlinear Dynamics, 70*:335–354.

Ghayesh, M.H., Amabili, M. (2013). Nonlinear vibrations and stability of an axially moving Timoshenko beam with an intermediate spring support. *Mechanismand Machine Theory, 67*:1–16.

Ghayesh, M.H. (2012c). Coupled longitudinal–transverse dynamics of an axially accelerating beam. *Journal of Sound and Vibration, 331*:5107–5124.

Han, H., Lee, K., Jeon, S. H., Park, S. (2017). Lateral-torsional coupled vibration of a propulsion shaft with a diesel engine supported by a resilient mount. *J. Mech. Sci. Technol. 31*(8):3727–3735.

Han, H., Lee, K. (2019). Experimental verification for lateral-torsional coupled vibration of the propulsion shaft system in a ship. *Engineering Failure Analysis, 104*:758-771.

Han, S.M., Benaroya, H. (2000a). Non-linear coupled transverse and axial vibration of a compliant structure, Part 1: formulation and free vibration, *Journal of Sound and Vibration, 237*: 837–873.

Han, S.M., Benaroya, H. (2000b). Non-linear coupled transverse and axial vibration of a compliant structure, Part 2: forced vibration. *Journal of Sound and Vibration, 237*:875–900.

Hong, J., Yu, P., Ma, Y., Zhang, D. (2020). Investigation on nonlinear lateral-torsional coupled vibration of a rotor system with substantial unbalance. *Chinese Journal of Aeronautics Volume, 33*(6):1642-1660.

Huang, Y., Horng, C. (1999). Analysis of torsional vibration systems by the extended transfer matrix method. *J. Vib. Acoust. 121* (02):250–255.

Huang, Q., Yan, X., Wang, Y., Zhang. C., Jin. Y. (2016). Numerical and experimental analysis of coupled transverse and longitudinal vibration of a marine propulsion shaft. *Journal of Mechanical Science and Technology, 30* (12):5405-5412.

Huang, Q., Yan, X., Wang, Y., Zhang, C., Wang, Z. (2017). Numerical modeling and experimental analysis on coupled torsional-longitudinal vibrations of a ship's propeller shaft. *Ocean Engineering, 136*:272–282.

Huang, Q., Yan, X., Zhang, C., Zhu, H. (2019). Coupled transverse and torsional vibrations of the marine propeller shaft with multiple impact factors. *Ocean Engineering, 178*:48-58.

Huang, Q., Zhang, C., Liu, J., Yan, X. (2015). Transient Analysis of Coupled Longitudinal and Transverse Vibration of Large Container Ship Propulsion Shafting. *ASME 2015 34th International Conference on Ocean. Offshore and Arctic Engineering.* May 31- June 5.

Jang, M., Kim, U., Park, Y., et al. (2004). A study on the coupled torsional-axial vibration of marine propulsion shafting system using the energy method. *J. Korean Soc. Mar. Eng. 03*:482–492.

Kang, W., Zhang, Z. , Zhou, K. , Chen, Y. (2019). The random vibration and force transmission characteristics of the elastic propeller-shafting system induced by inflow turbulence. *Ocean Eng. 188*(15):106317.

Kouroussis, G., Verlinden, O. (2015). Prediction of railway ground vibrations: accuracy of a coupled lumped mass model for representing the track/soil interaction. *Soil Dyn. Earthq. Eng. 69*:220–226.

Lenci, S., Rega, G. (2016). Axial–transversal coupling in the free nonlinear vibrations of Timoshenko beams with arbitrary slenderness and axial boundary conditions**.** *Proc. R. Soc. A,* 472 p.

Li, C., Huang, X., Hua, H. (2016). Dynamic modeling and analysis of axial vibration of a coupled propeller and shaft system. *J. Mech. Sci. Technol. 30*: 2953–2960.

Li, H., Sun, Q. (2003). Analysis of coupled torsional-axial vibration of crankshaft (in Chinese). *J. Lanzhou Jiaotong Univ. (Nat. Sci.) 23* (01): 107–110.

Mao, Y., Young, Y.L. (2016). Influence of skew on the added mass and damping characteristics of marine propellers. *Ocean Eng. 121*: 437–452.

Mohiuddin, M.A., Khulief, Y.A. (1999). Coupled bending torsional vibration of rotors using finite element. *J Sound Vib. 223* (2):297–316.

Morozov, N.F., Tovstik. P.E. (2013). Transverse rod vibrations under a short-term longitudinal impact**.** *Dokl. Phys. 58* (9):387-391.

Murawski, L. (2005). Shaft line alignment analysis taking ship construction flexibility and deformations into consideration. *Mar. Struct. 18*(1): 62–84.

Murawski, L. (2004). Axial vibrations of a propulsion system taking into account the couplings and boundary conditions. *J. Mar. Sci. Technol. 9*(4):171–181.

Murawski, L. (2012). Some aspects of torsional vibration analysis methods of marine power transmission systems. *Journal of Polish CIMAC, 7*(2):175-182.

Murawski, L., Charchalis, A. (2014). Simplified method of torsional vibration calculation of marine power transmission system. *Mar. Struct., 39*:335-349.

Parsons, M. (1983). Mode coupling in torsional and longitudinal shafting vibration. *Mar. Technol. 20*(3):257–271.

Pan, J., Farag, N., Lin, T., Juniper, R. (2002) Propeller induced structural vibration through the thrust bearing. *Innov. Acoust. Vib.* 390–399.

Qu, Y., Su, J., Hua, H., Meng, G. (2017). Structural vibration and acoustic radiation of coupled propeller-shafting and submarine hull system due to propeller forces. *J. Sound Vib. 401*:76–93.

Rao, M. A., Srinivas, J., Raju, V. B. V. R., Kumar, K. V. S. S. (2003). Coupled torsional-lateral vibration analysis of geared shaft systems using mode synthesis. *J. Sound Vib. 261*(2):359–364.

Sah, S.M., Thomsen, J.J., Tcherniak, D. (2019). Transverse vibrations induced by longitudinal excitation in beams with geometrical and loading imperfections. *J. Sound Vib. 444*:152-160.

Senjanovića, I., Ančića, I., Magazinovićb, G., Alujevića, N., Vladimira, N., Choc, D. (2019). Validation of analytical methods for the estimation of the torsional vibrations of ship power transmission systems. *Ocean Engineering, 184*:107–120.

Shi, L., Xue, D., Song, X. (2010). Research on shafting alignment considering ship hull deformations. *Mar. Struct. 23 (1)*:103–114.

Song, X., Song, T., Li, B. (1989). Coupled vibration of crankshaft system in piston engine. *J. Dalian Uni. Tech. 29* (6): 675–680.

Tian Ran, L., Jie, P., Peter, J.O'S., Chris, K.M. (2009). A study of vibration and vibration control of ship structures, *Marine Structures, 22*:730-743.

Wariko, R. and Haddara, M. R. (1992). Analysis of propeller shaft transverse vibrations. *Marine Structures, 5*:255-279.

Wu, J., Yang, I., Shea, P. O et al. (1995). Computer method for torsion-and-flexure coupled forced vibration of shafting system with damping. *J. Sound Vib. 180*(03): 417–435

Vlase, S., Marin, M., Scutaru, M., et al. 2017. Coupled transverse and torsional vibrations in a mechanical system with two identical beams. *AIP Adv. 7*(6):065301.

Xiang, L., Yang, S., Gan, C. (2012). Torsional vibration of a shafting system under electrical disturbances. *Shock Vib. 19*:01–11

Yang, Y., Che, C., Tang, W. (2014). Shafting coupled vibration research based on wave approach. *J. Shanghai Jiaot. Univ. (Sci.) 19*(3)*:*325–336

Yang Y., Tan W. Y., Huang X. C., Ma J. (2011). Optimal design for a VLCC propulsion system based on torsional vibration analysis. *Procedia Engineering, 15*:5378-5383.

Yuan, Z., Chu, F., Lin, Y. (2007). External and internal coupling effects of rotor's bending and torsional vibrations under unbalances. *Journal of Sound and Vibration, 299* (1–2):339-347

Zhang G. B., Zhao Y., Li T. Y., Zhu X. (2014). Propeller excitation of longitudinal vibration characteristics of marine propulsion shaft system. *Shock and Vibration*, ID: 413592.

Zhang, Z., Zhang, Z., Huang, X., Hua, H. (2014). Stability and transient dynamics of a propeller-shaft system as induced by nonlinear friction acting on bearing-shaft contact interface. *J. Sound Vib. 333*(12):2608–2630

Zou, D., Rao, Z., Ta, N. (2015). Coupled longitudinal-transverse dynamics of a marine propulsion shafting under superharmonic resonances, *J. Sound Vib. 346*: 248–264

Zou, D., Zhang, J., Ta, N., Rao, Z. (2019). Study on the axial exciting force characteristics of marine propellers considered the effect of the shaft and blade elasticity. *Appl. Ocean Res. 89*:141–153.

CURRICULUM VITAE

Name Surname **:** Akile Neşe HALİLBEŞE

EDUCATION **:**

- **B.Sc.** **:** 2012, Yıldız Technical University, Faculty of Naval Architecture and Maritime, Naval Architecture and Marine Engineering
- **M.Sc.** **:** 2015, Istanbul Technical University, Maritime Faculty, Naval Architecture and Ocean Engineering

PROFESSIONAL EXPERIENCE AND REWARDS:

- Research Assistant, Ordu University, Faculty of Marine Sciences (Jan. 2013–Ongoing).
- Research Assistant, Istanbul Technical University, Faculty of Naval Architecture and Ocean Engineering (2013–2020).
- Visiting Researcher, Reliability Engineering Institute, School of Energy and Power Engineering, Wuhan University of Technology (2019-2019).
- The Scientific and Technological Research Council of Turkey (TUBITAK) 2214-A International Doctoral Research Scholarship (2019–2019).

PUBLICATIONS, PRESENTATIONS AND PATENTS ON THE THESIS:

Halilbeşe, A. N., Zhang, C., Özsoysal, O. A. (2021) Effect of Coupled Torsional and Transverse Vibrations of the Marine Propulsion Shaft System. Journal of Marine Science and Application. DOI : 10.1007/s11804-021-00205-